
LST Validation and Algorithm Verification

**Technical assistance for the validation of AATSR land surface
temperature products**

ESA Contract Number: 19054/05/NL/FF

Issue 1A

Written by: D. Ghent

Approved by: G. Corlett

Summary

This report describes the work carried out at the University of Leicester within the framework of Work Package 410 of the ESA project “Long Term Land Surface Temperature Validation”. Work Package 410 concerns the continuation of the validation and algorithm verification activities carried out during ‘The Technical Assistance for the Validation of AATSR Land Surface Temperature Products’ (ESA Contract Number: 9054/05/NL/FF) and supplements the original contract final report and contract extension final report. In addition, this study extends the previous evaluation of the operational AATSR LST product to include the updated AATSR LST product produced by the University of Leicester, which incorporates recommendations made in the original contract for replacing the existing coarse resolution auxiliary datasets with approximately 1 km spatial resolution auxiliary datasets for land cover and fractional vegetation cover. Two further extensions to the original validation include the assessment of a larger number of *in situ* validation sites over a longer time frame, and a multi-sensor intercomparison exercise.



Table of Contents

1. INTRODUCTION	1
2. MODIFICATIONS TO THE AUXILIARY DATASETS	2
3. STUDY APPROACH	4
4. IN SITU VALIDATION	5
4.1. DESCRIPTION OF IN SITU DATA	5
4.1.1. ARM sites	5
4.1.2. Evora, Portugal	5
4.1.3. Gobebeb, Namibia	8
4.2. METHODOLOGY	8
4.2.1. Determining in situ LST	8
4.2.2. Cloud screening and snow masking	9
4.3. RESULTS	10
4.3.1. ARM sites	12
4.3.2. Evora, Portugal	13
4.3.3. Gobebeb, Namibia	14
4.4. SUMMARY.....	15
5. SENSITIVITY STUDY.....	17
5.1. METHODOLOGY	17
5.2. RESULTS	19
5.2.1. Response to emissivity	19
5.2.2. Response to water vapour	23
5.2.3. Response to atmospheric temperature.....	23
5.2.4. Response to skin temperature	24
5.2.5. Response to auxiliary fractional vegetation data	24
5.3. SUMMARY.....	29
6. MULTI-SENSOR INTERCOMPARISON.....	30
6.1. INSTRUMENTS.....	30
6.2. METHODOLOGY	31
6.3. RESULTS	31
6.4. SUMMARY.....	35
7. CONCLUSIONS	37
8. REFERENCES	39
9. ACKNOWLEDGEMENTS.....	41
APPENDIX A – IN SITU VALIDATION PLOTS	42
APPENDIX B – SENSITIVITY PLOTS.....	49

1. Introduction

The objective of the operational Land Surface Temperature (LST) product derived from data recorded by the Advanced Along-Track Scanning Radiometer (AATSR) has been to provide global observations of LST at 1 km spatial resolution, with a target accuracy of 2.5 K during the day and 1.0 K at night (Llewellyn-Jones *et al.*, 2001; Prata, 2002). In the final report documents for ESA contract number 19054/05/NL/FF, henceforth referred as the ‘original contract final report’ (Noyes, 2006a) and ‘contract extension final report’ (Noyes, 2007) respectively, recommendations were put forward to improve the spatial resolution of the auxiliary datasets utilised in the LST retrieval. The development of an updated LST product which implements the changed auxiliary files reported in Zeller (2010), and henceforth referred to as the updated LST, necessitates an appropriate validation study.

Continuation of the validation study reported in Noyes (2006a) and Noyes (2007) has therefore been undertaken on the updated LST (uLST). The nature of the validation study follows a similar methodology to the previous study. To summarise, the updated LST product has been validated with collocated *in situ* observations from the sites utilised previously. In these cases we report on the updated LST product and refer the reader to Noyes (2006a) for detailed results on the operational AATSR LST (oLST) product. Where new sites have been sourced then both operational LST and updated LST are assessed against *in situ* measurements.

In addition to the *in situ* validation a sensitivity analysis was performed whereby the sensitivity of the AATSR LST algorithm is assessed for the key variables in the retrieval. This is undertaken for each new biome classification, and a cursory comparison is made with the equivalent findings on the operational product from Noyes (2006a). An accurate comparison is not feasible since a one-to-one mapping between the Dorman and Sellers (DS) biomes (Dorman and Sellers, 1989) and the updated biome classification, henceforth referred to as the AATSR LST Biome classification version-2 (ALB2), which is based on the Globcover classification. Finally, both uLST and oLST were compared with equivalent data from other satellite sensors over southern Europe during 2006.

In section 2 a short summary on the new auxiliary datasets is presented here - for further details see Zeller (2010). We do however describe enhanced modifications made to these auxiliary datasets which have as yet to be documented. Section 3 presents an overview of the study approach, and sections 4, 5 and 6 detail the *in situ* validation, sensitivity study and multi-sensor intercomparison respectively. We summarise by assessing the overall accuracy of the updated product, and rationalise the results with respect to the findings presented both here and in Noyes (2006a) and Noyes (2007) regarding the accuracy of the operational LST. This study comes with a few caveats, which are discussed in the conclusions, and as a result of these findings recommendations for further investigation are proposed.

2. Modifications to the Auxiliary Datasets

During the original contract period, issues relating to the auxiliary biome and fractional vegetation data utilised by the product were identified. It was concluded that the resolution of these data were not high enough for their intended purpose. In some cases it was found that inaccuracies in the auxiliary data were culminating in large biases and absent values (i.e. where no LST retrieval was performed over land) in the AATSR LST data. As such, higher spatial resolution auxiliary datasets have been developed and reported in Zeller (2010). Here we expand upon the information within the aforesaid report by describing further work carried out to improve the classification of the bare soil regions of the globe.

Investigation revealed that emissivity values derived from the CIMSS dataset (Seemann *et al.*, 2008) for 11 and 12 μ m channels for the bare soil biome (ALB2-20) displayed substantial variations (see Figure 2.1(d) for 11 μ m), considerably larger than for any other biome. ALB2-20 regions were compared with a global soil map from United States Department of Agriculture (USDA) which classifies the orders and suborders of soil types (Soil Survey Staff, 1999). The outcome of this investigation was the creation of five additional biome classes (ALB2-21 to ALB2-25). The threshold for the creation of a new bare soil class was set as any soil type accounting for at least 0.5% of the global land surface. All remaining soil classes were grouped together under ALB2-20.

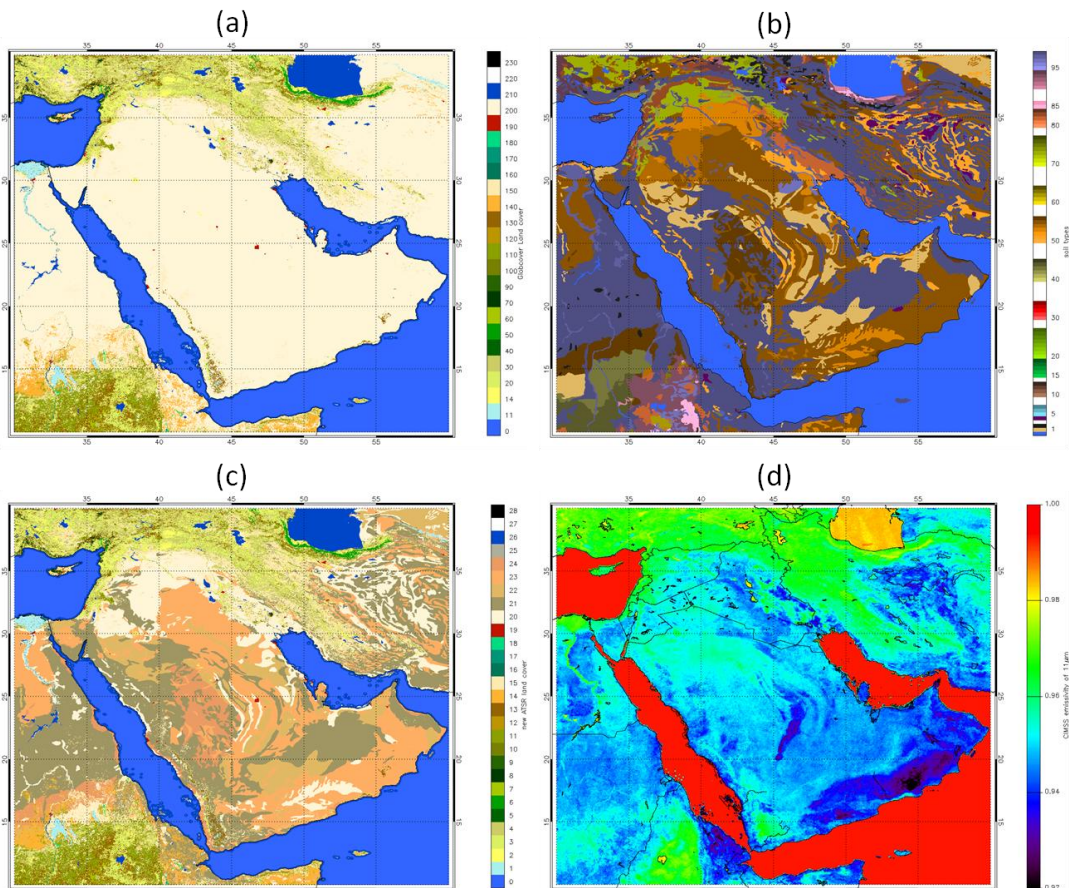


Figure 2.1: (a) Globcover biome map for Arabian Peninsula after changes described in Zeller (2010); (b) USDA soil map showing the suborders of the soil taxonomy; (c) new ATSR biome map (ALB2); (d) mean CIMSS emissivity for 2007 and 2008 for a wavelength of 11 μ m.

Figure 2.1 shows the biome classification as described in Zeller (2010) for the Arabian Peninsula (panel a) dominated by bare soil areas (previous classification GC200). The soil classification from the USDA, also displayed (panel b), illustrates the many different soil types of the region dominated specifically by Orthents from the Entisol order, shifting sand and Aridisols types. The modified biome classification (panel c) incorporates some of these dominating types and is now an improved representation of the emissivity variation (panel d). Similar patterns between emissivity and the soil classes are evident especially in the middle of the peninsula; with strong emissivity gradients both in the south of the peninsula and in Egypt appearing to be connected to soil type changes. Emissivity maxima over the mountains in Yemen and in the mountains parallel to the southern coast of the Caspian Sea may be due to maxima of vegetation density. A full listing of the ALB2 classes is provided in Table 2.1.

Table 2.1: ATSR LST biome classification version 2 (ALB2) derived from the Globcover classification.

No.	Legend	Based on
0	Water bodies of sea (>10km away from coast)	GC210 (GC0)
1	Post-flooding or irrigated croplands	GC11
2	Rainfed croplands	GC14
3	Mosaic Cropland (50-70%) / Vegetation (grassland, shrubland, forest) (20-50%)	GC20
4	Mosaic Vegetation (grassland, shrubland, forest) (50-70%) / Cropland (20-50%)	GC30
5	Closed to open (>15%) broadleaved evergreen and/or semi-deciduous forest (>5m)	GC40
6	Closed (>40%) broadleaved deciduous forest (>5m)	GC50
7	Open (15-40%) broadleaved deciduous forest (>5m)	GC60
8	Closed (>40%) needleleaved evergreen forest (>5m)	GC70
9	Open (15-40%) needleleaved deciduous or evergreen forest (>5m)	GC90
10	Closed to open (>15%) mixed broadleaved and needleleaved forest (>5m)	GC100
11	Mosaic Forest/Shrubland (50-70%) / Grassland (20-50%)	GC110
12	Mosaic Grassland (50-70%) / Forest/Shrubland (20-50%)	GC120
13	Closed to open (>15%) shrubland (<5m)	GC130
14	Closed to open (>15%) grassland	GC140
15	Sparse (>15%) vegetation (woody vegetation, shrubs, grassland)	GC150
16	Closed (>40%) broadleaved forest regularly flooded - Fresh water	GC160
17	Closed (>40%) broadleaved semi-deciduous and/or evergreen forest regularly flooded - Saline water	GC170
18	Closed to open (>15%) vegetation (grassland, shrubland, woody vegetation) on regularly flooded or waterlogged soil - Fresh, brackish or saline water	GC180
19	Artificial surfaces and associated areas (urban areas >50%)	GC190
20	Bare areas of soil types not contained in biomes 21 – 25	GC200 and other USDA soil types
21	Bare areas of soil type “Entisols – Orthents”	GC200 / USDA-99
22	Bare areas of soil type “Shifting sand”	GC200 / USDA-1
23	Bare areas of soil type “Aridisols - Calcids”	GC200 / USDA-55
24	Bare areas of soil type “Aridisols - Cambids”	GC200 / USDA-56
25	Bare areas of soil type “Gelisols - Orthels”	GC200 / USDA-7
26	Water bodies (inland lakes, rivers, sea: max 10km away from coast)	GC210
27	Permanent snow and ice	GC220 and ATSR land sea mask <60°S
28	No data (burnt areas, clouds, etc)	GC230

3. Study Approach

The traditional approach to validating geophysical products derived from satellite has been with respect to equivalent *in situ* data. Ideally this should be performed under the full range of expected conditions over the entire globe covering every biome classification. However in practise this is not feasible, with the recommendation being that most validation sites be larger than a satellite pixel, topographically flat and homogeneous in terms of surface cover. It is therefore prudent to supplement these with sensitivity studies to identify sources of any bias that are observed in the validation results. Furthermore, multi-sensor intercomparison studies enable differences between retrievals to be assessed. With this in mind, the following study approach, which builds on the findings of both Noyes (2006a) and Noyes (2007), has been adopted here:

1) **In situ validation (section 4)**

- a) Where existing validation sites have continued to measure *in situ* data validation efforts have continued in order to increase the number of matchups and the statistical significance of the results. Since no new data has been acquired from the NAFE sites these have not been included in this analysis.
- b) New validation data has been sourced, thereby expanding the original database. The aim has been to maximise the biome class representation. This has enabled a more comprehensive picture of the performance of both oLST and uLST.

2) **Theoretical sensitivity (section 5)**

- a) The theoretical sensitivity study that was initiated during the original contract period and continued during the contract extension has been extended to all the new biome classes, where sensitivity of the algorithm to surface temperature, emissivity, water vapour and atmospheric temperature has been investigated.
- b) A fast radiative transfer model (RTTOV) has been utilised to investigate the sensitivity to these key variables (Eyre, 1991); in this case version 10 of RTTOV was utilised. Here we have used the reference atmospheric profiles of Remedios (1999) for tropical, mid-latitude, polar-winter and polar-summer climatologies as input to RTTOV-10.

3) **Multi-sensor intercomparison (section 6)**

- a) A multi-sensor intercomparison has been carried out over southern Europe for the entirety of 2006. This has enabled a better identification of any seasonal differences between instruments and differences due to viewing angle.
- b) Southern Europe was chosen since it is covered by the spinning enhanced visible and infrared imager (SEVIRI) instrument on board the Meteosat Second Generation (MSG) geostationary satellites. The final instrument in the intercomparison was the moderate resolution imaging spectroradiometer (MODIS) instrument on board the sun-synchronous, near-polar orbiting satellite Terra.

4. In situ validation

In Table 4.1 a summary of existing field sites which have continued to produce *in situ* measurements and have been included in the current study is presented together with new sites which have been identified since the original contract and extension. For each site the new ALB2 biome class has been determined and included for reference.

In this section we describe a selection of the new sites and present our results on the validation of oLST and uLST for both the new sites and for the existing sites where *in situ* measurements have continued to be collected beyond the time window reported in both Noyes (2006a) and Noyes (2007).

4.1. Description of *in situ* Data

4.1.1. ARM sites

In addition to the existing ARM sites described in Noyes (2007), several further ARM sites have been included in this study. Most sites are equipped with a range of instrumentation including upward and downward-looking ground radiometers for measuring both the brightness temperatures (BTs) of the sky and surface respectively. In addition, the sites also house a range of standard meteorological equipment, such as humidity sensors, thermometers, and ceilometers. Specifics can be found in the ARM Infrared Thermometer Handbook (ARM, 2005). The downward-looking radiometers take average measurements every 60 seconds of the surface. A feature of the ARM sites is that in general the data sets recorded are near continuous.

4.1.2. Evora, Portugal

The Evora site (38.54°N, 8.00°W) is part of the global flux network of measurements - Fluxnet (Baldocchi *et al.*, 2001). In addition to instruments taking meteorological measurements a rotating radiometer measures LST from the 28m tower. Measurements are taken in the 8–12 μ m spectral range, with a target accuracy of 0.2 K. Calibration is performed automatically during every measurements cycle utilising both heated and ambient temperature blackbodies. The head of the radiometer rotates about a perpendicular axis to the viewing direction, which enables a scene to be viewed over a range of zenith angles and for different scenes. As such, BTs are measured for three scenes (endmembers) on the ground corresponding to deciduous tree crown, sunlit grass, and grass in shadow; with a periodicity of 2-minutes and an instantaneous field of view of approximately 6 m. For the comparison with satellite-derived LST the *in situ* BTs were calculated as a weighted average of the BTs of these three endmembers; with the estimates of the weights being 0.37 (tree crown), 0.315 (sunlit grass), and 0.315 (shadow grass). Further details can be found in Trigo *et al.* (2008a) and Kabsch *et al.* (2008).

Table 4.1: Summary of *in situ* LST data for each site for the validation of AATSR LSTs. The table groups the sites by ALB2 biome classification, and for each site the 4-character site “callsign” and its long name are given, plus the geolocation information and time period over which *in situ* measurements are available. The minimum number of matchups expected before cloud screening is also presented.

Biome	Site	Site name	Lon, Lat	Data Period	Average number of matchups per months for descending (D) and ascending (A) overpasses																								Comments
					Jan		Feb		Mar		Apr		May		Jun		Jul		Aug		Sep		Oct		Nov		Dec		
					A	D	A	D	A	D	A	D	A	D	A	D	A	D	A	D	A	D	A	D	A	D			
1	vlnc	Valencia site, Spain	-0.29, 39.24	2002/07/10 - 2004/08/12	0	0	0	0	0	0	0	0	0	0	0	0	0	0	0	0	0	0	0	0	0	0	0	Data recorded at intervals to coincide with AATSR overpass	
2	card	Cardington site	-0.42, 52.10	2004/05/28 - 2006/11/30	6	6	6	6	7	6	6	6	6	7	7	5	6	7	6	6	6	5	6	7	7	7	5	4	Data recorded every 10 minutes
	evra	ARM Evora site	-8.00, 38.54	2005/08/02 - 2006/07/18	2	2	3	4	4	4	3	3	4	4	1	2	1	1	1	1	3	3	1	2	2	1	0	0	Data recorded every 2 minutes
	okla	ARM Oklahoma South Great Plains (USA)	-97.48, 36.60	2003/12/18 - 2010/12/31	6	6	6	6	6	6	5	6	6	6	5	6	5	6	5	6	5	6	6	5	6	6	6	Data recorded once a minute	
	shxn	ARM Shouxian, China	116.78, 32.55	2008/05/11 - 2008/12/28	0	0	0	0	0	0	0	0	4	5	5	5	7	7	5	6	7	6	7	7	6	7	8	8	Data recorded once a minute
3	azrs	ARM Azores site	-28.02, 39.09	2009/05/01 - 2010/12/31	4	3	3	3	4	4	4	3	8	5	8	7	7	8	8	7	9	7	6	6	6	7	8	7	Data recorded once a minute
	manu	ARM Manus Tropical Western Pacific	147.42, -2.06	2003/10/13 - 2010/12/31	4	8	3	8	4	9	4	7	4	8	4	9	4	9	4	8	4	7	4	9	4	10	4	10	Data recorded once a minute
6	blkf	ARM Black Forest site	8.39, 48.54	2007/04/01 - 2008/01/01	0	0	0	0	0	0	8	7	4	8	9	6	8	9	8	9	9	7	9	9	9	10	9	7	Data recorded once a minute

	ptry	ARM Point Reyes, California	-122.95, 38.09	2005/02/14 - 2005/09/15	0	0	3	4	8	7	5	7	7	8	7	5	6	8	7	7	4	4	0	0	0	0	0	0	Data recorded once a minute
12	barr	ARM Barrow, North Slope of Alaska	-156.60, 71.32	2003/10/13 - 2010/12/31	2	30	15	15	17	17	21	8	34	0	33	0	33	0	32	2	15	16	18	18	9	27	0	35	Data recorded once a minute
15	niam	ARM Niger, Africa	2.1758, 13.47	2005/11/24 - 2007/01/07	3	2	2	2	1	2	2	2	2	2	2	2	2	2	1	1	2	1	2	2	2	2	3	4	Data recorded once a minute
18	atqs	ARM Atqasuk, North Slope of Alaska	-157.40, 70.47	2003/10/13 - 2010/12/31	4	27	14	14	17	16	19	9	32	0	31	0	31	0	28	3	15	15	18	16	11	23	0	33	Data recorded once a minute
19	darw	ARM Darwin site	130.89, -12.42	2003/10/13 - 2010/12/31	4	3	4	3	5	4	5	5	5	5	5	5	5	5	5	6	5	5	6	5	6	5	5	4	Data recorded once a minute
20	gbeb	Gobabeb, Namibia	15.03, -22.33	2008/01/29 - 2009/12/31	3	4	7	6	6	5	6	6	7	7	5	4	1	2	3	3	6	7	7	6	5	6	5	5	Data recorded once a minute
26	naur	ARM Nauru Tropical Western Pacific	166.91, -0.52	2003/10/13 - 2010/12/31	5	10	4	10	5	10	4	9	5	10	4	10	5	10	5	11	4	9	5	11	5	11	5	11	Data recorded once a minute
27	g_09	Greenland site 09	-49.68, 69.49	2000/01/01 - 2004/05/22	4	18	8	9	12	12	13	7	19	0	12	0	13	0	17	4	10	10	10	8	9	11	0	21	Data recorded once an hour
	g_17	Greenland site 17	-50.05, 69.42	2000/01/01 - 2004/05/26	4	18	8	10	11	12	11	7	21	0	12	0	12	0	15	4	8	10	11	9	9	12	0	23	Data recorded once an hour
	gnld	Greenland site	-38.50, 72.57	2000/01/01-2004/06/14	0	17	6	7	12	9	14	4	21	0	13	0	15	0	24	1	10	11	12	9	4	14	0	16	Data recorded once an hour

4.1.3. Gobebeb, Namibia

The Gobabeb site (22.33°S, 15.03°E) is located on large gravel plains (>900 km²) at an altitude of 408m; these plains are sparsely covered by desiccated grass. To measure LST two self-calibrating KT-15 IR-radiometers are mounted on the 30m tower taking measurements in the 9.6-11.5 μ m range with a target accuracy of ± 0.3 K (Goettsche - personal communication). The two radiometers observe neighbouring areas of the gravel surface from the north with a 30° viewing angle. Such a viewing angle is justified since angular anisotropic emissivity values for sand, grass, and gravel are negligible up to 30° (Sobrino and Cuenca, 1999). An additional KT-15 radiometer measures the effective brightness temperature of the sky at 53° to zenith. Only measurements from the east-facing radiometer have been included in the matchup process since these have been found to be more representative (Goettsche - personal communication).

4.2. *Methodology*

All the comparison results reported in this section of the report have been produced both for the operational 1 km AATSR LST data and updated LST based on the high resolution auxiliary datasets. The general methodology adopted for comparing the satellite-derived LST with the corresponding *in situ* data is as follows:

1. If required the *in situ* radiometric temperatures are corrected for surface emissivity effects and an estimate of skin temperature is derived (see section 4.2.1).
2. For each AATSR overpass the nominal 1 km pixel containing the location of the *in situ* observation is extracted.
3. The AATSR LST for this pixel and the *in situ* observation that is temporally closest to the exact time of the AATSR overpass are recorded as a matchup. The threshold for the temporal offset between the time of the AATSR overpass and the *in situ* observation is set as ± 90 minutes. In practise, only a small proportion of the matchups have a temporal offset greater than ± 5 minutes – almost all of these are for the three Greenland sites which only take *in situ* measurements every 60 minutes.
4. Any matchups flagged cloudy by the updated cloud detection methods (see section 4.2.2) are rejected.
5. The mean and standard deviation of AATSR LST minus *in situ* LST is calculated for all cloud-free matchups. In addition robust statistics – median and median absolute deviation – are determined for all cloud-free matchups per site. The rationale here is that these statistics are not adversely influenced by outliers. In this study outliers may be problematic *in situ* measurements or incorrect cloud screening.

4.2.1. Determining *in situ* LST

Surface temperature observations made by an *in situ* radiometer operating in the infrared do not represent the true kinetic temperature of the surface, since the Earth's surface is not a blackbody and its thermal emissivity not unity. This results in surface temperatures typically 1-4 K higher than the observed at-surface radiometric BTs. For *in situ* measurements made at the surface of the earth the radiative transfer equation can be expressed as:

$$B_c(T_c) = \varepsilon_c B_c(T_{sfc}) + (1 - \varepsilon_c) B_c(T_{sky})$$

Where $B_c(T_c)$ is the measured radiance given by the Planck function for effective brightness temperature T_c in the radiometer channel c , $B_c(T_{sfc})$ is the emitted surface radiance given by the Planck function for surface temperature T_{sfc} in channel c , and $B_c(T_{sky})$ is the down-welling atmospheric radiance given by the Planck function for effective brightness temperature T_{sky} of the atmosphere; ε_c is the emissivity of the Earth's surface in channel c . The non-uniformity of the surface emissivity means that the down-welling atmospheric radiance has a small, but significant impact on LST, so regular radiometric measurements of this correction factor are important, particularly if the sky is not homogeneous. In practice, this is carried out with a radiometer facing the sky at approximately 53° from zenith (Kondratyev, 1969; Coll *et al.*, 2005).

For fifteen of the eighteen sites LST data was available and no calculation was applied. For the other three sites (Cardington, Evora and Gobebeb) LST was determined from the BTs and estimates of emissivity. Where *in situ* observations of emissivity were not available data from the ASTER Spectral Library (1999) plus information regarding the ground cover in the radiometer instantaneous field of view (IFOV) for each site has been used to determine the estimates. The ASTER spectral library contains reflectance spectra corresponding to visible and infrared wavelengths for almost 2000 natural and man-made materials. Table 4.2 quantifies the 11 and $12\mu\text{m}$ emissivities for the surface types at Cardington and Evora.

Table 4.2: 11 and $12\mu\text{m}$ channel emissivities derived from data provided by the Aster Spectral Library (1999) for green grass, dry grass and deciduous trees.

Surface	11 μm channel	12 μm channel
Green grass	0.984	0.989
Dry grass	0.912	0.915
Deciduous trees	0.973	0.973

For Cardington the radiometer IFOV covers 100 % green grass. As such the channel emissivities for green grass from the ASTER spectral library have been used. For Gobebeb, which is treated as a homogenous site with a single endmember emissivities for both 11 and $12\mu\text{m}$ was set as 0.96 (Goettsche – personal communication). For Evora, emissivities were derived from the ASTER spectral library for green grass and deciduous trees. Over the course of a year the deciduous tree cover remains relatively constant throughout the year; the emissivity remains constant as well. However, the grass coverage changes with the seasons so different emissivities need to be applied. In the winter months (October to January) the emissivity is that of green grass, whereas in the summer months the emissivity is taken as that of dry grass.

4.2.2. Cloud screening and snow masking

Due to known problems with undetected cloud in AATSR data over land, it has been necessary to employ alternative cloud screening of the AATSR LSTs used in this study. Cloud screening work carried out at the University of Leicester has found that the use of the Gross Cloud Test (GCT) and Thin Cirrus Test (TCT) from the AATSR operational cloud product and an adaptation to the

MODIS $11\mu\text{m} - 3.9\mu\text{m}$ brightness temperature difference test has resulted in the most effective cloud mask. This latter test applies the difference between the 11 and $3.9\mu\text{m}$ channels to thresholds set both for day and night and additionally for polar and non-polar latitudes. This test has been adapted for AATSR data by using the $3.7\mu\text{m}$ instead of the $3.9\mu\text{m}$ channel. Further details on this test and its performance within the MODIS cloud mask can be found in the report on improvements on MODIS cloud detection by Frey *et al.* (2008).

For the snow masking, the method developed by Istomina *et al.* (2010) has been used. This exploits all seven AATSR channels to produce a snow/cloud clearing mask. The algorithm attempts to account for the many factors that can affect the spectral signature of snow, such as atmospheric aerosol, ground contamination and snow grain size - setting criteria to describe the spectral shape of snow: 3 VIS/NIR criteria and 3 TIR criteria. The VIS/NIR criteria should be sufficient to screen optically thick warm clouds, but will have difficulty with cirrus and optically thin clouds as they do not significantly disturb the spectral signature of snow in those spectral regions, therefore the TIR channels provide the necessary additional cloud screening.

4.3. Results

Once we have established a set of cloud-free matchups for each site, statistics for mean bias and standard deviation – and for median and median absolute deviation - are calculated according to step 5 of the methodology outlined in section 4.2. We present these statistics in Table 4.3, and investigate in detail select sites. For these select sites results are represented graphically where the bias (AATSR LST minus *in situ* LST) is represented on the y-axis with time on the x-axis. A common y-axis scale (-10 to +10 K) is used for all figures where possible; however, in cases where the bias is considerably larger than this then a scale of -60 to +60 K is used.

Overall Table 4.3 presents evidence that the updated AATSR LST outperforms the operational AATSR LST in general. If we first consider the daytime, and concentrate on the robust statistics, then several conclusions may be drawn. First, in the cases where the median for oLST minus *in situ* are strongly negative the corresponding biases for uLST minus *in situ* are all much reduced in magnitude. The most feasible explanation for this is that the new auxiliary dataset – and the corresponding coefficients in the LST algorithm - provide a much more representative description of the land cover at these sites. Second, for the majority of sites the median absolute deviation for uLST minus *in situ* LST is lower than for oLST minus *in situ* LST. Furthermore, in all but three cases the median absolute deviation for uLST minus *in situ* LST is within the daytime target accuracy of 2.5 K. The median absolute deviation for oLST minus *in situ* LST fails to meet this target accuracy in six cases. Finally, a few sites demonstrate large discrepancies with respect to the *in situ* measurements; where in the case of Darwin for example (Appendix A) the larger median bias is affected by the asymmetric distribution between the first half of the comparison window and the second half. Furthermore, the *in situ* radiometer at this site is measuring bare soil, whereas the ALB2 classification is urban with the AATSR LST being an aggregate of the temperature of several surface types including vegetation which generally has lower surface temperatures. Nauru (Appendix A) on the other hand which is a coastal site and classified as inland water (ALB2-26) may be an extreme case for this biome class whereby the coefficients which are globally optimum for inland water may not be optimum here.

Table 4.3: Results of comparisons between AATSR LST - both operational (oLST) and updated (uLST) - and collocated *in situ* LST data.

Site	Version	Day				Night			
		Mean bias	Std. Dev.	Median bias	Med. Abs. Dev.	Mean bias	Std. Dev.	Median bias	Med. Abs. Dev.
atqs	oLST	-0.71	6.15	0.79	2.27	-2.30	4.73	-0.76	1.57
	uLST	-1.12	5.28	0.64	2.13	-2.07	4.90	-0.39	1.55
azrs	oLST	-11.68	6.78	-11.48	5.27	-6.53	5.51	-5.44	2.94
	uLST	-4.86	6.84	-3.35	4.26	-2.61	6.34	-0.71	3.73
barr	oLST	-1.24	6.19	-0.57	2.42	-3.01	6.82	-1.90	2.07
	uLST	-1.01	6.24	-0.45	2.39	-2.38	6.39	-0.96	2.13
blkf	oLST	-5.79	4.88	-4.40	2.33	-0.49	7.66	2.64	3.35
	uLST	-5.10	5.89	-2.21	2.68	-0.82	7.34	2.25	3.24
card	oLST	-2.73	4.83	-1.21	1.74	-2.89	7.56	0.21	2.46
	uLST	-3.28	5.62	-1.31	2.21	-2.63	7.24	0.70	2.18
darw	oLST	-13.79	8.71	-14.22	3.49	-9.11	8.51	-8.12	2.85
	uLST	-3.61	8.86	-3.26	2.88	-3.73	8.59	-2.23	2.10
evra	oLST	-0.31	7.58	0.36	2.91	-3.85	6.56	-1.83	1.16
	uLST	-2.73	6.74	-0.56	1.80	-3.68	5.95	-1.84	1.42
gbeb	oLST	2.05	3.77	1.99	2.53	-3.89	5.96	-2.84	1.17
	uLST	3.43	3.70	3.78	1.86	-0.83	6.06	0.78	0.96
g_09	oLST	-1.54	5.23	0.66	1.43	-4.12	5.93	-2.90	3.25
	uLST	-3.00	5.16	-1.00	1.49	-5.26	5.94	-3.73	3.10
g_17	oLST	-1.22	5.58	1.25	0.79	-4.92	7.41	-2.28	2.79
	uLST	-2.65	5.60	-0.14	0.77	-6.79	6.56	-4.44	3.08
gnld	oLST	-1.25	4.24	-0.55	2.31	-1.07	3.80	-1.13	1.95
	uLST	-2.37	4.25	-1.70	2.27	-1.89	4.07	-2.05	1.95
manu	oLST	-16.86	7.87	-17.37	1.89	-6.96	6.25	-5.57	1.61
	uLST	-6.19	8.51	-5.65	1.75	0.80	5.90	2.36	1.70
naur	oLST	-18.38	12.04	-19.10	3.63	-6.36	7.55	-5.25	1.95
	uLST	-11.08	12.30	-11.88	4.18	0.25	7.87	1.53	1.49
niam	oLST	-0.15	2.92	0.53	1.71	-0.62	2.17	-0.40	1.31
	uLST	-2.43	3.84	-1.55	2.04	-0.86	2.30	-0.75	0.96
okla	oLST	-0.49	5.33	0.07	1.87	-1.44	7.30	0.15	1.70
	uLST	-0.38	5.21	0.24	1.67	-0.99	7.16	0.93	1.27
ptry	oLST	-4.46	3.35	-3.91	1.88	-2.78	7.54	-1.22	1.11
	uLST	-0.78	4.31	1.35	1.72	-1.19	7.52	0.87	1.09
shxn	oLST	2.19	4.64	3.15	2.66	2.74	11.32	7.15	3.33
	uLST	-3.50	3.64	-2.93	1.57	-1.55	10.27	2.95	2.08
vlnc	oLST	3.48	1.10	3.49	0.81	No data	No data	No data	No data
	uLST	2.74	0.68	2.92	0.51	No data	No data	No data	No data

For night-time comparisons the same overall improvements in uLST minus *in situ* LST compared with oLST minus *in situ* LST are evident in terms of median bias and median absolute deviation; however, several distinctions are apparent. First, in most cases the magnitude of the median biases and median absolute deviations are lower than for the corresponding daytime cases. Although, in only two cases is the night-time target accuracy of 1 K met for uLST minus *in situ* LST, for oLST minus *in situ* LST this target accuracy is not achieved at all. Several explanations are possible, such as the coefficients for the corresponding biomes being non-optimal for these specific sites, or deficiencies in the cloud masking during the night. Finally, the largest median biases for uLST minus *in situ* LST occurred for the three Greenland sites. The most likely explanation here is a combination of failures in the cloud masking over ice and globally optimised coefficients that are non-optimal at these sites.

4.3.1. ARM sites

Here we look at a couple of ARM sites in more detail, Atqasuk (Figure 4.4) and Oklahoma (Figure 4.5).

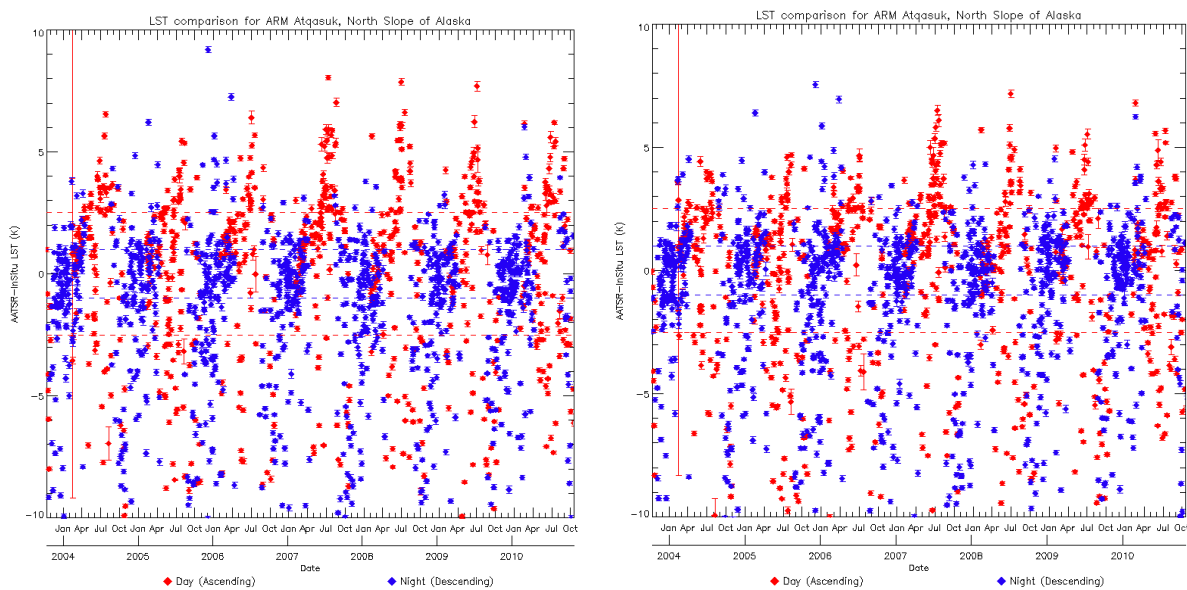


Figure 4.4: Comparison between AATSR operational LST (left) and updated LST (right) with respect to *in situ* LST data over the ARM-Atqasuk field site from 2004 to 2010 inclusive. The dashed lines show the target accuracy of the AATSR LST product during the day (red) and night (blue). The error bars represent the estimated errors on the point *in situ* LST observations.

The results illustrated in these figures and their robust statistics demonstrate that the AATSR LST product agrees reasonably well with the *in situ* data recorded for these field sites both during the day and night. Indeed, the absolute median bias is less than 1 K for both sites – day and night - and for both uLST and oLST comparisons. The median absolute deviations are also within the 2.5 K target accuracy for daytime, and although outside the 1 K night-time target accuracies, values of 1.27 K and 1.70 K for uLST and oLST comparisons respectively are less than 1 K outside the target accuracy.

Several features are evident and worth further comment. Distinct seasonal patterns for instance can be discerned for both sites. As detailed in both Noyes (2006a) and Noyes (2007), and corroborated here, a cold-bias in the winter and warm-bias in the summer is evident for Oklahoma. Moreover, this same finding is also apparent – and indeed magnified - at Atqasuk; a plausible explanation in this latter case is that the *in situ* radiometer is measuring the surface temperature of seasonally flooded grassland, whereas nearby there is an airstrip - the surface temperature of which in summer is likely to be higher than that measured by the radiometer - which would contribute to the AATSR LST. This is particularly evident for the daytime comparisons, and is most likely due to surface heterogeneity producing extreme variations in surface temperature on the sub-pixel scale. These variations in surface temperature may also be present during the night, but to a lesser extent as solar heating is absent.

A further seasonal pattern is evident for both sites, whereby large negative biases are more concentrated during the winter months. The most feasible explanation here is that there are increased failures of the cloud screening during these months as a result of the presence of ice and snow. Two distinct failures are possible: first, the ground is covered by snow / ice and the cloud screening process is missing the presence of clouds; second, the ground is not covered by snow / ice but the snow mask is incorrectly interpreting cloud as snow / ice and applying inappropriate coefficients in the LST retrieval.

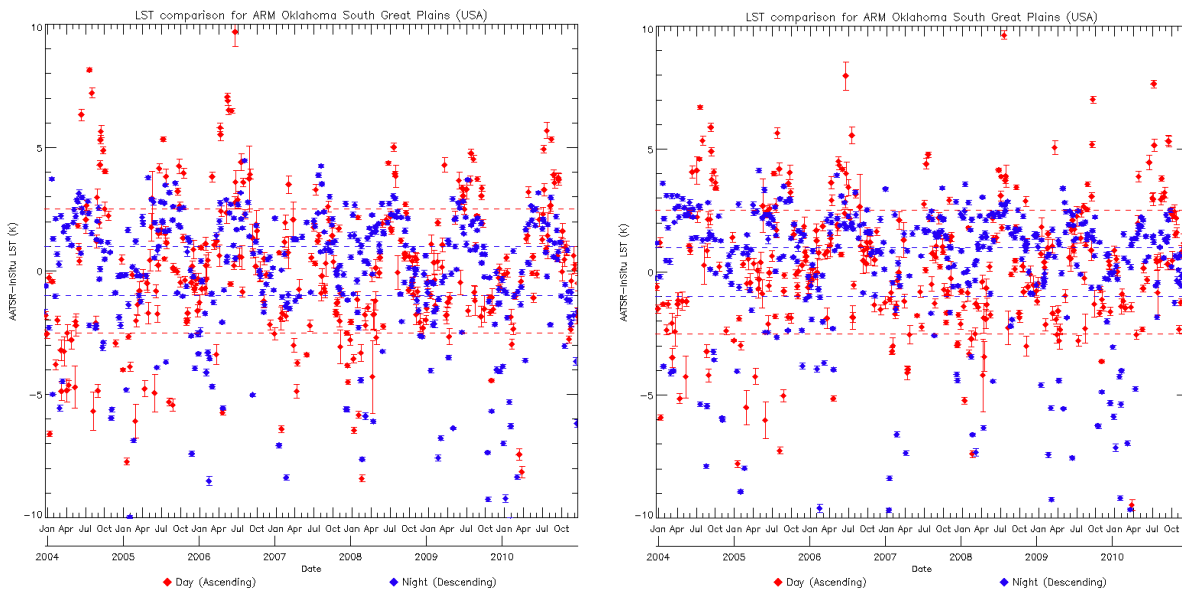


Figure 4.5: Comparison between AATSR operational LST (left) and updated LST (right) with respect to *in situ* LST data over the ARM-Oklahoma field site from 2004 to 2010 inclusive. The dashed lines show the target accuracy of the AATSR LST product during the day (red) and night (blue). The error bars represent the estimated errors on the point *in situ* LST observations.

4.3.2. Evora, Portugal

The AATSR retrieved LST shows good agreement with the *in situ* LST at Evora for both AATSR LST products. Small daytime biases were recorded for both uLST and oLST comparisons of 0.36 K and -0.56 K respectively. The corresponding median absolute deviations were 2.91 K and 1.80 K

respectively; indicating that the recent developments to the LST retrieval have enabled the 2.5 K daytime target accuracy to be met. Night-time biases are higher, -1.83 K and -1.84 K respectively, with the median absolute deviations (1.16 K and 1.42 K respectively) not quite meeting the 1 K target accuracy. As suggested above, despite the rigorous approach to cloud screening the night-time cloud masking tests may not be optimum for all scenes. Another source of discrepancy between satellite and *in situ* is the upscaling of the endmember *in situ* measurements to an area average. Here the endmember proportions are based on the overlying SEVIRI pixel which may have considerably different endmember proportions to each AATSR overstrike. Figure 4.6 shows the difference for each individual comparison following cloud screening.

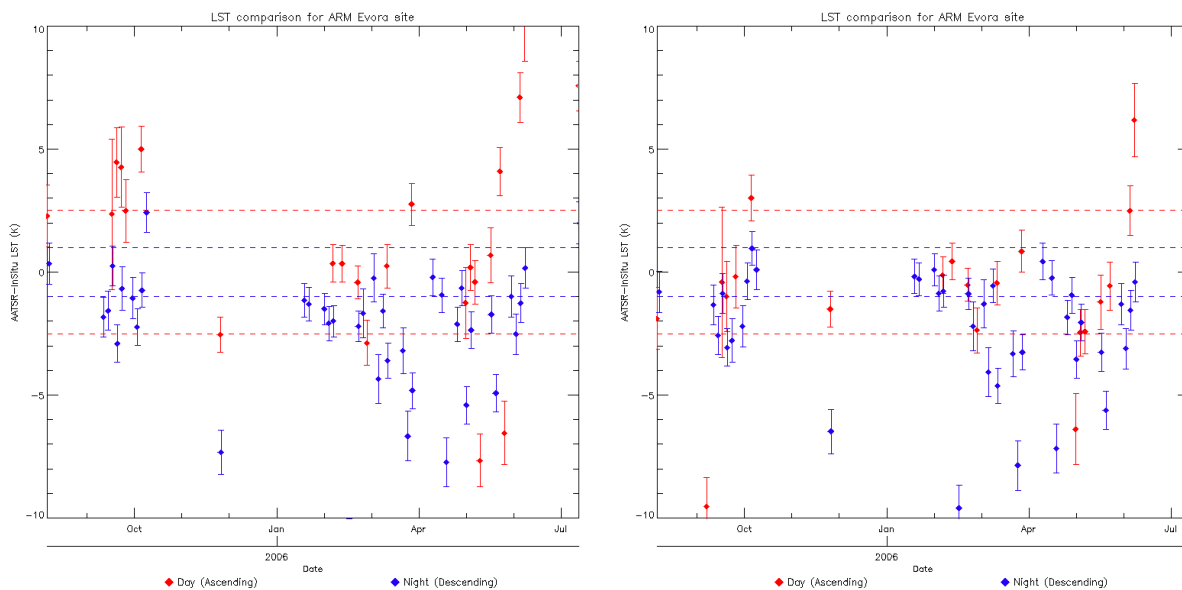


Figure 4.6: Comparison between AATSR operational LST (left) and updated LST (right) with respect to *in situ* LST data over the Evora field site from August 2005 to July 2006. The dashed lines show the target accuracy of the AATSR LST product during the day (red) and night (blue). The error bars represent the estimated errors on the point *in situ* LST observations.

4.3.3. Gobebeb, Namibia

As with Evora, the AATSR retrieved LST shows good agreement with the *in situ* LST at Gobebeb for both AATSR LST products. For uLST minus *in situ* LST both daytime (1.86 K) and night-time (0.96 K) median absolute deviations are within their corresponding target accuracies – an improvement on oLST. In addition, the large negative night-time bias for oLST minus *in situ* LST has switched to a smaller positive 0.78 K bias. However, the existing positive daytime bias of 1.99 K for oLST minus *in situ* LST has increased to 3.78 K with uLST. It seems likely that the daytime coefficient for ALB2-20, which is a global optimum, may not be optimum for this site. Further investigation is warranted here and will be included in the accompanying report to deliverable 5.2 of the current contract.

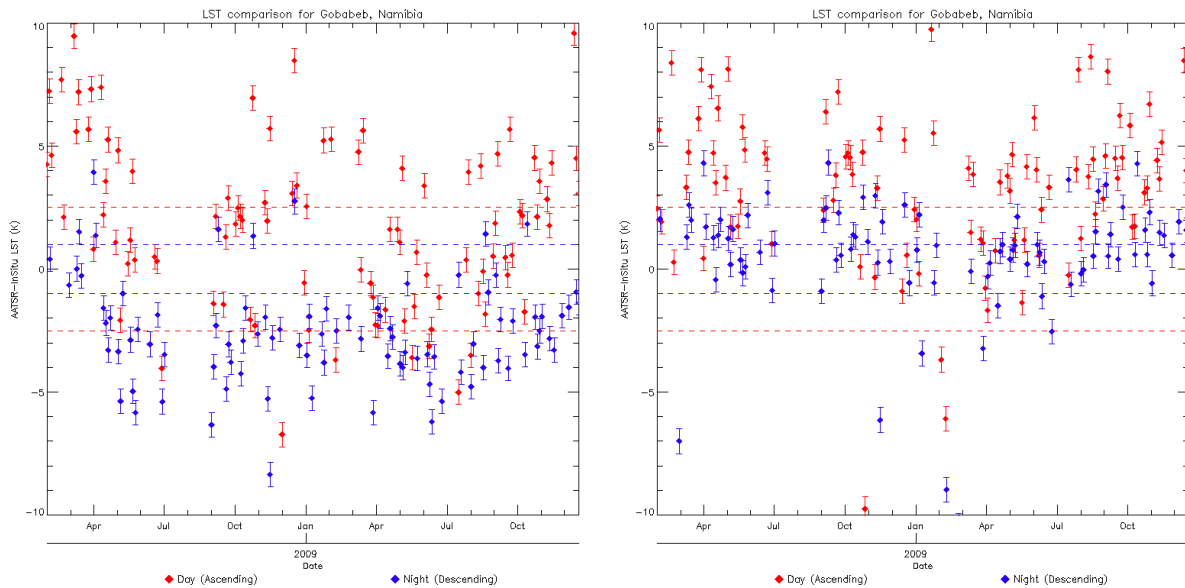


Figure 4.7: Comparison between AATSR operational LST (left) and updated LST (right) with respect to *in situ* LST data over the Gobebeeb field site from March 2008 to December 2009 inclusive. The dashed lines show the target accuracy of the AATSR LST product during the day (red) and night (blue). The error bars represent the estimated errors on the point *in situ* LST observations.

4.4. Summary

In this section, we have reported on the results of comparisons between AATSR and *in situ* LST data both for the operational product and the updated product over eighteen sites. Numerous sites have been operating on a continuous basis for several years enabling an excellent opportunity to perform long-term validation of AATSR LST data. For the uLST scenario the median absolute deviations are within 2.5 K over fifteen sites; this suggests that the updated AATSR LST algorithm is approaching consistency within the target accuracy during the day. During the night overall median bias and median absolute deviations are lower than for the day, with uLST being an improvement on oLST. However, several median biases are still high and for only two sites is the 1 K target accuracy met. Indeed, in most cases a cold bias exists and needs addressing; the suspicion being that failures in the cloud screening are primarily responsible. Furthermore, it should be noted that for several sites the quantity of matchups are relatively few, in some cases only a couple of matchups per month, and the results for these sites may be an artefact of the small sampling size.

A key result from this work is confirmation of the seasonal bias in the AATSR LST product over the ARM-Oklahoma field site that was reported in the reports for both the original contract and contract extension. In fact a similar seasonal bias, whereby AATSR LST is higher than *in situ* during the summer months and lower during the winter months, is also evident at other Northern Hemisphere sites – most notable ARM-Atqasuk and ARM-Barrow. While apparent in both daytime and night-time comparisons, it is during the day when the amplitude of the seasonal difference with respect to *in situ* is greatest.

While providing useful indications of the performance of LST retrievals from satellite-borne instruments comparisons between ground and satellite data must be viewed with several cautions. First, such comparisons will inevitably contain outliers and conclusions drawn from snapshot assessments may be biased by such outliers, even when the use of robust statistics is applied; this can be most acute when the sampling size is small, such as for dedicated short term field campaigns where only a few matchups are recorded. Second, comparisons over heterogeneous sites are extremely difficult to interpret due to the uncertainty associated with any methodology for upscaling from a 'point' source to that of a satellite pixel owing to the various assumptions that are necessarily made. A first assumption is that the precise geolocation and surface area of a satellite pixel can be guaranteed; a second, is that for each pixel validated the same generic land cover classes can be reliably classified; and a third, is that within and between each pixel the thermal behaviour of each land cover class remains invariant - in reality this is not the case. Finally, the ± 90 minute tolerance window adhered to here, represents a large time frame for LST variability; even though the majority of matchups were within ± 5 minutes this still represents adequate opportunity for differences to develop between the LST measured by the *in situ* radiometers and that viewed by the satellite instrument. A further point to consider here is that any temporal difference in a matchup presents an opportunity for a cloud contaminated measurement to be compared against a clear-sky measurement.

Additional further detailed analysis of these data is required to fully understand the biases which remain, including an improved categorisation of any cloud contamination and the assessment of matchups for a variety of zenith viewing angles. Although this is beyond the scope of this current study, it is required to fully understand the results. Overall, this experiment provides valuable information on the performance of the AATSR LST algorithm and a quantification of the improvements made as a result of the incorporation of the high resolution auxiliary datasets. In addition, it highlights the benefit of the creation of the matchup database for storing extensive, long term records of well characterised *in situ* LST data.

5. Sensitivity study

In Section 4, we presented the results of comparisons between AATSR and collocated *in situ* LST data over eighteen field sites. Whilst a good proportion of the median absolute deviations are within the aforementioned target accuracies, particularly for daytime, the results have highlighted a number of anomalies that necessitate further investigation. For example, the apparent seasonal bias in the AATSR operational LST at the ARM-Oklahoma and ARM-Atqasuk field sites, as identified in the previous contract, remains in the AATSR updated LST, suggesting that the LST retrieval algorithm is subject to seasonal bias.

In this section, we describe the research into sources of bias in the AATSR LST product that has been carried out within the framework of this study. Such biases may result not only from cloud contamination or instrument -related problems, but also from the LST retrieval coefficients and the tuning parameters utilised in the LST retrieval process, such as fractional vegetation, biome classification and precipitable water. Here we report on a sensitivity analysis of key parameters in the retrieval: 1) emissivity, both explicit and in terms of fractional vegetation cover; 2) atmospheric water vapour; 3) atmospheric temperature; and 4) surface temperature. This work is an extension of the work reported in the final reports for both the original contract and contract extension.

5.1. Methodology

In this study we repeat the methodology based Noyes *et al.* (2006), which was employed in the original contract and contract extension. Here we briefly summarise the process. AATSR top-of-atmosphere (TOA) BTs are simulated for the 11 and 12 μ m channels using the fast radiative transfer model RTTOV-10 for a given set of reference atmospheric and surface conditions and for a 0 $^\circ$ zenith viewing angle. In this study, we have utilised the reference atmospheric profiles of Remedios (1999) for tropical, mid-latitude, polar-winter and polar-summer climatologies. Figure 5.1 shows the water vapour and temperature profiles for these reference atmospheres.

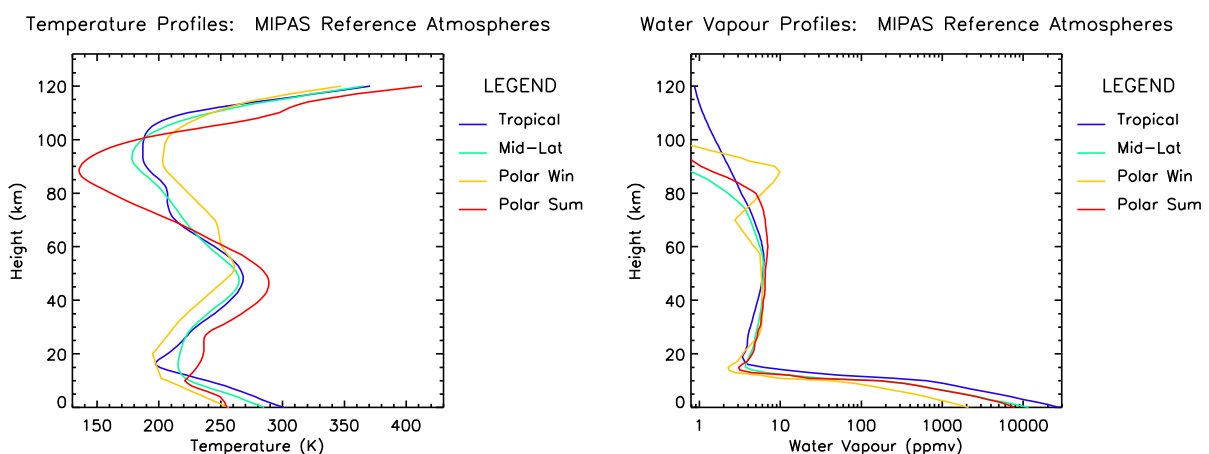


Figure 5.1: Temperature and water vapour profiles for the atmospheres used in the sensitivity study. These data are from Remedios (1999).

The operational AATSR LST algorithm is applied to these BTs to provide a simulated LST retrieval for each set of conditions; this is then compared to the skin temperature input into the RTTOV-10 model. Theoretically under these test conditions a perfectly modelled algorithm should retrieve LST

equal to the skin temperatures input into the radiative transfer model. Differences between these estimates provide an indication of bias in the algorithm that would occur under these conditions. The principal assumptions in this method are that we have an accurate radiative transfer model, and that the model parameters are realistic for the individual biomes within the latitudinal bands.

This methodology is applied to every ALB2 class for each of the four reference atmospheres (where no combination of biome class – latitudinal band exists the results are not included in the analysis). Surface emissivities derived for each AATSR thermal channel from the ASTER spectral library and the AATSR 11 and 12 μ m spectral response functions corresponding to a fractional vegetation of 0.5 (50% bare soil, 50% green vegetation) have been used for each simulation. That is, emissivities for each channel for green vegetation (an average of the channel emissivities for each green vegetation type) and bare soil have been averaged. The green vegetation and bare soil emissivities are shown in Table 5.1.

Table 5.1: AATSR 11 and 12 μ m channel emissivities derived from data provided by the Aster Spectral Library (1999) for green grass, and bare soil. Column ‘N’ denotes the number of samples used in the mean and standard deviation (Std. Dev).

Surface	N	11 μ m Channel		12 μ m Channel	
		Mean	Std. Dev.	Mean	Std. Dev.
Green vegetation	3	0.982	0.008	0.984	0.010
Soil	58	0.967	0.013	0.975	0.007

The reference surface temperatures used in the simulations have been selected to be very close to the temperature at 0 km height given in the reference atmosphere profiles, such that the surface-near-surface air temperature difference is approximately zero. Table 5.2 shows these for each of the four latitudinal bands.

Table 5.2: Near-surface (2m) air temperatures and skin temperatures corresponding to each reference atmosphere as quoted in Noyes (2006b).

Atmosphere	2m air temperature	T _{skin}
Tropical	300.93	301.00
Mid-latitude	285.15	285.00
Polar Summer	254.90	255.00
Polar Winter	256.70	257.00

To test the sensitivity of the LST retrieval to each of the model input parameters perturbations from the reference values are made to each of the parameters in turn. As an example, take the sensitivity to changing skin temperature. In this case RTTOV-10 is run over a range of different skin temperatures whereby constant atmospheric profiles and surface emissivities are maintained. The bias in the LST retrieval can then be quantified as a function of skin temperature variation. Perturbation steps and limits were selected as follows:

1. For emissivity each channel emissivity was perturbed in steps of 0.005 between ± 0.01 .
2. For water vapour the entire profile was perturbed in 10% increments over $\pm 50\%$. That is the value at each height level given in the reference atmosphere is reduced or increased in increments of 10% of the value at that height level.

3. For water vapour the entire profile was perturbed in 1% increments over $\pm 3\%$. As with the water vapour profiles, the value at each height level given in the reference atmosphere is reduced or increased by the fixed percentage of the value at that height level.
4. Skin temperature was perturbed in increments of 1K between $\pm 10\text{K}$.
5. Fractional vegetation was perturbed in increments of 0.1 between ± 0.5 , which since the reference fractional vegetation was set at 0.5 effectively means the whole range of fractional vegetation cover between 0 and 1.0 was sampled.

The limits of the atmospheric perturbations have been assigned using the companion minimum and maximum atmospheric profiles of Remedios (1999) to ensure physically realistic, but also extreme, ranges of Earth conditions.

5.2. Results

In Figures 5.2, 5.3 and 5.4 we show the results of the sensitivity studies for ALB2 biomes 2, 18 and 20. For each figure the difference between the simulated LST and the reference input skin temperature (y-axis) is plotted against the parameter perturbation (x-axis). These selected biomes correspond with the *in situ* sites analysed in detail above: biome 2 (ARM-Oklahoma and Evora); biome 18 (ARM-Atqasuk); and biome 20 (Gobebeb). The overall nature of these results is typical of those for the other 24 biomes for which the results are presented in Appendix B. The calculated response parameters for each test covering each biome are presented in Tables 5.3 to 5.6. In each case, we consider the retrieved LST deviation to be the simulated retrieved LST minus the skin temperature input into the simulation. Overall the sensitivity of the uLST retrieval to changes in key parameters is less than that of the oLST retrieval reported in Noyes (2006a) and Noyes (2007). It should be noted that in the majority of test cases where the sensitivity is very large this is a result of an inappropriate combination of biome and reference atmosphere.

5.2.1. Response to emissivity

Given a constant skin temperature we expect some deviation in the response of the BTs simulated by the radiative transfer model to variations in surface emissivity. For each biome, we perturbed the emissivity separately for each of the split-window channels in increments of 0.005. The overall outcome here is that an increase in the $11\mu\text{m}$ emissivity (ϵ_{11}) with respect to the reference value leads to an increase in LST bias in a positive direction, with a decrease in ϵ_{11} leading to an increase in LST bias in a negative direction. The upshot being that a change in ϵ_{11} of 0.01 can for some biomes result in a change in LST bias of greater than 3 K. The situation is reversed in the ϵ_{12} case, whereby a positive change in emissivity leads to an increasing negative LST bias. If we consider each reference atmosphere test case separately the tropical atmosphere elicits the smallest change in LST bias with respect to the change in either ϵ_{11} or ϵ_{12} . A further feature is that the bare soil biomes (20 to 25) display - for the most part - the largest sensitivity to emissivity change in the tropic and mid-latitude scenarios (Tables 5.3 and 5.4); only examples of biome 25 can be found in the polar latitudes.

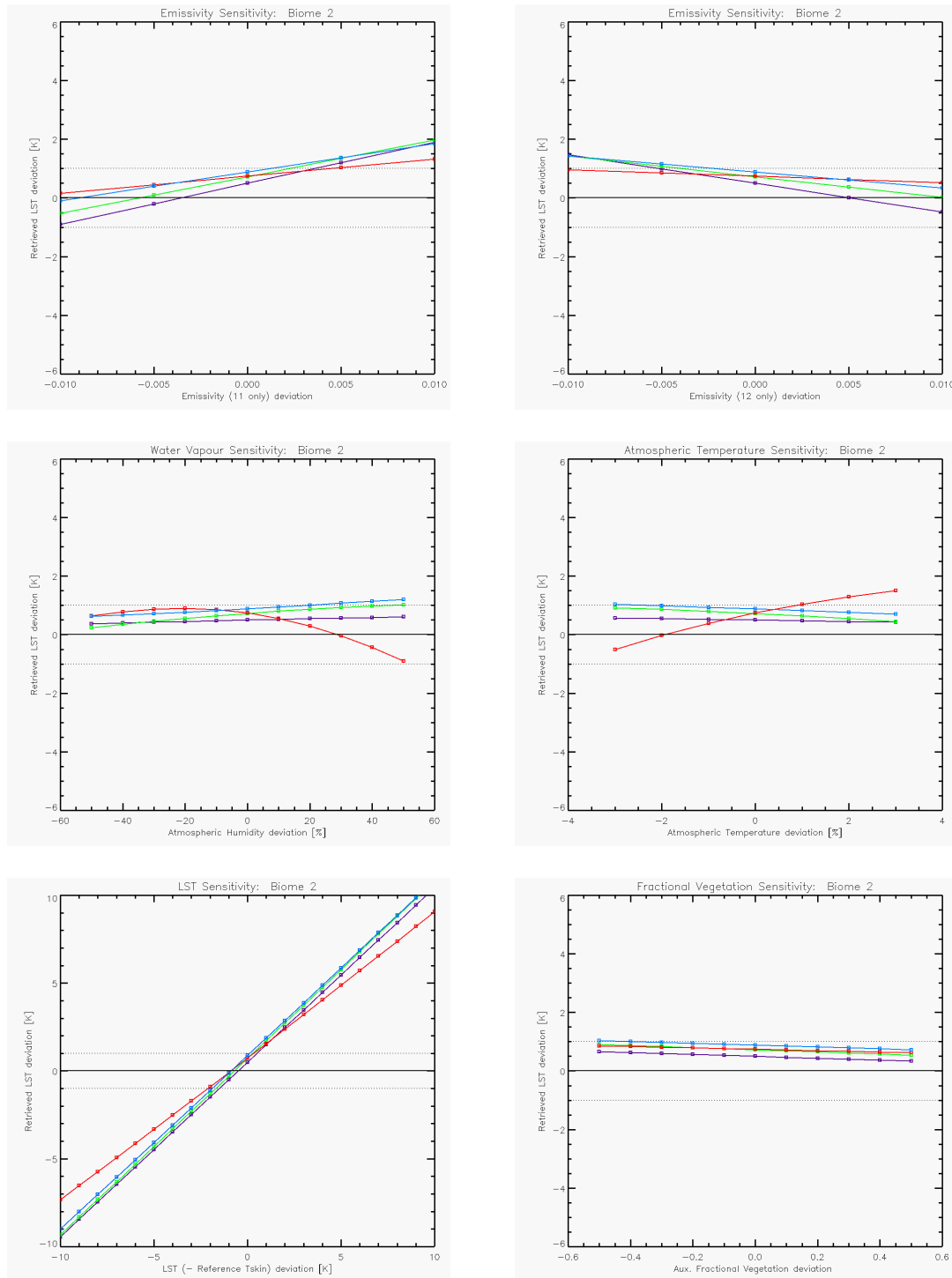


Figure 5.2: Sensitivity results for the AATSR updated LST algorithm (nadir view geometry) for ALB2 biome 2 (Evora and Oklahoma) for varying surface 11 and 12 μ m emissivities, atmospheric water vapour and temperature, skin temperature and the auxiliary fractional vegetation data utilised by the LST algorithm. ‘Tropical’ (red), ‘Mid-latitude’ (green), ‘Polar-Winter’ (light blue) and ‘Polar-Summer’ (purple) refer to the reference atmosphere used in each case.

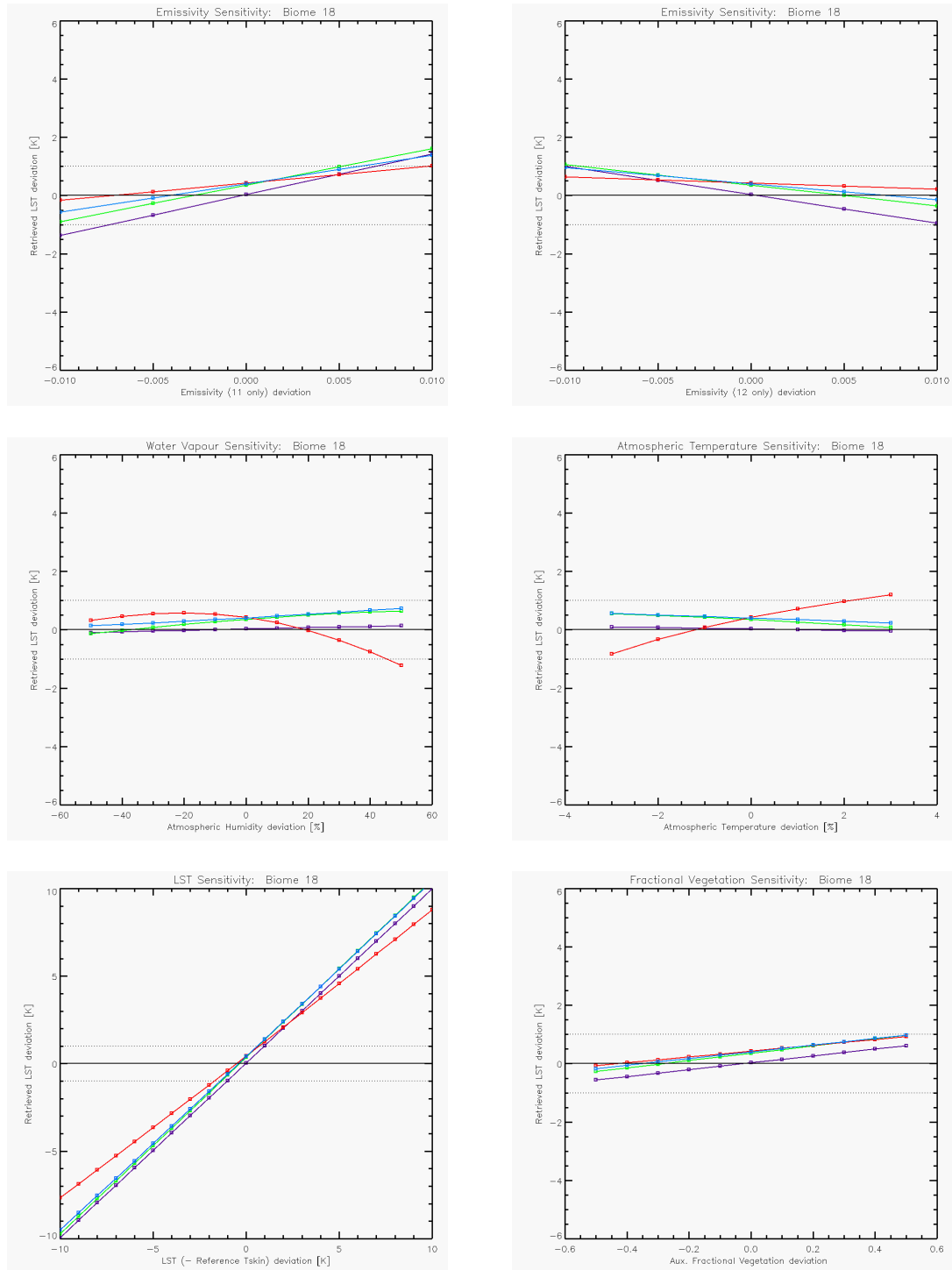


Figure 5.3: Sensitivity results for the AATSR updated LST algorithm (nadir view geometry) for ALB2 biome 18 (ARM - Atqusak) for varying surface 11 and 12 μ m emissivities, atmospheric water vapour and temperature, skin temperature and the auxiliary fractional vegetation data utilised by the LST algorithm. ‘Tropical’ (red), ‘Mid-latitude’ (green), ‘Polar-Winter’ (light blue) and ‘Polar-Summer’ (purple) refer to the reference atmosphere used in each case.

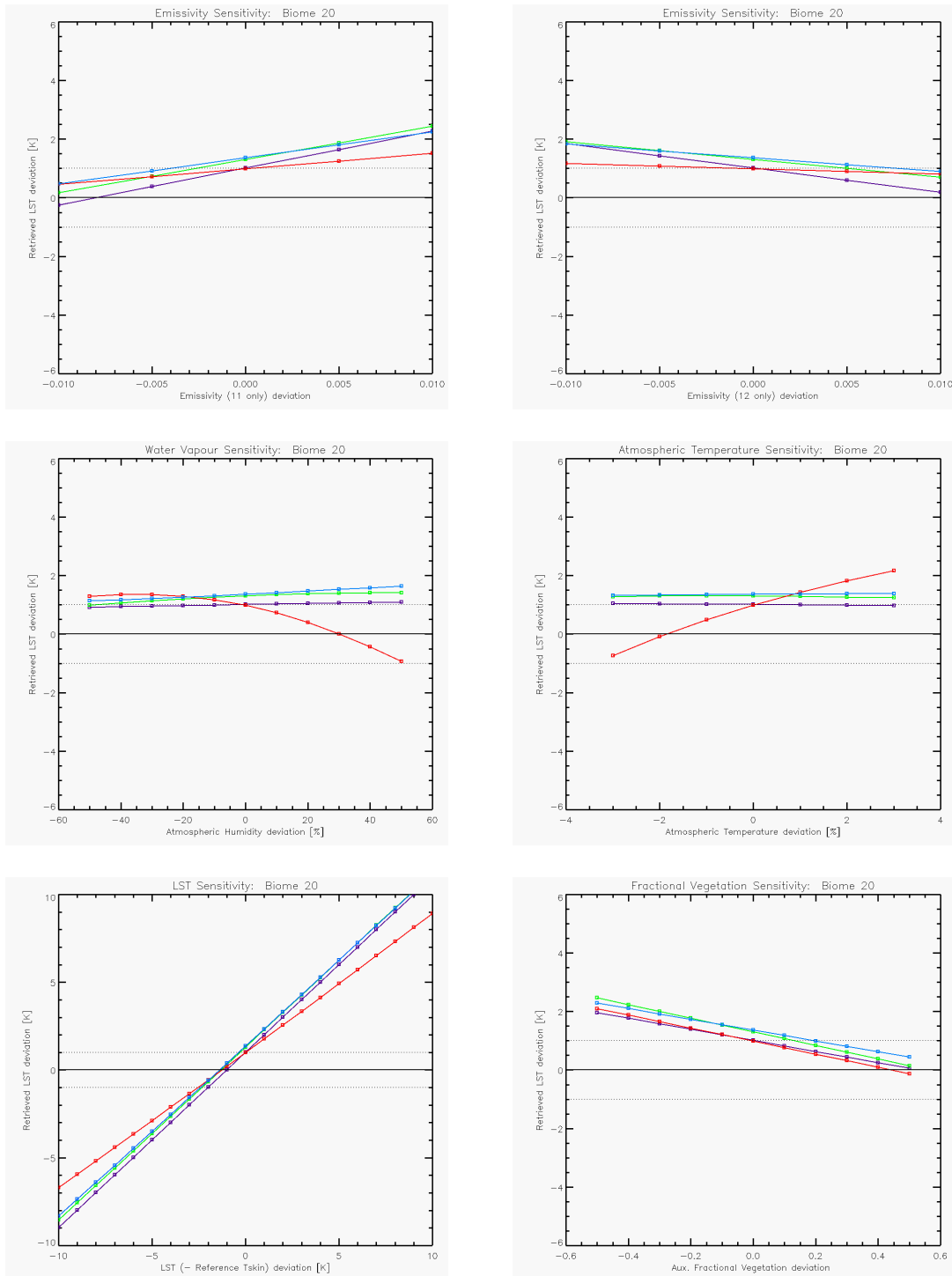


Figure 5.4: Sensitivity results for the AATSR updated LST algorithm (nadir view geometry) for ALB2 biome 20 (Gobebeb) for varying surface 11 and 12 μ m emissivities, atmospheric water vapour and temperature, skin temperature and the auxiliary fractional vegetation data utilised by the LST algorithm. ‘Tropical’ (red), ‘Mid-latitude’ (green), ‘Polar-Winter’ (light blue) and ‘Polar-Summer’ (purple) refer to the reference atmosphere used in each case.

5.2.2. Response to water vapour

For the mid-latitude and polar atmosphere scenarios, the results indicate that the bias in the LST algorithm will increase with increasing water vapour. For the mid-latitude and polar-summer scenarios the response is approximately 0.1 K per 10% change in total column water vapour; the response for polar-winter is less than half of this. For every applicable biome the tropical atmosphere scenario displays a highly non-linear response – for drier tropical atmospheres an increase in water vapour results in an increase in LST bias of the same magnitude to the mid-latitude atmosphere, whereas for more humid tropical atmospheres an increase in water vapour has the opposite effect, decreasing the LST bias in the retrieval. These findings for the uLST retrieval are consistent with those of Noyes (2006a) and Noyes (2007) for the oLST retrieval.

Overall, our findings suggest that changes in atmospheric water vapour could significantly impact on the LST retrieval accuracy. Indeed, the response of the algorithm to changing atmospheric water vapour does not conform to the ideal situation of a zero gradient, which is a typical response for split window algorithms. The general case for all biomes is an increase in water vapour resulting in an increase in LST bias, with the exception of very wet atmospheres in which the LST bias begins to decrease. In such extreme cases the negative LST bias may be greater than 2 K. Furthermore, since atmospheric water vapour is a parameter exhibiting strong seasonal variation, this implies that seasonally dependent coefficients may be required to rectify seasonal variations in LST bias in the AATSR algorithm. As with the analysis of Noyes (2006a) and Noyes (2007) direct comparisons between the absolute results for different atmospheres are difficult to assess since the profiles have been perturbed by a percentage at each height level rather than by absolute amounts.

5.2.3. Response to atmospheric temperature

For the mid-latitude and polar atmosphere scenarios, the results indicate that for most biomes the bias in the LST algorithm will decrease with increasing atmospheric temperature. For the mid-latitude and polar-summer scenarios the response is approximately 0.1 K per 1% change in atmospheric temperature; the response for polar-winter is less than half of this. For some biomes though the reverse situation applies; for example the aridisols-calcids biome (ALB2-23) and permanent ice biome (ALB2-27) both respond with an increase in LST bias to increases in atmospheric temperature. These responses are near-linear, whereas for tropical atmospheres the response is more non-linear; however, the response is similar here for all biomes being up to 0.5 K per 1% change. For the most part these findings for the uLST retrieval are consistent with those of Noyes (2006a) and Noyes (2007) for the oLST retrieval, the exception being the few exceptional cases of increasing LST bias to increasing atmospheric temperature for mid-latitude and polar-summer atmospheres encountered in this study.

As for water vapour the response of the LST algorithm does not conform to the optimum response of zero. Overall, our results indicate that the uLST retrieval is sensitive to changes in atmospheric temperature, particularly in tropical latitudes. This provides evidence for the derivation of latitudinal dependent coefficients to mitigate the occurrence of LST biases due to atmospheric temperature variation. Also since atmospheric temperature may exhibit seasonal variation this could result seasonally dependent biases. Again as with the water vapour analysis direct comparisons between the absolute results for different atmospheres are difficult to assess since the profiles have been perturbed by a percentage at each height level rather than by absolute amounts.



5.2.4. Response to skin temperature

For the mid-latitude and polar reference atmosphere scenarios the response to variation in skin temperature for all biomes, with the exception of inland water (ALB2-26) and permanent ice (ALB2-27), where cases of the respective biome falls within the respective latitudinal band is near unity. For inland water and permanent ice although larger the variation in LST bias is still within 2 K. The tropical scenario is rather different, whereby variation in LST bias is up to and above 4 K across the ± 10 K range from the corresponding perturbed skin temperature. In other words, an increase in skin temperature results in a decrease in LST bias in the algorithm, probably the result of non-linear response in the retrieval for tropical atmospheres.

An optimised retrieval algorithm would have a gradient of unity with respect to the true surface temperature; in other words, for every 1 K change in actual surface temperature the LST retrieved by the algorithm would also change by 1 K. For most biomes and for mid-latitude and polar latitude atmospheres scenarios this is primarily the case. For this parameter, the ideal algorithm would incorporate a latitudinal dependency, whereby for tropical latitudes additional functionality in the algorithm would offset the average -0.2 K deviation to the 1 K change in LST for every 1 K increase in actual surface temperature. In these tropical latitudes where the variation in surface temperature is seasonal, this could result in an algorithm bias that is also seasonal; this though requires further investigation.

5.2.5. Response to auxiliary fractional vegetation data

In the LST algorithm variation in surface emissivity is expressed as a fraction of vegetation cover. Here we have explicitly varied the auxiliary fractional vegetation in the retrieval algorithm and investigated the effect on the LST bias. Starting with an initial state of 0.5 we varied this in increments of 0.1 between 0 and 1.0, thereby covering the entire possible range of fractional vegetation cover. The magnitude of the response is biome specific, as is the direction of the response. For the bare soil biomes (ALB2 biomes 20 to 25), and other biomes where bare soil constitutes a considerable fraction of the land surface, an increase in fractional vegetation cover leads to an decrease in the LST bias; with the response being greatest for the Entisols-Orthents biome (ALB2-21) – a 3 K difference between the LST bias for a bare soil state compared with a fully vegetated state. Despite this sensitivity for the bare soil biomes the fact remains that these biomes tend to experience very low intra- and interannual changes in fractional vegetation.

Table 5.3: Response parameters for the tropical atmosphere, where the equation $y=A+Bx$ has been fitted to the results for changing skin temperature, mean surface emissivity for 11 and 12 μm , and the auxiliary fractional vegetation data utilised by the AATSR LST algorithm. The equation $y=A+Bx+Cx^2$ has been fitted for water vapour and atmospheric temperature. In each case, the parameter A is the bias in the algorithm for zero deviation in the test parameter. Skin temperature response is per 1 K change; emissivity response is per 0.005 change; water vapour response is per 10% change at each height level; atmospheric temperature response is per 1% change at each height level.

Biome	Skin Temperature		Emissivity		Water Vapour			Atmospheric Temperature			Fractional vegetation	
	A (K)	B (K)	A (K)	B (K/0.005)	A (K)	B (K/10%)	C (K/10%) ²	A (K)	B (K/1%)	C (K/1%) ²	A (K)	B (K/0.1)
1	1.51	-0.16	1.46	38.60	1.29	-0.01	0.00	1.38	0.24	0.00	1.46	0.00
2	0.79	-0.18	0.74	37.30	1.00	0.01	0.00	1.00	0.01	0.00	0.74	-0.24
3	0.95	-0.18	0.90	37.20	1.00	0.01	0.00	1.00	0.01	0.00	0.90	0.77
4	0.94	-0.18	0.89	37.16	1.00	0.01	0.00	1.00	0.01	0.00	0.89	0.68
5	0.75	-0.17	0.70	37.60	1.00	0.01	0.00	1.00	0.01	0.00	0.70	0.58
6	0.16	-0.19	0.11	36.66	1.00	0.01	0.00	1.00	0.01	0.00	0.11	0.12
7	1.00	-0.18	0.94	36.90	1.00	0.01	0.00	1.00	0.01	0.00	0.94	0.58
8	0.11	-0.19	0.06	36.80	1.00	0.01	0.00	1.00	0.01	0.00	0.06	0.55
9	-0.71	-0.27	-0.76	32.06	1.00	0.01	0.00	1.00	0.01	0.00	-0.76	0.27
10	-0.42	-0.23	-0.47	34.16	1.00	0.01	0.00	1.00	0.01	0.00	-0.47	0.15
11	0.54	-0.17	0.49	37.70	1.00	0.01	0.00	1.00	0.01	0.00	0.49	0.10
12	0.76	-0.18	0.71	36.90	1.00	0.01	0.00	1.00	0.01	0.00	0.71	0.59
13	1.20	-0.18	1.15	36.98	1.00	0.01	0.00	1.10	0.36	0.00	1.15	0.13
14	0.81	-0.19	0.76	36.76	1.00	0.01	0.00	1.00	0.01	0.00	0.76	-0.86
15	-0.07	-0.21	-0.12	35.68	1.00	0.01	0.00	1.00	0.01	0.00	-0.12	-0.09
16	1.21	-0.07	1.15	42.38	1.00	0.01	0.00	1.10	0.28	0.00	1.15	-0.01
17	1.08	-0.14	1.03	39.56	1.00	0.01	0.00	1.00	0.01	0.00	1.03	0.45
18	0.48	-0.18	0.43	37.40	1.00	0.01	0.00	1.00	0.01	0.00	0.43	0.99
19	0.75	-0.18	0.70	37.10	1.00	0.01	0.00	1.00	0.01	0.00	0.70	-0.84
20	1.04	-0.22	0.99	34.96	1.00	0.01	0.00	1.00	0.01	-0.01	0.99	-2.23
21	1.51	-0.22	1.46	34.96	1.18	-0.02	0.00	1.38	0.47	0.00	1.46	-2.78
22	1.91	-0.2	1.86	35.96	1.49	-0.02	0.00	1.84	0.42	0.00	1.86	-2.25
23	2.27	-0.25	2.23	32.78	2.02	-0.03	0.00	2.20	0.66	0.00	2.23	0.00
24	1.67	-0.23	1.62	34.56	1.43	-0.02	0.00	1.52	0.51	0.00	1.62	-1.03
25	-0.69	-0.28	-0.73	31.60	1.00	0.01	0.00	1.00	0.01	0.00	-0.73	-0.12
26	-0.26	-0.11	-0.31	41.24	1.00	0.01	0.00	1.00	0.01	0.00	-0.31	-0.24
27	-2.58	-0.31	-2.63	30.06	1.00	0.01	0.00	1.00	0.01	0.00	-2.62	0.00

Table 5.4: Response parameters for the mid-latitude atmosphere, where the equation $y=A+Bx$ has been fitted to the results for changing skin temperature, mean surface emissivity for 11 and 12 μm , and the auxiliary fractional vegetation data utilised by the AATSR LST algorithm. The equation $y=A+Bx+Cx^2$ has been fitted for water vapour and atmospheric temperature. In each case, the parameter A is the bias in the algorithm for zero deviation in the test parameter. Skin temperature response is per 1 K change; emissivity response is per 0.005 change; water vapour response is per 10% change at each height level; atmospheric temperature response is per 1% change at each height level.

Biome	Skin Temperature		Emissivity		Water Vapour			Atmospheric Temperature			Fractional vegetation	
	A (K)	B (K)	A (K)	B (K/0.005)	A (K)	B (K/10%)	C (K/10%) ²	A (K)	B (K/1%)	C (K/1%) ²	A (K)	B (K/0.1)
1	1.27	0.02	1.26	55.60	1.22	0.01	0.00	1.25	-0.12	0.00	1.26	0.00
2	0.74	0.01	0.73	54.90	1.00	0.01	0.00	1.00	0.01	0.00	0.73	-0.36
3	0.92	0.01	0.90	54.84	1.00	0.01	0.00	1.00	0.01	0.00	0.90	1.11
4	0.89	0.01	0.87	54.88	1.00	0.01	0.00	1.00	0.01	0.00	0.87	1.03
5	0.32	0.03	0.31	56.08	1.00	0.01	0.00	1.00	0.01	0.00	0.31	0.92
6	0.16	0.01	0.14	54.66	1.00	0.01	0.00	1.00	0.01	0.00	0.14	0.21
7	0.85	0.01	0.83	55.14	1.00	0.01	0.00	1.00	0.01	0.00	0.83	0.69
8	0.13	0.00	0.11	54.64	1.00	0.01	0.00	1.00	0.01	0.00	0.11	0.69
9	0.05	-0.04	0.03	51.74	1.00	0.01	0.00	1.00	0.01	0.00	0.03	0.34
10	0.02	-0.02	0.01	52.98	1.00	0.01	0.00	1.00	0.01	0.00	0.01	0.29
11	0.37	0.01	0.36	55.30	1.00	0.01	0.00	1.00	0.01	0.00	0.36	0.22
12	0.68	0.01	0.66	54.94	1.00	0.01	0.00	1.00	0.01	0.00	0.67	0.74
13	1.13	0.01	1.12	54.90	1.09	0.01	0.00	1.10	-0.06	0.00	1.12	0.32
14	0.81	0.01	0.80	54.64	1.00	0.01	0.00	1.00	0.01	0.00	0.80	-0.90
15	0.10	0.00	0.08	54.06	1.00	0.01	0.00	1.00	0.01	0.00	0.08	-0.02
16	-0.69	0.12	-0.71	61.24	1.00	0.01	0.00	1.00	0.01	0.00	-0.70	-0.02
17	0.49	0.04	0.48	56.84	1.00	0.01	0.00	1.00	0.01	0.00	0.48	0.59
18	0.37	0.01	0.36	55.10	1.00	0.01	0.00	1.00	0.01	0.00	0.36	1.25
19	0.71	0.01	0.69	54.80	1.00	0.01	0.00	1.00	0.01	0.00	0.69	-1.06
20	1.32	-0.01	1.31	53.56	1.27	0.00	0.00	1.30	-0.01	0.00	1.31	-2.32
21	1.79	-0.01	1.77	53.60	1.76	0.00	0.00	1.77	-0.01	0.00	1.77	-2.74
22	2.05	0.00	2.03	54.14	2.01	0.01	0.00	2.02	-0.04	0.00	2.03	-2.37
23	2.74	-0.02	2.72	52.74	2.70	0.00	0.00	2.72	0.08	0.00	2.72	0.00
24	1.98	-0.01	1.96	53.40	1.95	0.00	0.00	1.95	0.01	0.00	1.96	-1.18
25	0.17	-0.04	0.15	51.40	1.00	0.01	0.00	1.00	0.01	0.00	0.15	-0.11
26	-1.07	0.05	-1.08	57.70	1.00	0.01	0.00	1.00	0.01	0.00	-1.08	-0.50
27	-1.38	-0.07	-1.40	50.16	1.00	0.01	0.00	1.00	0.01	0.00	-1.40	0.00

Table 5.5: Response parameters for the polar-summer atmosphere, where the equation $y=A+Bx$ has been fitted to the results for changing skin temperature, mean surface emissivity for 11 and 12 μ m, and the auxiliary fractional vegetation data utilised by the AATSR LST algorithm. The equation $y=A+Bx+Cx^2$ has been fitted for water vapour and atmospheric temperature. In each case, the parameter A is the bias in the algorithm for zero deviation in the test parameter. Skin temperature response is per 1 K change; emissivity response is per 0.005 change; water vapour response is per 10% change at each height level; atmospheric temperature response is per 1% change at each height level.

Biome	Skin Temperature		Emissivity		Water Vapour			Atmospheric Temperature			Fractional vegetation	
	A (K)	B (K)	A (K)	B (K/0.005)	A (K)	B (K/10%)	C (K/10%) ²	A (K)	B (K/1%)	C (K/1%) ²	A (K)	B (K/0.1)
1	1.51	0.00	1.49	43.48	1.49	0.01	0.00	1.49	-0.09	0.00	1.49	0.00
2	0.91	-0.01	0.88	42.90	0.88	0.01	0.00	1.00	0.01	0.00	0.88	-0.32
3	1.09	-0.01	1.07	42.86	1.07	0.01	0.00	1.07	-0.05	0.00	1.07	1.00
4	0.99	-0.01	0.96	42.86	0.96	0.01	0.00	1.00	0.01	0.00	0.96	0.82
5	-0.46	0.02	-0.48	43.80	-0.48	0.01	0.00	1.00	0.01	0.00	-0.48	0.60
6	0.17	-0.01	0.15	42.70	0.15	0.01	0.00	1.00	0.01	0.00	0.15	0.23
7	0.56	0.00	0.53	43.08	0.53	0.01	0.00	1.00	0.01	0.00	0.53	-0.28
8	0.28	-0.01	0.26	42.68	0.26	0.01	0.00	1.00	0.01	0.00	0.26	0.55
9	0.13	-0.05	0.11	40.40	0.11	0.00	0.00	1.00	0.01	0.00	0.11	0.36
10	0.17	-0.03	0.14	41.40	0.14	0.00	0.00	1.00	0.01	0.00	0.14	0.34
11	0.39	0.00	0.37	43.20	0.37	0.01	0.00	1.00	0.01	0.00	0.37	0.25
12	0.60	0.00	0.58	42.90	1.00	0.01	0.00	1.00	0.01	0.00	0.58	0.68
13	1.12	-0.01	1.09	42.90	1.09	0.01	0.00	1.09	-0.04	0.00	1.09	0.16
14	0.86	-0.01	0.83	42.74	0.83	0.01	0.00	1.00	0.01	0.00	0.83	-0.66
15	0.14	-0.02	0.11	42.20	0.11	0.01	0.00	1.00	0.01	0.00	0.11	0.01
16	-3.57	0.11	-3.59	47.90	-3.59	0.01	0.00	1.00	0.01	0.00	-3.59	-0.15
17	0.16	0.03	0.14	44.44	0.14	0.01	0.00	1.00	0.01	0.00	0.14	0.22
18	0.43	0.00	0.41	43.06	0.41	0.01	0.00	1.00	0.01	0.00	0.41	1.15
19	0.79	-0.01	0.76	42.84	0.76	0.01	0.00	1.00	0.01	0.00	0.76	-0.92
20	1.39	-0.03	1.37	41.86	1.37	0.01	0.00	1.37	0.01	0.00	1.37	-1.85
21	1.82	-0.02	1.79	41.88	1.79	0.01	0.00	1.79	0.01	0.00	1.79	-1.39
22	2.14	-0.02	2.12	42.28	2.12	0.01	0.00	2.12	-0.02	0.00	2.12	-1.63
23	2.29	-0.03	2.26	41.20	2.26	0.00	0.00	2.26	0.09	0.00	2.26	0.00
24	1.92	-0.03	1.89	41.74	1.89	0.00	0.00	1.89	0.03	0.00	1.89	-0.90
25	0.30	-0.06	0.27	40.12	0.27	0.00	0.00	1.00	0.01	0.00	0.27	-0.08
26	-1.27	0.04	-1.29	45.12	-1.29	0.01	0.00	1.00	0.01	0.00	-1.29	-0.80
27	-0.99	-0.08	-1.02	39.16	-1.02	0.00	0.00	1.00	0.01	0.00	-1.02	0.00

Table 5.6: Response parameters for the polar-winter atmosphere, where the equation $y=A+Bx$ has been fitted to the results for changing skin temperature, mean surface emissivity for 11 and 12 μ m, and the auxiliary fractional vegetation data utilised by the AATSR LST algorithm. The equation $y=A+Bx+Cx^2$ has been fitted for water vapour and atmospheric temperature. In each case, the parameter A is the bias in the algorithm for zero deviation in the test parameter. Skin temperature response is per 1 K change; emissivity response is per 0.005 change; water vapour response is per 10% change at each height level; atmospheric temperature response is per 1% change at each height level.

Biome	Skin Temperature		Emissivity		Water Vapour			Atmospheric Temperature			Fractional vegetation	
	A (K)	B (K)	A (K)	B (K/0.005)	A (K)	B (K/10%)	C (K/10%) ²	A (K)	B (K/1%)	C (K/1%) ²	A (K)	B (K/0.1)
1	1.08	-0.01	1.08	41.54	1.08	0.00	0.00	1.08	-0.03	0.00	1.08	0.00
2	0.50	-0.01	0.50	42.34	0.50	0.00	0.00	1.00	0.01	0.00	0.50	-0.33
3	0.68	-0.01	0.68	42.40	0.68	0.00	0.00	1.00	0.01	0.00	0.68	1.03
4	0.58	0.00	0.58	42.54	0.58	0.00	0.00	1.00	0.01	0.00	0.58	0.86
5	-0.80	0.03	-0.80	44.06	-0.80	0.00	0.00	1.00	0.01	0.00	-0.8	0.65
6	-0.22	0.00	-0.22	42.96	-0.22	0.00	0.00	1.00	0.01	0.00	-0.22	0.24
7	0.18	0.01	0.18	43.40	0.18	0.00	0.00	1.00	0.01	0.00	0.19	-0.18
8	-0.12	-0.01	-0.12	42.56	-0.12	0.00	0.00	1.00	0.01	0.00	-0.12	0.57
9	-0.21	0.00	-0.21	45.00	-0.21	0.00	0.00	1.00	0.01	0.00	-0.21	0.36
10	-0.21	0.00	-0.21	43.86	-0.21	0.00	0.00	1.00	0.01	0.00	-0.21	0.34
11	-0.01	0.00	-0.01	42.46	-0.01	0.00	0.00	1.00	0.01	0.00	-0.01	0.26
12	0.21	0.00	0.21	43.00	0.21	0.00	0.00	1.00	0.01	0.00	0.21	0.70
13	0.72	0.00	0.72	42.86	0.72	0.00	0.00	1.00	0.01	0.00	0.72	0.19
14	0.46	0.00	0.46	42.86	0.46	0.00	0.00	1.00	0.01	0.00	0.47	-0.68
15	-0.24	0.00	-0.24	43.36	-0.24	0.00	0.00	1.00	0.01	0.00	-0.24	0.01
16	-3.83	0.09	-3.83	46.10	-3.83	0.00	0.00	1.00	0.01	0.00	-3.83	-0.14
17	-0.23	0.01	-0.23	42.30	-0.23	0.00	0.00	1.00	0.01	0.00	-0.23	0.26
18	0.03	0.00	0.03	42.50	0.03	0.00	0.00	1.00	0.01	0.00	0.03	1.18
19	0.39	0.00	0.39	42.60	0.39	0.00	0.00	1.00	0.01	0.00	0.39	-0.95
20	1.02	0.00	1.01	43.64	1.01	0.00	0.00	1.01	-0.01	0.00	1.02	-1.90
21	1.44	0.00	1.44	43.72	1.44	0.00	0.00	1.44	-0.01	0.00	1.44	-1.51
22	1.76	0.00	1.76	43.14	1.76	0.00	0.00	1.76	-0.02	0.00	1.76	-1.70
23	1.97	0.02	1.97	45.66	1.97	0.00	0.00	1.97	0.00	0.01	1.97	0.00
24	1.55	0.00	1.55	44.10	1.55	0.00	0.00	1.55	-0.01	0.00	1.55	-0.93
25	-0.05	0.00	-0.05	45.06	-0.05	0.00	0.00	-0.05	0.00	0.02	-0.05	-0.09
26	-1.69	0.00	-1.69	41.20	-1.69	0.00	0.00	1.00	0.01	0.00	-1.69	-0.79
27	-1.34	-0.01	-1.34	45.26	-1.34	0.00	0.00	1.00	0.01	0.00	-1.34	0.00

5.3. Summary

The purpose of these experiments has been to investigate the sensitivity of the LST bias to incremental changes in the state parameters. The change in bias in the uLST retrievals is a result of changes in water vapour, atmospheric temperature, emissivity and skin temperature. In most cases when considering the mid-latitude and polar scenarios much of the sensitivity in the LST retrieval results from variations in the surface emissivity (represented in the LST algorithm by fractional vegetation). If we take the mid-latitude scenario as an example, the following in general holds for most biomes:

- An increase in ϵ_{11} results in an increase in LST bias
- An increase in ϵ_{12} results in a decrease in LST bias
- An increase in water vapour results in an increase in LST bias
- An increase in atmospheric temperature results in a decrease in LST bias

The lower sensitivity to change in key parameters exhibited by the uLST retrieval is evidence that the updated coefficients have been derived from profiles which encompass a wider range of possible atmospheric and surface states. Even so our results support the conclusions of Noyes (2006a) and Noyes (2007) in which it was suggested that the retrieval scheme may benefit from the incorporation of some latitudinal dependency in the retrieval coefficients.

Another characteristic encountered in this study is that in many cases an underlying bias exists between the skin temperature input into the radiative transfer model and the simulated LST from the AATSR algorithm even when no perturbations are applied – these biases are presented in each of “A” columns in Tables 5.3 to 5.6. In extreme cases this bias can be greater than ± 2 K. Although errors in the radiative transfer model could be one source of the discrepancies, more likely it is that the reference states used in these experiments are not representative of the average biome conditions from which the retrieval coefficients were derived. However, these initial state biases are on average lower than those recorded in Noyes (2006a) and Noyes (2007) for the Dorman and Sellers biomes implying that the profiles employed to generate the uLST coefficients captured a greater range of the possible atmospheric and surface conditions indicative of each biome. The non-optimisation of the Dorman and Sellers coefficients is supported by the algorithm evaluation results of Noyes (2006a) and Noyes (2007).

A final point on this investigation is that all simulations were all carried out with a single set of reference atmospheres, rather than seasonally varying ones. Furthermore, only simulated zenith viewing angles of 0° were considered. Further investigation is required to see if similar conclusions can be drawn for the full range of AATSR nadir viewing angles, which range from 0 to approximately 22° .

6. Multi-sensor intercomparison

In the previous sections, we have used both *in situ* measurements and theoretical methods to investigate possible sources of bias in the AATSR LST algorithm. Here, we supplement this study by assessing the differences between satellite retrieved LST from multiple sensors, specifically AATSR, MODIS on board Terra, and SEVIRI. The MODIS instrument on board Aqua was not included here due to the substantial difference in local overpass time with respect to Envisat.

6.1. Instruments

The SEVIRI instrument is the main payload on board the Meteosat Second Generation (MSG) geostationary satellites, which fly at an altitude of approximately 36000km above the equator. An image is acquired every 15 minutes, with the pixel size a function of the viewing angle. For Europe, this equates to pixel sizes between 5km and 6km. LST retrieval is a more challenging undertaking than for the polar-orbiting satellites, particularly at higher latitudes, as a result of increased atmospheric attenuation due to higher viewing zenith angles. A generalised split-window algorithm is used to estimate LST as a linear function of TOA BTs for the 10.8 μ m and 12 μ m channels, in which surface emissivity depends on land cover classes and the fraction of vegetation cover (Peres and DaCamara 2005; Trigo *et al.*, 2008b). SEVIRI LST products are generated and disseminated by the Satellite Application Facility on Land Surface Analysis (LandSAF). They use cloud masking software developed by the Nowcasting and Very Short-Range Forecasting Satellite Application (<http://www.nwcsaf.org>) to identify clear sky pixels. Validation of LST retrievals indicates a bias free algorithm, with increasing random errors as a response to increasing viewing zenith angles (Trigo *et al.*, 2008a), in which the accuracy for most simulations between nadir and 50° viewing zenith angle can be potentially as low as 1.5K (Sobrino and Romaguera, 2004). The product user manual provides a comprehensive description of the LST retrieval algorithm, and can be accessed from the LandSAF web site (<http://landsaf.meteo.pt/>).

MODIS instruments are part of the payload of two sun-synchronous, near-polar orbiting satellites, Terra and Aqua. The large swath width of these instruments, 2330km, enables each satellite to provide a pair of observations globally every day. Terra retrievals were used and these correspond to approximately 10:30 local solar time in descending mode, and approximately 22:30 local solar time in ascending mode. Here only version-5 of the 1km swath LST product MOD11_L2 acquired from Terra was used, since meaningful intercomparison between Aqua retrievals and AATSR retrievals could not be achieved due to a mismatch in local overpass times. LST is estimated using the generalised split-window algorithm of Wan and Dozier (1996) as a linear function of TOA BTs for bands 31 (11 μ m) and 32 (12 μ m), in which surface emissivity is dependent on land cover class and a linear correction for the satellite viewing angle (Wan *et al.*, 2002). The cloud masking algorithm used in version-5 includes refinements to account for surface elevation in an attempt to minimise the significant cloud contamination symptomatic of earlier versions, resulting in a reported accuracy better than 1.0K (Wan, 2008). Full details of MODIS LST retrieval is provided in the user manual, which is available from <http://www.icesb.ucsb.edu/modis/LstUsrGuide/>.

6.2. Methodology

The intercomparison was carried out over southern Europe within the processed region of the SEVIRI instrument for 2006. Since precise temporal matchups between AATSR and MODIS are not common all comparisons were made with respect to SEVIRI as the reference point. For each intercomparison the following process was followed:

1. Prior to intercomparison all data was quality checked by removing pixels that did not meet the highest quality control.
2. Any pixels flagged as cloudy for any of the LST products were also discarded.
3. In order to compare data, spatial regridding onto a common $0.05^\circ \times 0.05^\circ$ grid was carried out. This was done by averaging all the pixels whereby the centre coordinates lay within each $0.05^\circ \times 0.05^\circ$ grid box.
4. For temporal matching, time interpolation was carried using up to six consecutive SEVIRI measurements (within ± 45 minutes of the respective AATSR or MODIS overpass time). For each of the AATSR LST products and for MODIS LST the value of the SEVIRI LST used in the matchup was interpolated to correspond to the overpass time of the respective polar orbiting satellite.
5. Average daytime and night-time products of LST differences were created for each month. The three products created were AATSR oLST vs. SEVIRI LST, AATSR uLST vs. SEVIRI LST, and Terra MODIS LST vs. SEVIRI LST.
6. The mean and standard deviation of each daytime and night-time intercomparison for each month for all cloud-free matchups were recorded. From these seasonal differences could be analysed.

6.3. Results

One of the most striking improvements the uLST retrieval has made on the oLST retrieval is the elimination of the sharp gradients between a group of pixels and the surrounding pixels as illustrated by the “blocking” effect in Figures 6.1 (top row) and 6.2 (top row). This “blocking” is completely absent for the uLST retrieval intercomparison with SEVIRI (Figures 6.1 (middle row) and 6.2 (middle row)).

The intercomparison also illustrates the coverage differences between AATSR and MODIS. The wider swath of MODIS, with extreme zenith viewing angles greater than 60° , facilitates a greater number of inter-comparable grid cells. However, the wider swath brings with it larger differences in the proportions of sunlit and shadow scenes observed between MODIS and SEVIRI.

Other key insights were uncovered by the intercomparison. First, the seasonal bias present at some of the Northern Hemisphere *in situ* sites is also evident in the AATSR vs. SEVIRI intercomparison. Both oLST and uLST retrieve higher LST than SEVIRI during the summer months over Europe and lower LST over the winter months (Figures 6.1 to 6.4). The amplitude of this seasonal bias is larger during the day than at night, most probably due to the spatial anisotropy of LST from different viewing perspectives which is particularly apparent during the day when solar heating occurs.

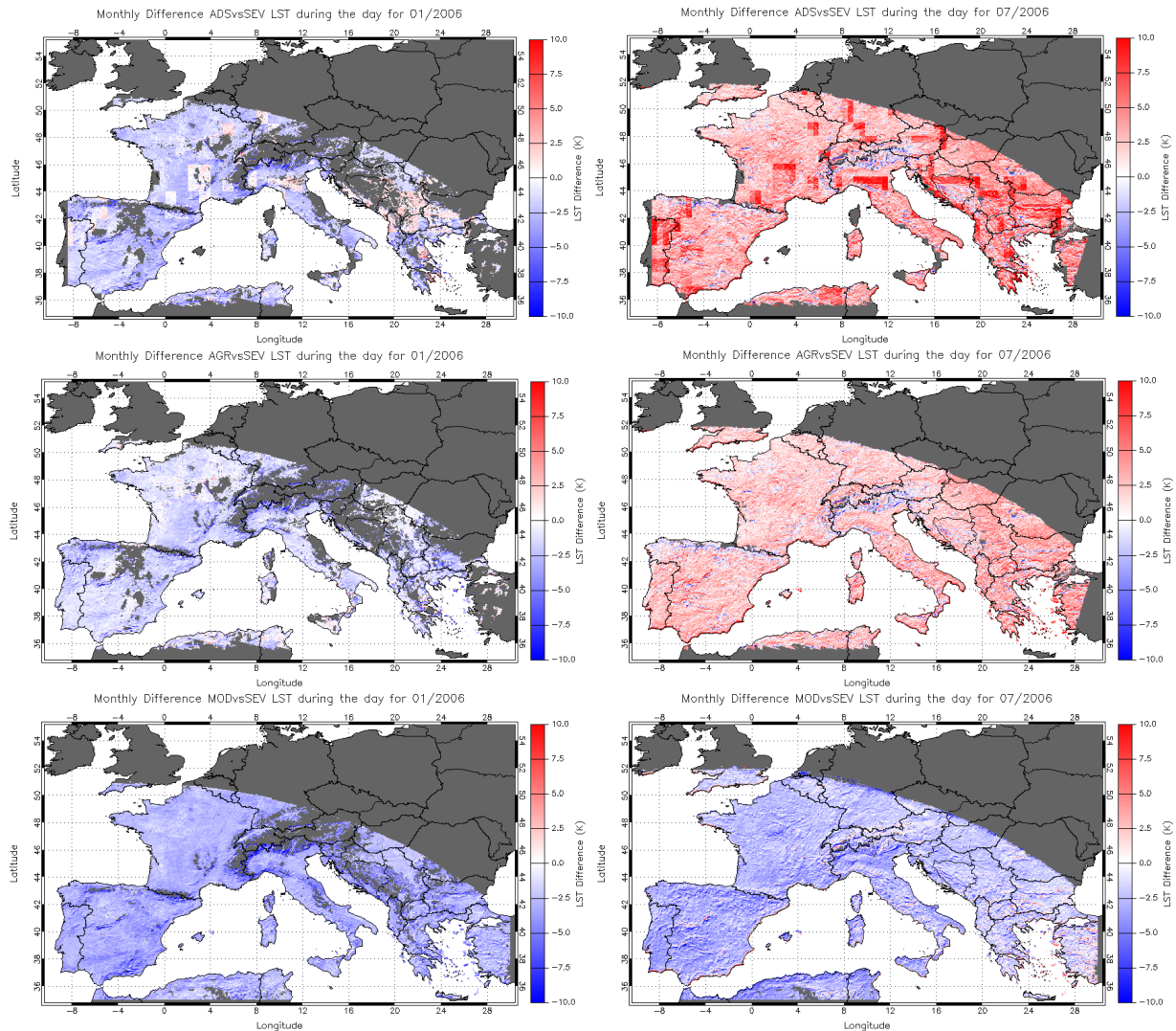


Figure 6.1: Daytime inter-comparison over southern Europe with respect to SEVIRI average monthly LST as the reference point for January 2006 (left column) and July 2006 (right column) - AATSR operational LST vs. SEVIRI (top); updated LST vs. SEVIRI (middle); and Terra MODIS vs. SEVIRI (bottom).

Second, MODIS consistently retrieves lower LST than SEVIRI. This negative difference increases with the size of the viewing angle, probably as a result of differential heating rates between sunlit and shadow scenes. SEVIRI on the other hand, observes predominantly sunlit scenes. Despite this consistent negative difference, the seasonal cycle of MODIS vs. SEVIRI is remarkably similar to that of AATSR vs. SEVIRI, whereby this negative difference is reduced during the summer months.

Finally, topographical features can be distinguished in the difference plots for both AATSR and MODIS (Figures 6.2 and 6.2). Specifically, the mountainous regions of southern and central Europe are exhibiting a cold / colder difference for AATSR / MODIS with respect to SEVIRI. Again this more pronounced during the day is due to SEVIRI observing proportionally more of the sunlit side of mountains than AATSR or MODIS.

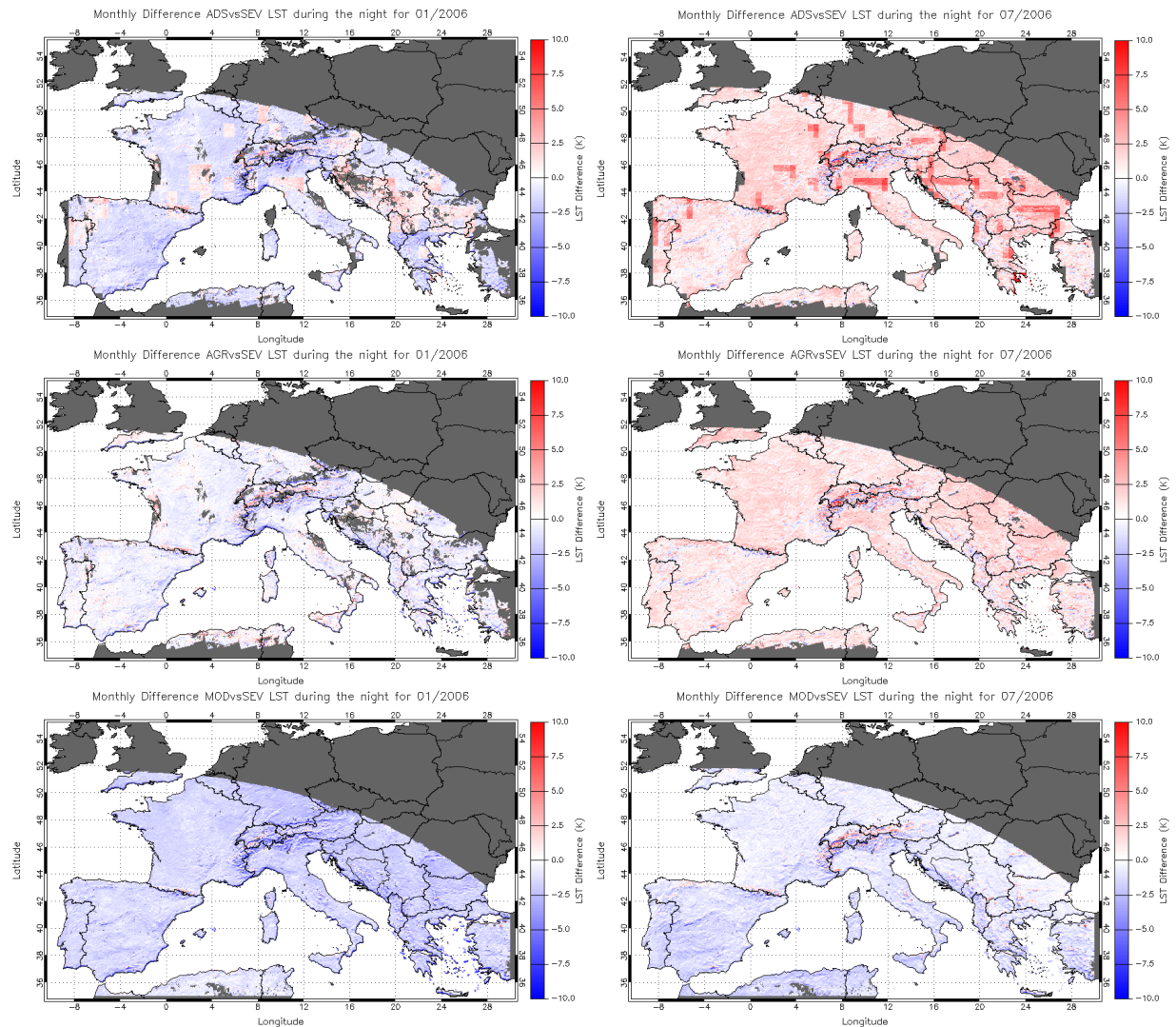


Figure 6.1: Night-time inter-comparison over southern Europe with respect to SEVIRI average monthly LST as the reference point for January 2006 (left column) and July 2006 (right column) - AATSR operational LST vs. SEVIRI (top); updated LST vs. SEVIRI (middle); and Terra MODIS vs. SEVIRI (bottom).

These findings are consistent with that of Noyes *et al.* (2006) in their study across sites in Europe; they also found SEVIRI to systematically record higher LST than MODIS; as did Trigo *et al.* (2008a) in their study over the Iberian Peninsula. MODIS viewing angle variation was also considered to be the primary cause of the negative LST difference with respect to SEVIRI in this latter study.

Figures 6.3 (bottom-right) and 6.4 (bottom-right) illustrate the change in the seasonal cycle of uLST minus SEVIRI compared with oLST minus SEVIRI. They highlight that the amplitude of the seasonal difference between AATSR and SEVIRI has been reduced. Over the year of 2006 the mean discrepancy between AATSR and SEVIRI has been reduced from 0.90 K to 0.41 K during the daytime and from 0.69 K to 0.65 K at night.

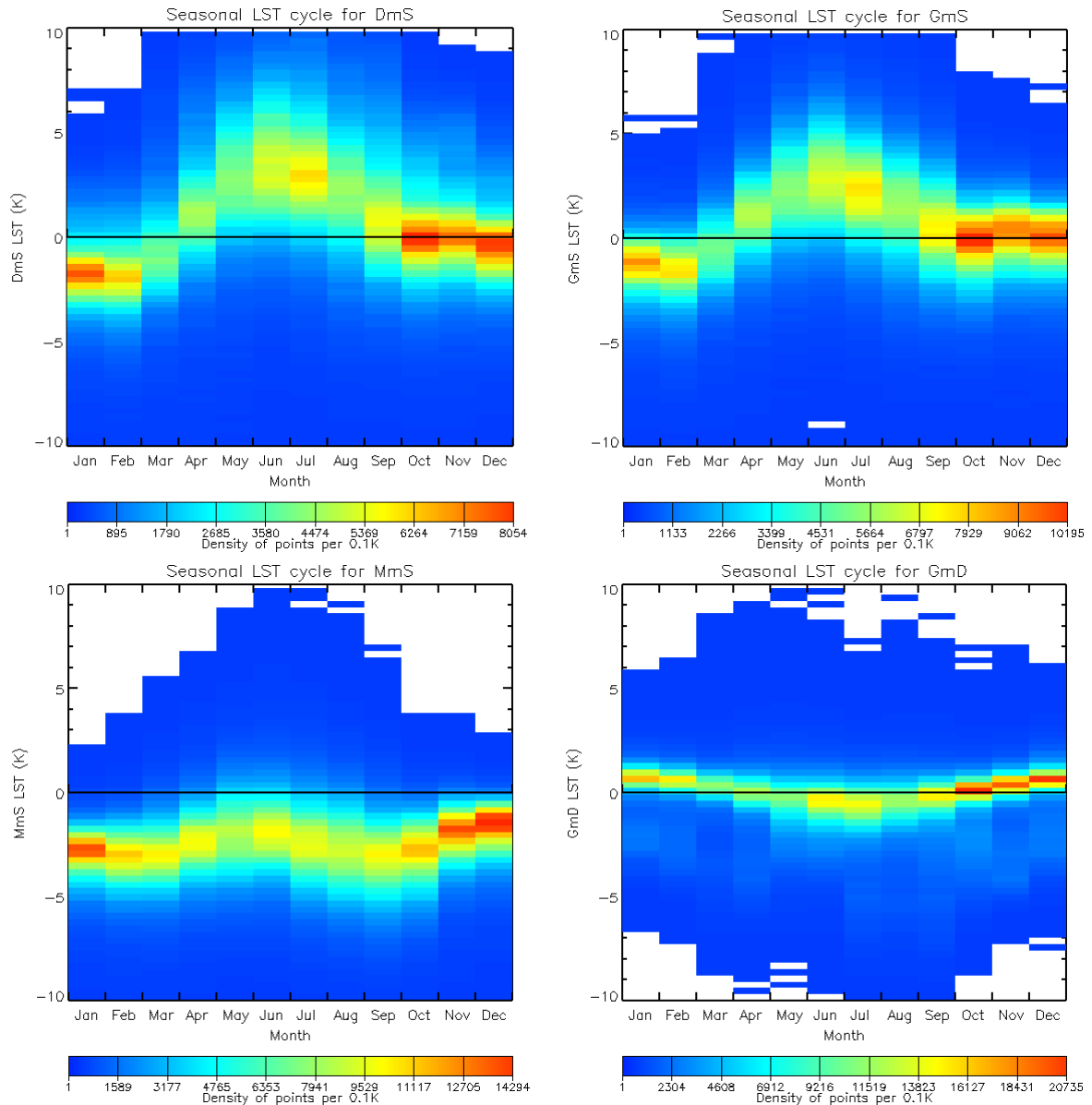


Figure 6.3: Daytime inter-comparison for 2006 for AATSR operational LST vs. SEVIRI (top left), AATSR updated LST vs. SEVIRI (top right), MODIS vs. SEVIRI (bottom left) and AATSR updated LST vs. AATSR operational LST (bottom right) illustrating the seasonal patterns.

In an additional investigation evidence was gathered for the MODIS zenith viewing angle being the primary cause of the negative discrepancy between MODIS and SEVIRI. When only retrievals within 22° were included in the intercomparison the mean discrepancy over the year in question was reduced from -2.59 K to -1.64 K during the day and from -1.08 K to -0.49 K at night.

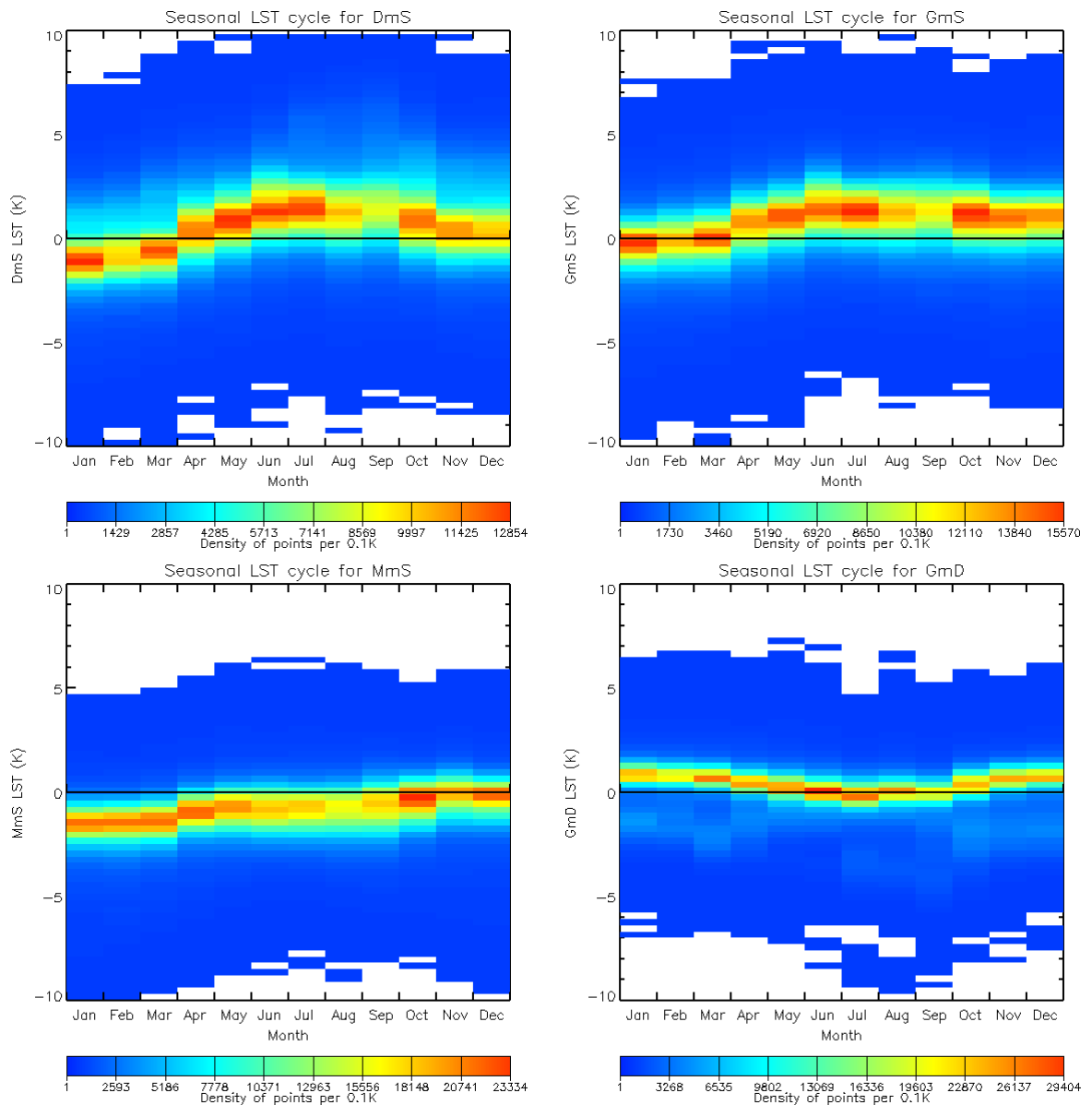


Figure 6.3: Night-time inter-comparison for 2006 for AATSR operational LST vs. SEVIRI (top left), AATSR updated LST vs. SEVIRI (top right), MODIS vs. SEVIRI (bottom left) and AATSR updated LST vs. AATSR operational LST (bottom right) illustrating the seasonal patterns.

6.4. Summary

The intercomparison exercise carried out here generated, for the most part, findings which concur with previous studies (Madeira *et al.*, 2005; Noyes *et al.*, 2006; Trigo *et al.*, 2008a). A number of factors may have contributed to the differences encountered here and indeed in these prior studies.

Firstly, this was not a strict three-way comparison since Envisat has an equatorial crossing time of ~10:00 in descending mode and ~22:00 in ascending mode; for Terra they are ~10:30

and ~22:30 respectively. This temporal difference allows for significant changes in surface temperature. As such AATSR and MODIS were compared to a reference LST product, namely SEVIRI. More specifically each LST retrieved from the polar-orbiting satellites was compared with time interpolated LST from SEVIRI so as to enable a matchup at the overpass time. This is of course subject to uncertainty in the interpolation process; and additionally the difference between AATSR and SEVIRI cannot be directly compared with the difference between MODIS and SEVIRI since the LST difference trajectory between the AATSR overpass time and that of MODIS for each instrument-pair may not be linear. Second, discrepancies in geolocation can affect the heterogeneity of the surface which is analysed. Thirdly, the land surface is viewed from a different perspective by each satellite sensor, with the proportion of sunlit or shadow scenes viewed being a factor of the viewing angle.

A final point is that there are inherent differences in the way TOA radiances are processed by each sensor. Examples include the accuracy of instrument calibration, the application of different emissivity maps, and unique cloud clearing algorithms. Considering this further, cloud contamination limits the available imagery ensuring intercomparison exercises remain challenging undertakings; this was particularly the case with respect to AATSR retrievals because of the longer repeat cycle.

Overall though, the findings of the intercomparison illustrate that the mean difference between AATSR and SEVIRI is within 1 K both day and night, with this discrepancy reduced when utilising the uLST product. Furthermore, the uLST retrieval demonstrates significant improvement over the oLST product in that the “blocking” effect has been eliminated as a result of the move to approximately 1 km resolution auxiliary land cover and fractional vegetation datasets. Both AATSR products exhibit a seasonal warm bias during the European summer and a cold bias during the European winter with respect to SEVIRI. This is consistent with the findings from the *in situ* validation in section 4 for some Northern Hemisphere sites. Even so, the amplitude of this seasonal difference between AATSR and SEVIRI has been reduced for the uLST product.

7. Conclusions

This report has described the activities undertaken by the University of Leicester during the ESA contract for “Long Term Land Surface Temperature Validation”. For the most part, the results obtained within the framework of this LST validation continuation study confirm the conclusions of Noyes (2006a) and Noyes (2007). Key findings include first, confirmation that the AATSR LST algorithm is seasonally biased, in which a peak in the difference between AATSR and the third-party source occurs during the warmest months of the year. Second, a sensitivity analysis of key parameters in the LST retrieval scheme indicates that the accuracy of the algorithm is crucially dependent on emissivity but also on water vapour and atmospheric temperature. Moreover, the sensitivity and bias of the algorithm varies significantly between biomes.

Despite this, crucial differences between the operational LST product and the updated LST product exist. The auxiliary data utilised by the algorithm is critical to the accuracy of the LST product. Biome misclassification and poor agreement between the auxiliary fractional vegetation and estimates using AATSR visible channels may have resulted in LST discrepancies of several K as reported previously. The evidence acquired to date suggests the use of finer spatial and temporal resolution auxiliary datasets has alleviated some of these discrepancies.

A clear conclusion we can make here is that the findings presented here indicate that uLST retrieval is producing an improved performance on the oLST retrieval, in terms of lower sensitivity to variations in parameter states, on average lower median biases and median absolute deviations with respect to *in situ* measurements, and a lower amplitude in the seasonal bias with respect to the SEVIRI LST product. However, the updated retrieval is still not optimum – this is particularly the case for the bare soil biomes and further tuning of the coefficients is recommended.

Further caveats to this study include the fact that a +0.2 K offset to the AATSR 12 μ m BT (Nightingale and Birks, 2004) was not applied in any test and so remains a further consideration to investigate. In addition, the Oxford Reference Forward Model (RFM) was used in the original contract (and extension) for radiative transfer modelling, whereas in this study the fast model RTTOV-10 was used. Variations between the models in the simulation of BTs were not quantified and may be a source of differences between findings. Finally, all experiments have been carried out with the operational form of the AATSR LST algorithm, albeit with / without the use of the high resolution auxiliary datasets. No attempt at this stage has been made to evaluate alternative forms of the algorithm - further work is required to examine other forms.

Considering the above, several items require further investigation. First, the coefficients for the uLST retrieval require fine tuning, and indeed results from the sensitivity study (section 5) imply that latitudinal dependent coefficients may be better equipped to reduce water vapour and atmospheric temperature sensitivity. An alternative method could be to develop a water vapour correction to the existing algorithm for example. Second, the improvements incorporated for the auxiliary biome and fractional vegetation datasets should be extended to the inclusion of a finer spatial and temporal resolution precipitable water dataset. Third,

issues remain with the cloud screening and further improvements are necessary to eliminate some of the large negative biases in the matchup database. Finally, there is a requirement to assess whether similar conclusions can be drawn for the full range of AATSR nadir viewing angles.

8. References

- ARM, 2005, Infrared Thermometer Handbook (download from www.arm.gov/publications/tech_reports/handbooks/irt_handbook.pdf)
- ASTER Spectral Library, 1999, Reproduced from the ASTER Spectral Library through the courtesy of the Jet Propulsion Laboratory, California Institute of Technology, Pasadena, California.
- Baldocchi, D., Falge, E., Gu, L. H., Olson, R., Hollinger, D., Running, S., Anthoni, P., Bernhofer, C., Davis, K., Evans, R., Fuentes, J., Goldstein, A., Katul, G., Law, B., Lee, X. H., Malhi, Y., Meyers, T., Munger, W., Oechel, W., Paw, K. T., Pilegaard, K., Schmid, H. P., Valentini, R., Verma, S., Vesala, T., Wilson, K., and Wofsy, S., 2001. FLUXNET: A new tool to study the temporal and spatial variability of ecosystem-scale carbon dioxide, water vapor, and energy flux densities. *Bulletin of the American Meteorological Society*, **82**, 2415–2434.
- Coll, C., Caselles, V., Galve, J. M., Valor, E., Niclos, R., Sanchez, J. M., and Rivas, R., 2005. Ground measurements for the validation of land surface temperatures derived from AATSR and MODIS data. *Remote Sensing of Environment*, **97**, 288-300.
- Dorman, J. L. and Sellers, P. J., 1989, A global climatology of albedo, roughness length and stomatal resistance for atmospheric general circulations models as represented by the Simple Biosphere Model (SiB), *Journal of Applied Meteorology*, **28**, 833-855.
- Eyre J.R. 1991: A fast radiative transfer model for satellite sounding systems. *ECMWF Research Dept. Tech. Memo. 176*.
- Frey, R. A., Ackerman, S. A., Liu, Y., Strabala, K. I., Zhang, H., Key, J. R., and Wang, X., 2008, Cloud Detection with MODIS. Part I: Improvements in the MODIS Cloud Mask for Collection 5, *Journal of Atmospheric and Oceanic Technology*, **25**, 1057-1072.
- Istomina, L., G., von Hoyningen_Huene, W., Kokhanovsky, A. A., and Burrows, J. P., 2010, The detection of cloud free snow covered areas using AATSR measurements, *Atmospheric Measurement Techniques*, **3**, 1005-1017.
- Kabsch, E., Olesen, F. S., and Prata, F., 2008, Initial results of the land surface temperature (LST) validation with the Evora, Portugal ground-truth station measurements. *International Journal of Remote Sensing*, **29**, 5329-5345.
- Kondratyev, K. Y., 1969, Radiation in the Atmosphere, New York Academic Press.
- Llewellyn-Jones, D. Edwards, M. C., Mutlow, C. T., Birks, A. R., Barton, I. J., and Tait, H., 2001. AATSR: Global-Change and Surface-Temperature Measurements from Envisat. ESA bulletin February 2001, pp. 11–21.
- Madeira, C., Dash, P., Olesen, F., and Trigo, I. F., 2005, Intercomparison of Meteosat-8 derived LST with MODIS and AATSR similar products, in *Proceedings of the 2005 EUMETSAT Meteorological Satellite Conference*, Dubrovnik, Croatia, September 2005.
- Nightingale, T.J., and A.R. Birks, 2004. AATSR Algorithm Verification: Comparison of AATSR and ATSR-2 Data, AATSR Technical Note, Rutherford Appleton Laboratory.
- Noyes, E., Good, S., Corlet, G., Kong, X., Remedios, J., and Llewellyn-Jones, D., 2006. AATSR LST product validation. in *Proceedings of the Second Working Meeting on MERIS and AATSR Calibration and Geophysical Validation (MAVT-2006)*. ESRIN, Frascati, Italy.

- Noyes, E. J., 2006a, Technical Assistance for the Validation of AATSR Land Surface Temperature Products, Final Report – February 2006, *ESA Contract Number: 19054/05/NL/FF*
- Noyes, E. J., 2006b, An Investigation into the Accuracy of Surface Temperature Retrievals from the AATSR, *PhD Thesis*, University of Leicester.
- Noyes, E. J., 2007, Technical Assistance for the Validation of AATSR Land Surface Temperature Products, Contract Extension Final Report – January 2007, *ESA Contract Number: 19054/05/NL/FF*
- Peres, L. F., and DaCamara, C. C., 2005, Emissivity maps to retrieve land-surface temperature from MSG/SEVIRI. *IEEE Transactions on Geoscience and Remote Sensing*, **43**, 1834–1844.
- Prata, A. J., 2002, Land Surface Temperature Measurement from Space: AATSR Algorithm Theoretical Basis Document, *CSIRO report*.
- Remedios, J. J., 1999, MIPAS equatorial atmospheric data set designed for use with Oxford RFM, http://www-atm.physics.ox.ac.uk/RFM/rfm_downloads.html#atm
- Seemann, S.W., Borbas, E. E., Knuteson, R. O., Stephenson, G. R., and Huang, H.-L. 2008, Development of a Global Infrared Land Surface Emissivity Database for Application to Clear Sky Sounding Retrievals from Multi-spectral Satellite Radiance Measurements, *Journal of Applied Meteorology and Climatology*, **47**, 108-123.
- Sobrino, J. A., and Cuenca, J., 1999, Angular variation of thermal infrared emissivity for some natural surfaces from experimental measurements, *Applied Optics*, **38**, 3931-3936.
- Sobrino, J. A., and Romaguera, M., 2004. Land surface temperature retrieval from MSG1-SEVIRI data. *Remote Sensing of Environment*, **92**, 247-254.
- Soil Survey Staff, Soil Taxonomy - A Basic System of Soil Classification for Making and Interpreting Soil Surveys Second Edition, Agriculture Handbook No 436 edited by United States Department of Agriculture, Natural Resources Conservation Service, Washington, D. C., second edition, 1999
- Trigo, I. F., Monteiro, I. T., Olesen, F., and Kabsch, E., 2008a. An assessment of remotely sensed land surface temperature. *Journal of Geophysical Research-Atmospheres*, **113**, 12.
- Trigo, I. F., Peres, L. F., DaCarnara, C. C., and Freitas, S. C., 2008b. Thermal land surface emissivity retrieved from SEVIRI/meteosat. *IEEE Transactions on Geoscience and Remote Sensing*, **46**, 307-315.
- Wan, Z., and Dozier, J., 1996. A generalized split-window algorithm for retrieving land surface temperature from space. *IEEE Transactions on Geoscience and Remote Sensing*, **34**, 892–905.
- Wan, Z., Zhang, Y., Zhang, Y. Q., and Li, Z. L., 2002. Validation of the land-surface temperature products retrieved from Terra Moderate Resolution Imaging Spectroradiometer data. *Remote Sensing of Environment*, **83**, 163–180.
- Wan, Z., 2008. New refinements and validation of the MODIS landsurface temperature/emissivity products. *Remote Sensing of Environment*, **112**, 59- 74.
- Zeller, O., Technical Assistance for the Validation of AATSR Land Surface Temperature Products, Contract Extension Task 3 Report: New auxiliary files for the AATSR LST retrieval, *ESA Contract Number: 19054/05/NL/FF*, 2010.

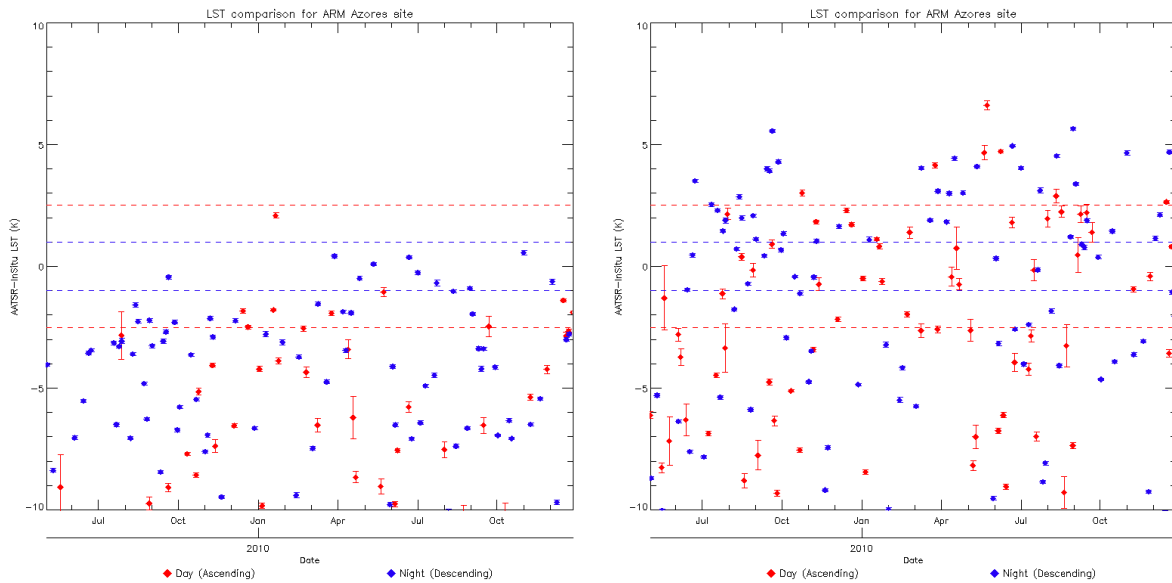
9. Acknowledgements

The *in situ* radiometric data acquired over all the ARM sites were supplied by the Atmospheric Radiation Measurement (ARM) Program. Data for Evora and Gobebeb were supplied by Frank Goettsche. Furthermore, we are grateful to the British Atmospheric Data Centre (BADC) which provided us with access to the Met Office Cardington dataset. Finally, the AATSR operational LST data used in this study were provided by ESA and the NEODC, SEVIRI data were provided by LandSAF and MODIS data were available from USGS.

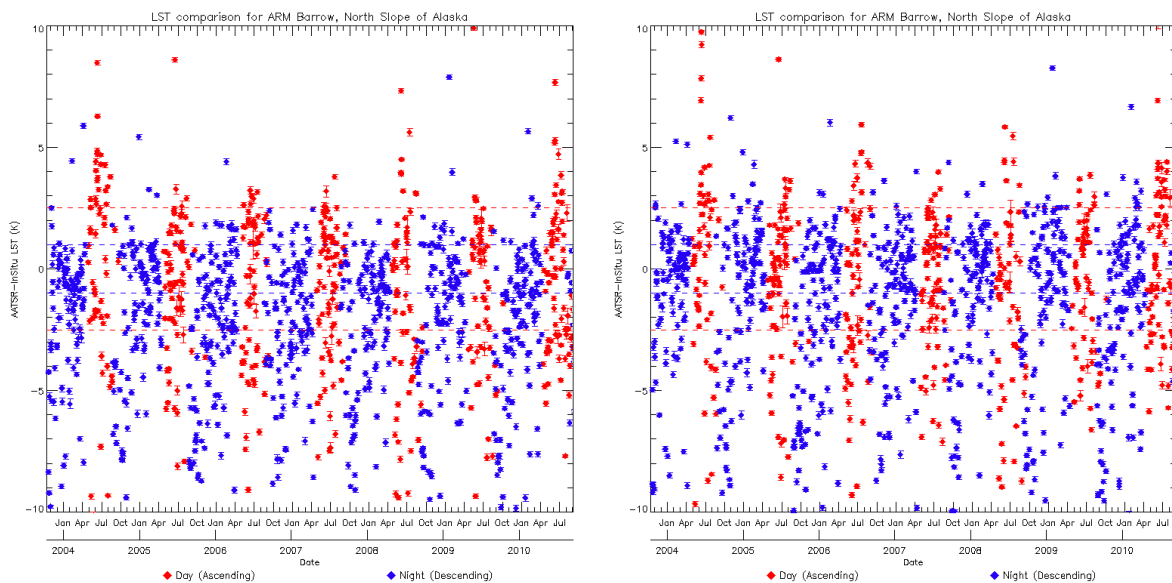
Appendix A – in situ validation plots

Comparisons between AATSR operational LST (left) and updated LST (right) with respect to *in situ* LST data over the remaining *in situ* validation sites. The dashed lines show the target accuracy of the AATSR LST product during the day (red) and night (blue). The error bars represent the estimated errors on the point *in situ* LST observations. For sites where the median biases are larger than the (-10, 10) range comparisons are plotted on a (-60, 60) range.

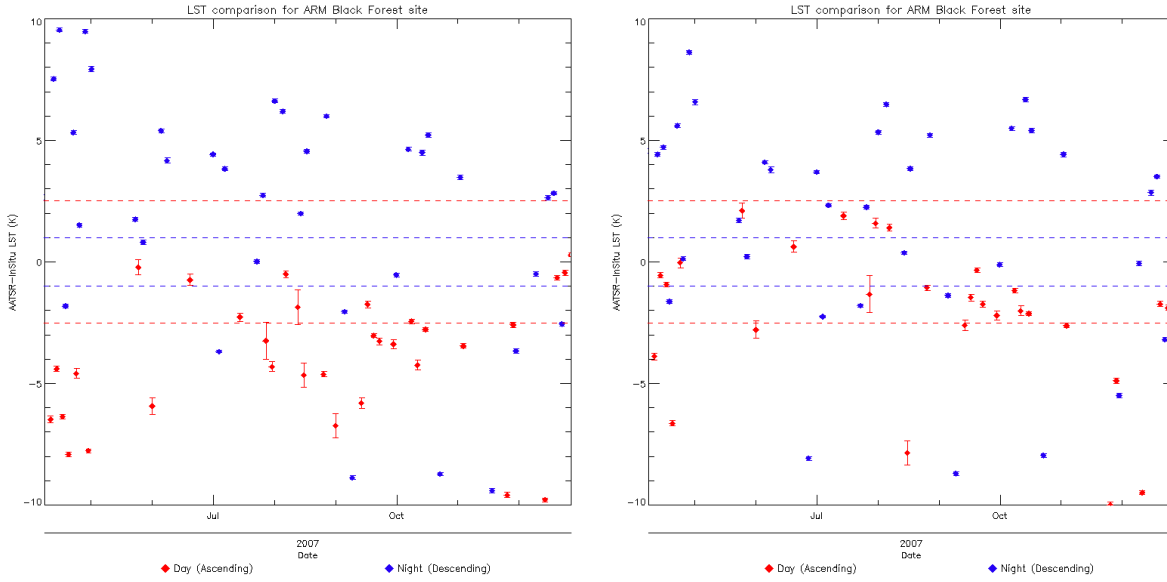
ARM Azores



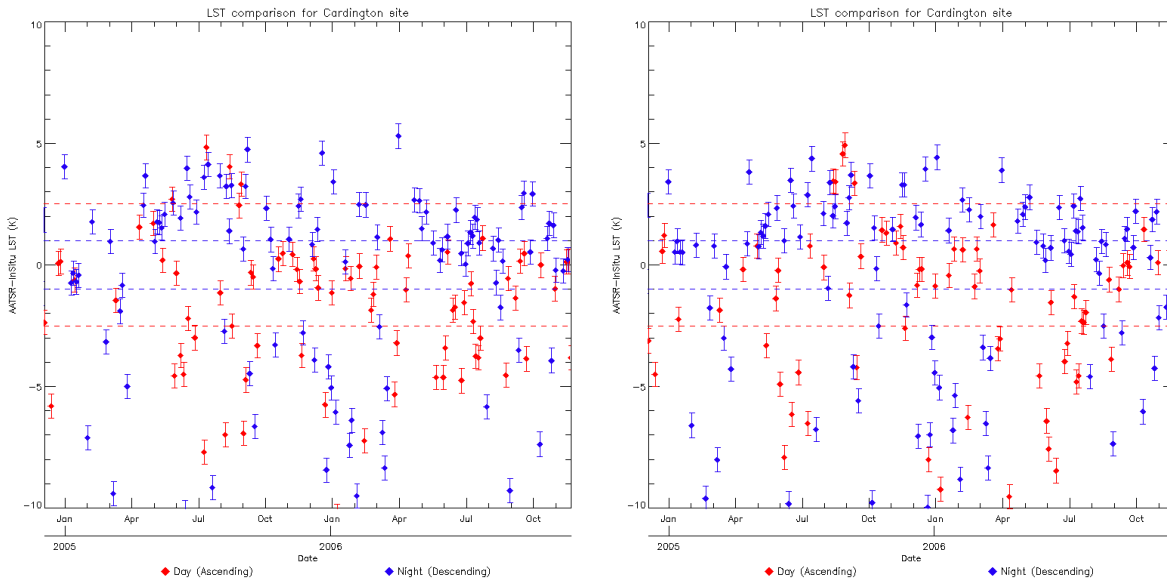
ARM Barrow



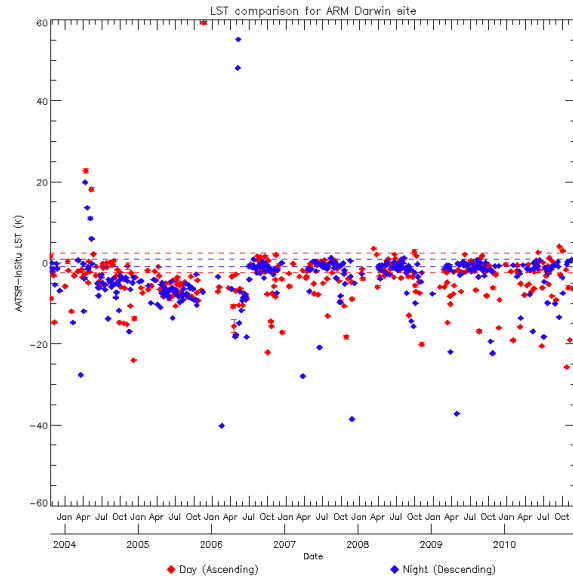
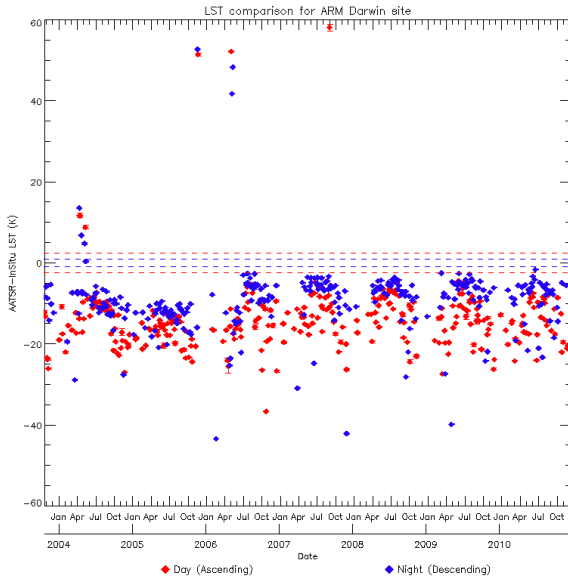
ARM Black Forest



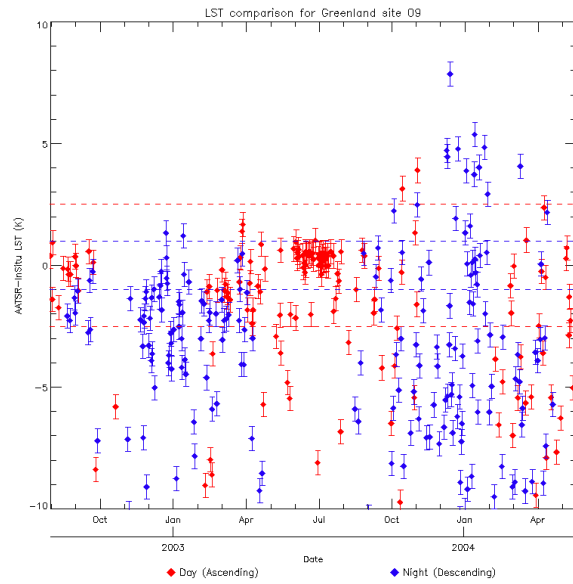
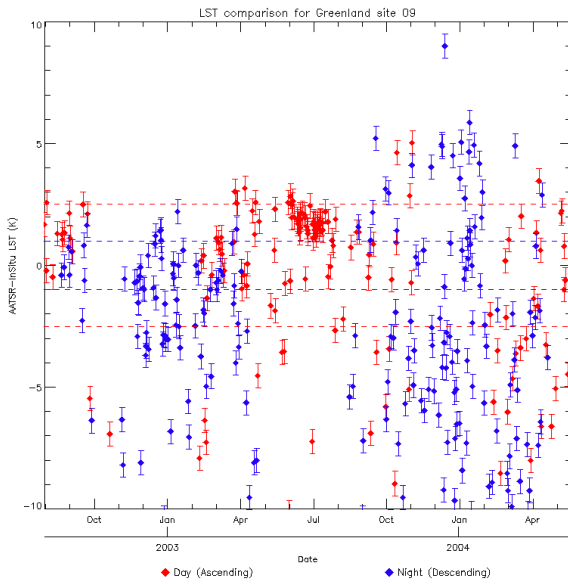
Cardington



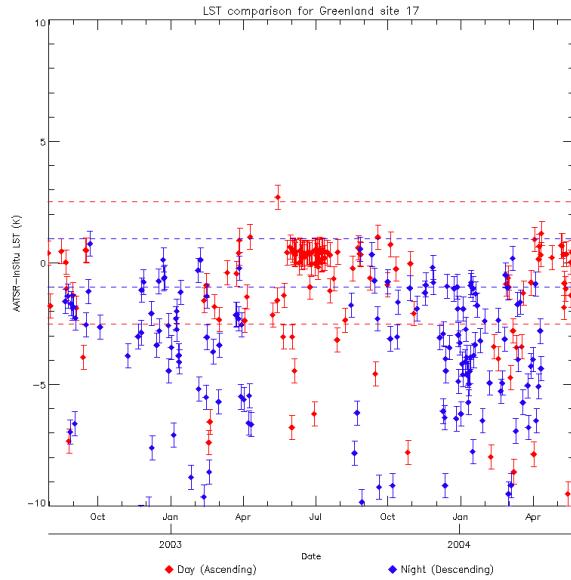
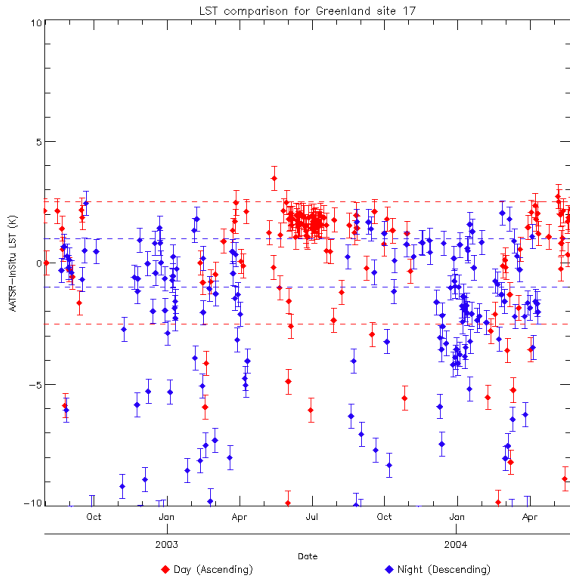
ARM Darwin



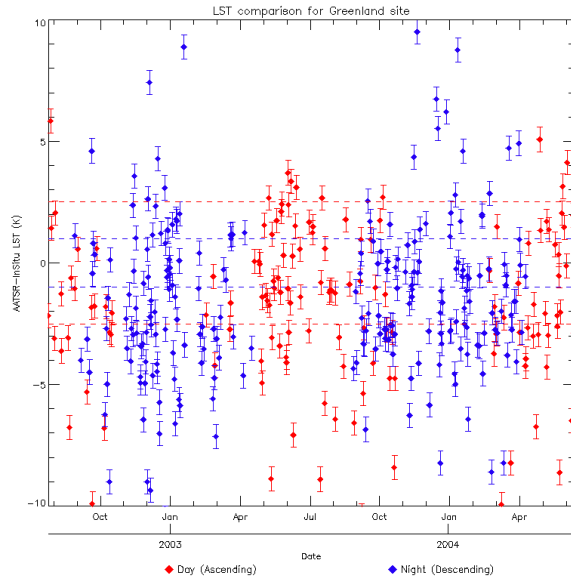
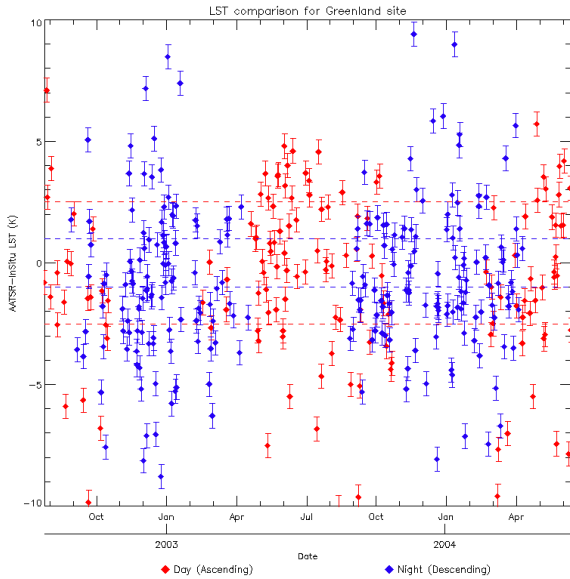
Greenland site 09



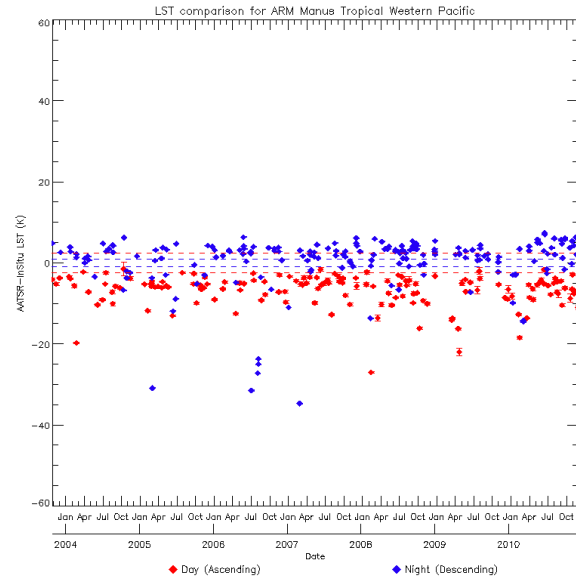
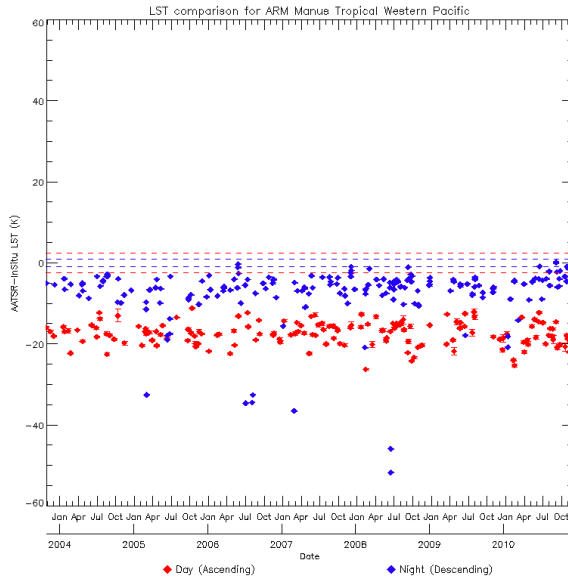
Greenland site 17



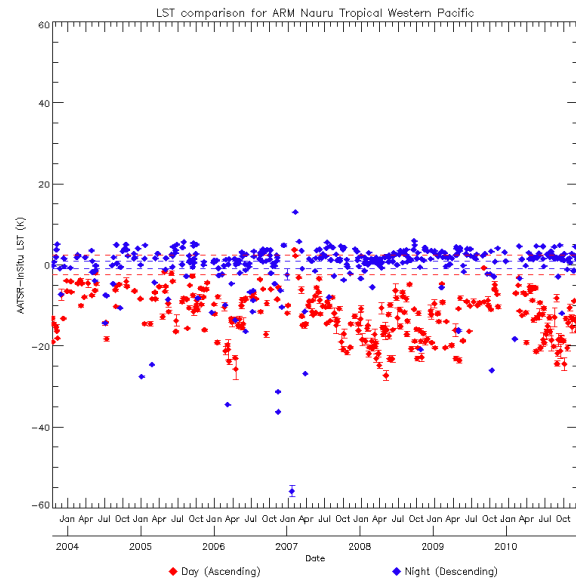
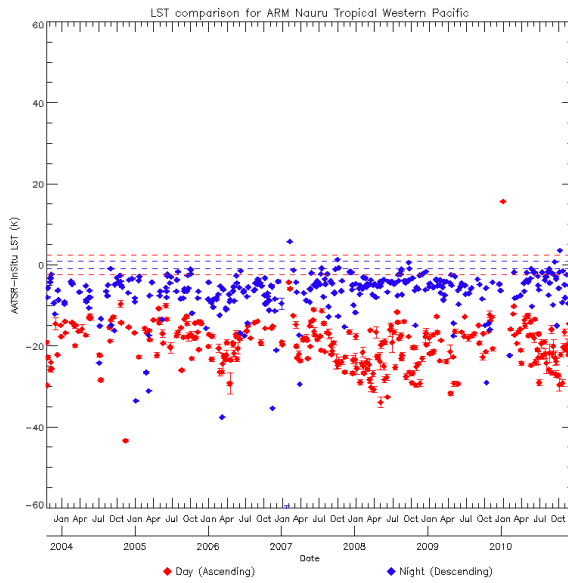
Greenland



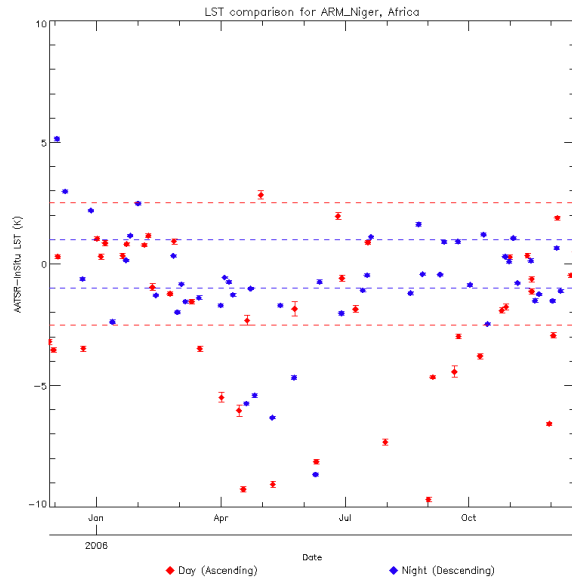
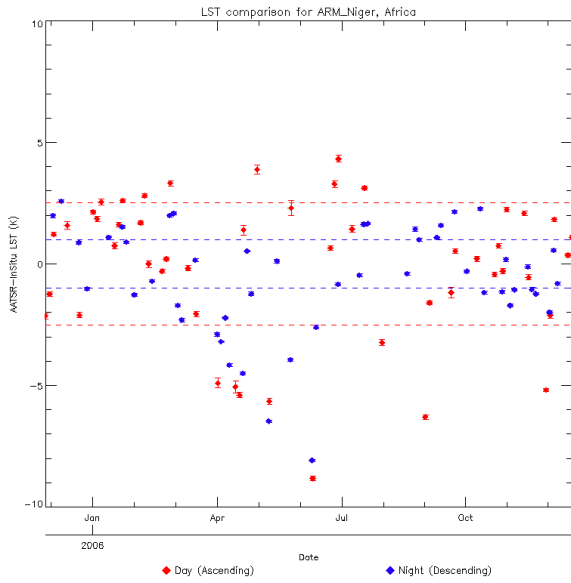
ARM Manus



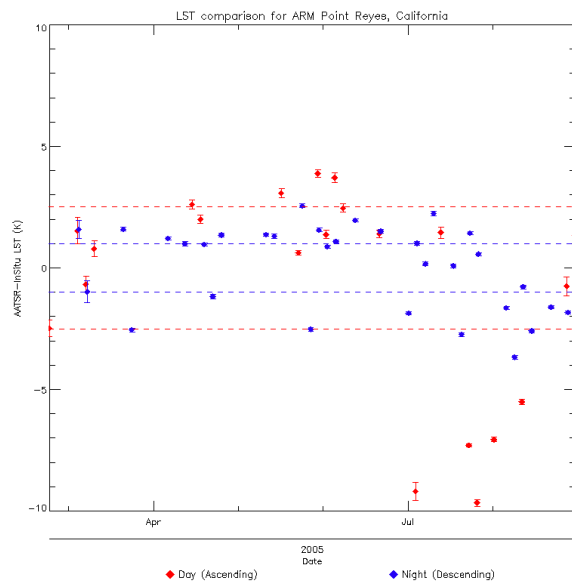
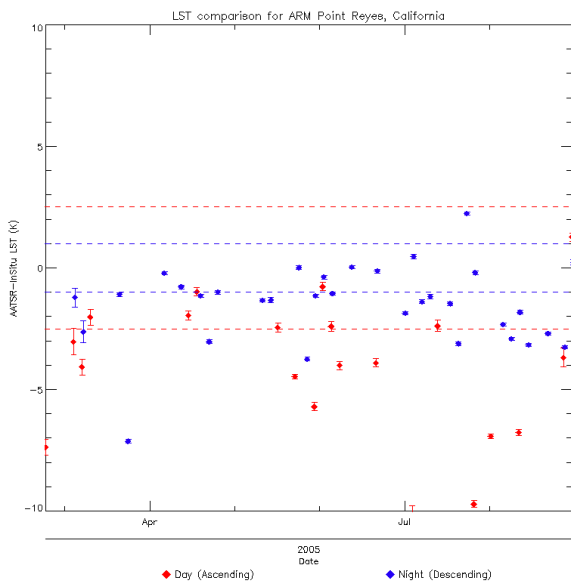
ARM Nauru



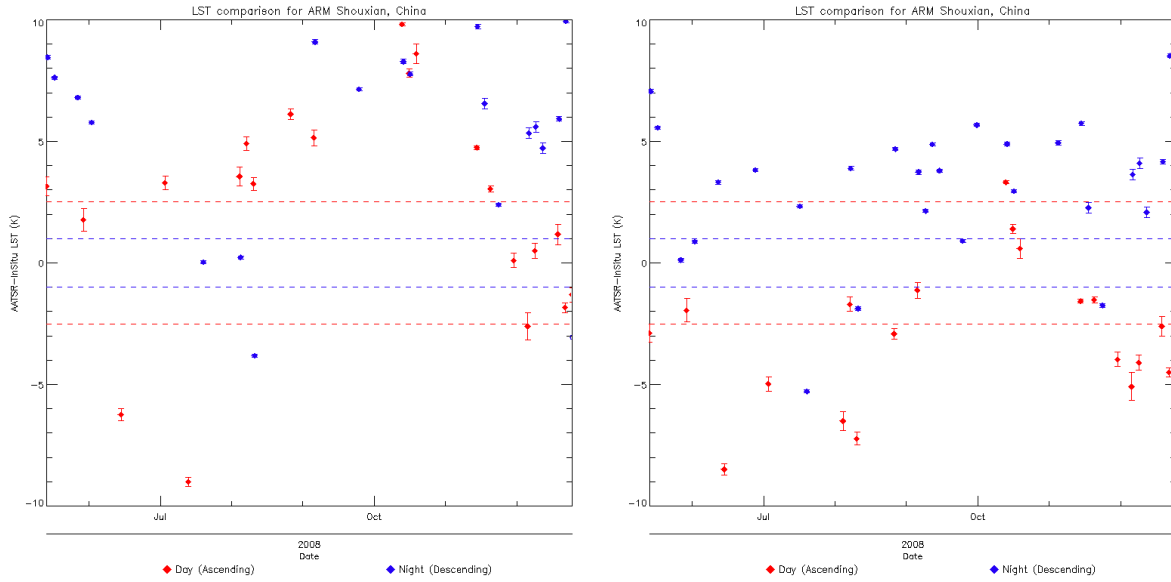
ARM Niamey



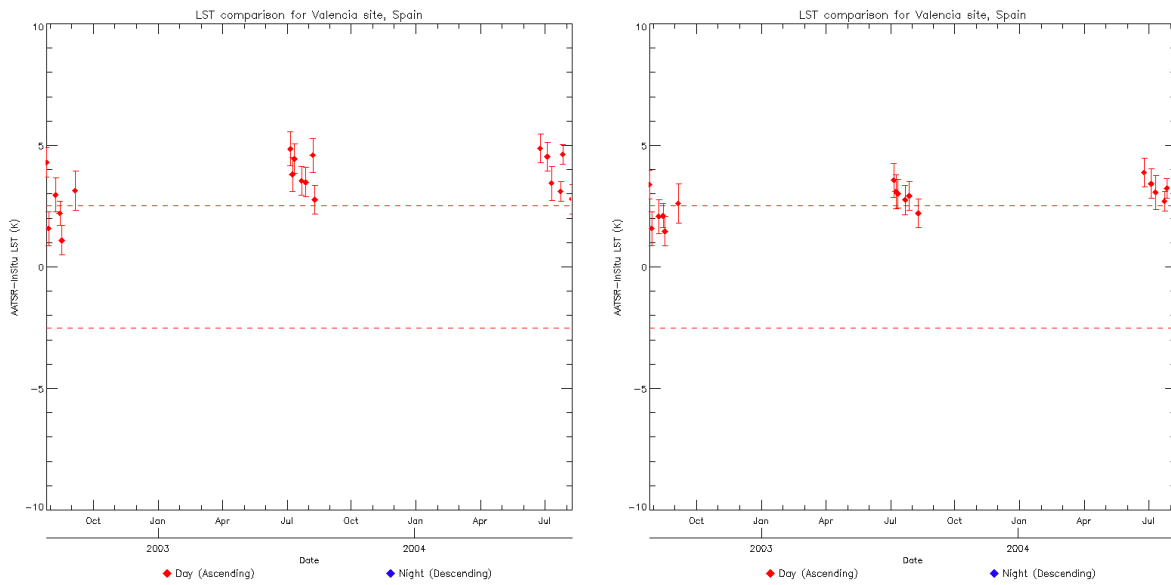
ARM Point Reyes



ARM Shouxian

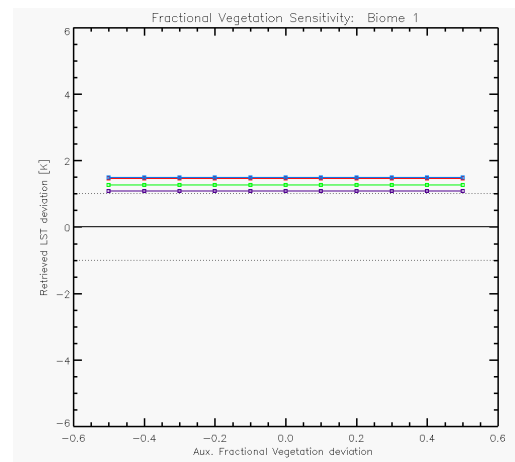
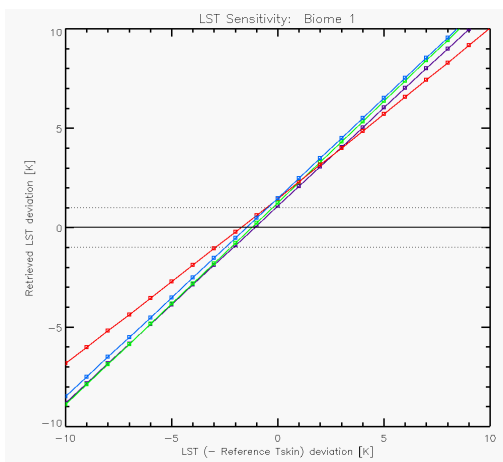
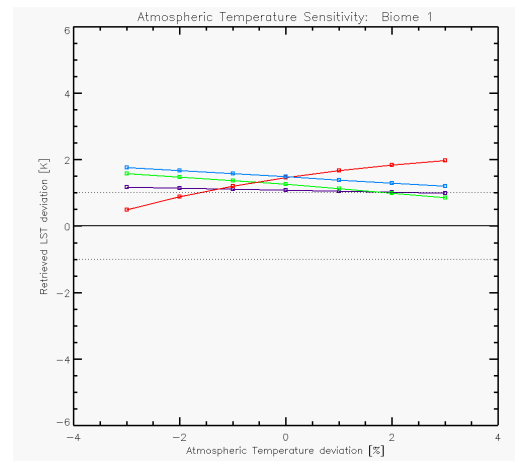
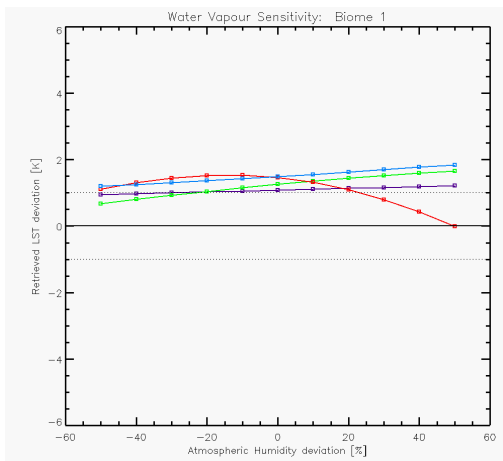
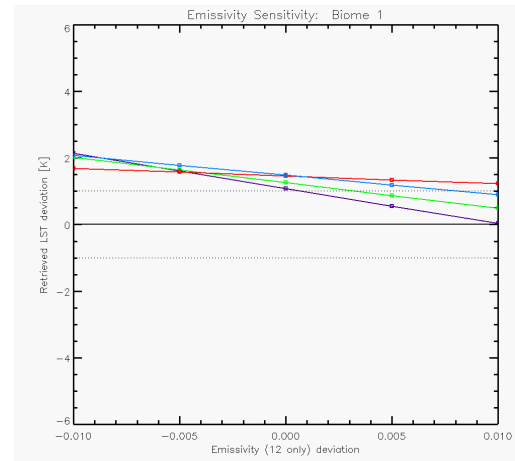
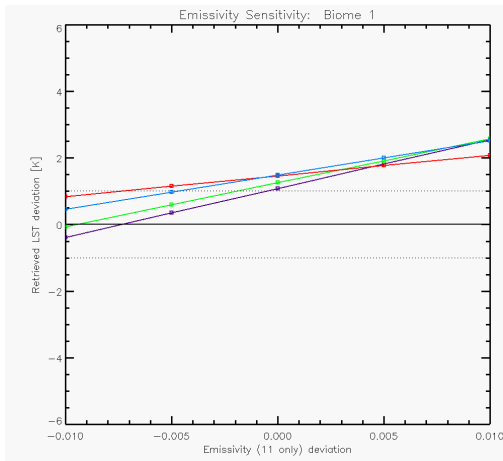


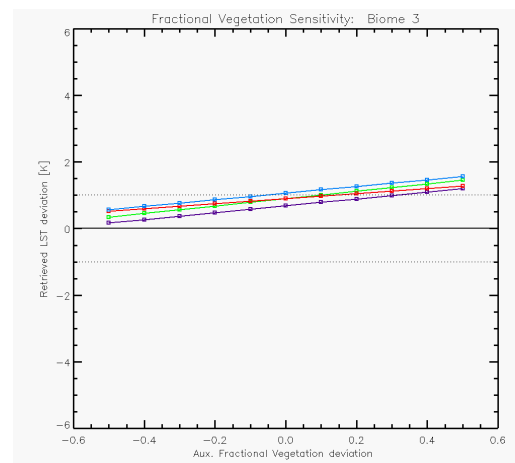
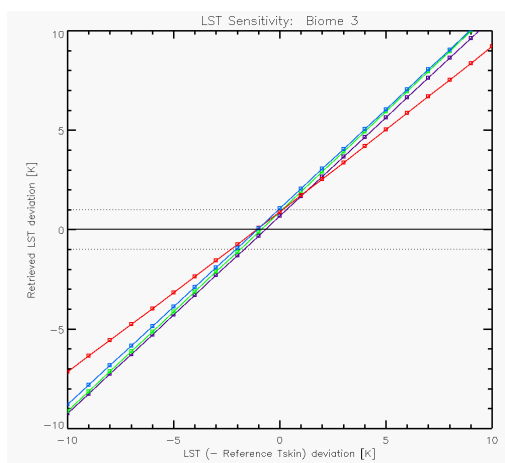
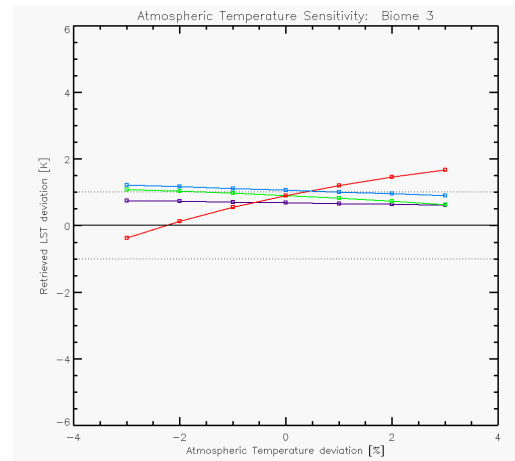
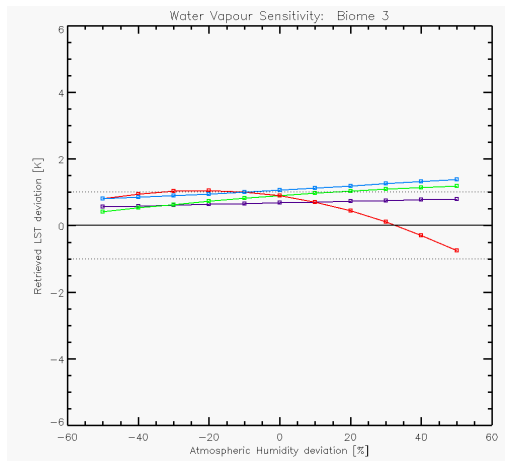
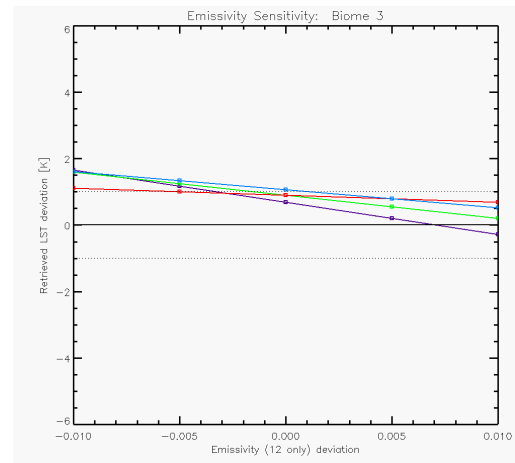
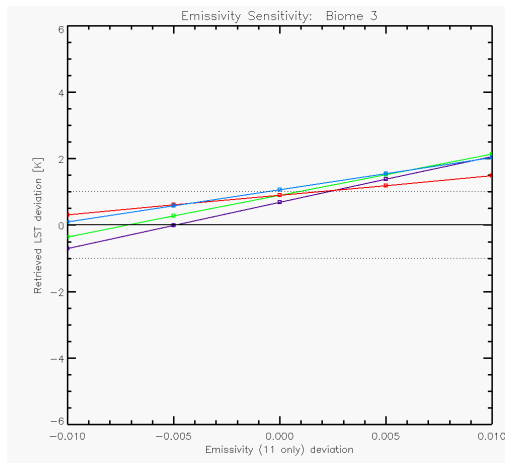
Valencia



Appendix B – sensitivity plots

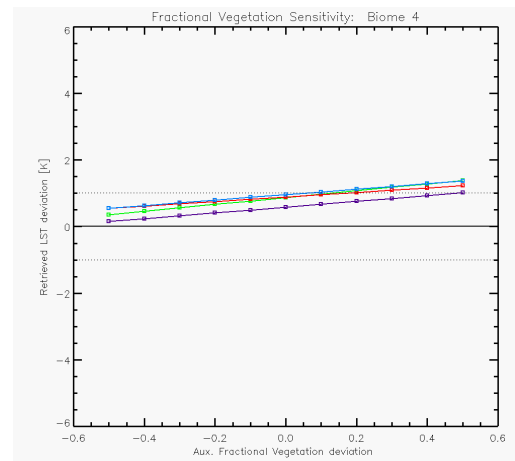
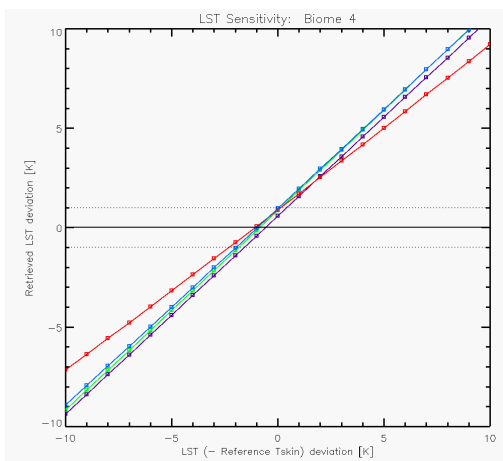
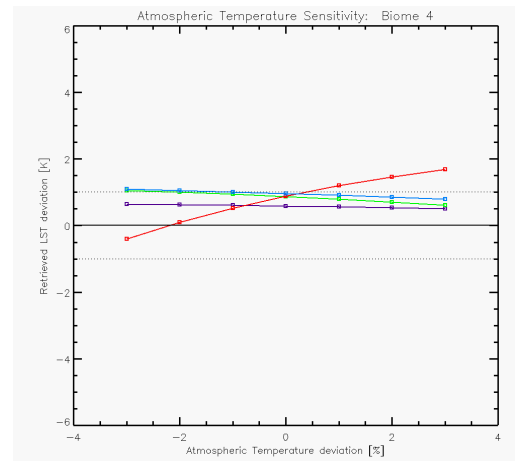
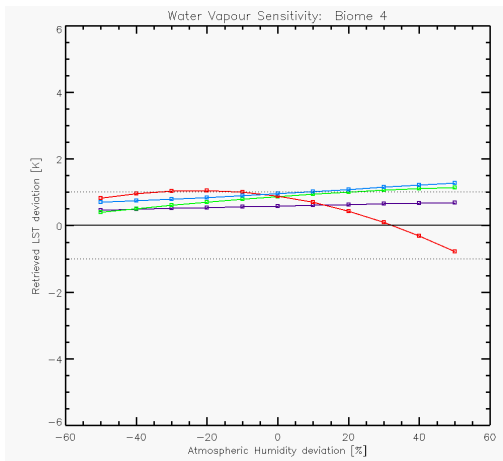
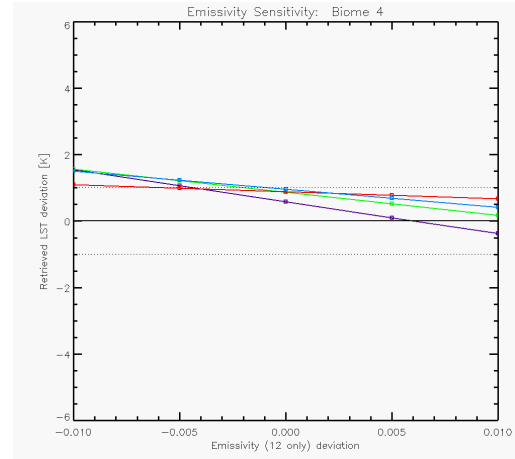
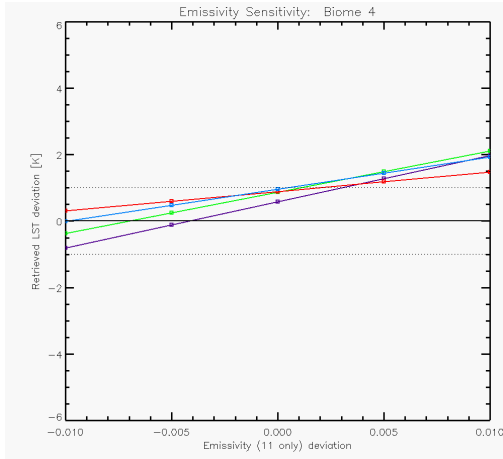
ALB2 Biome 1



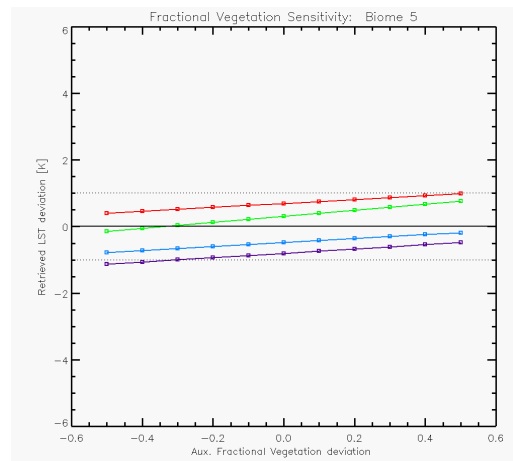
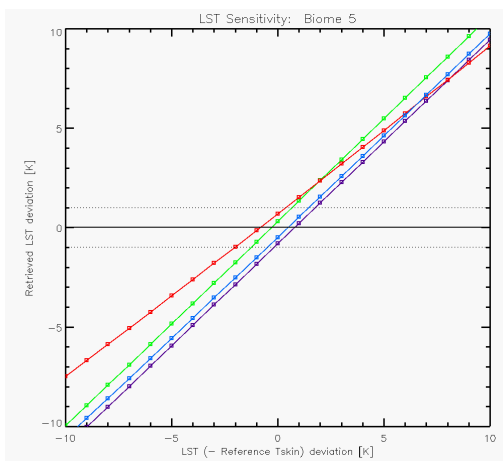
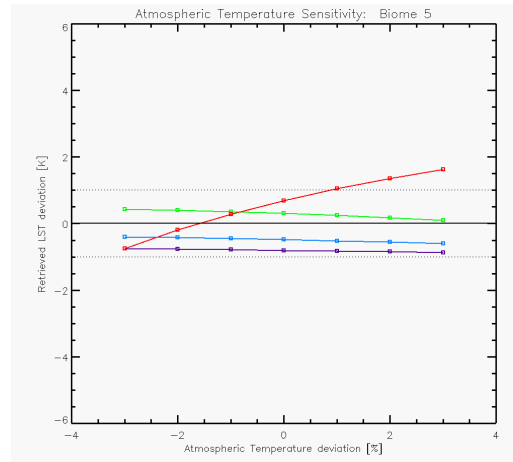
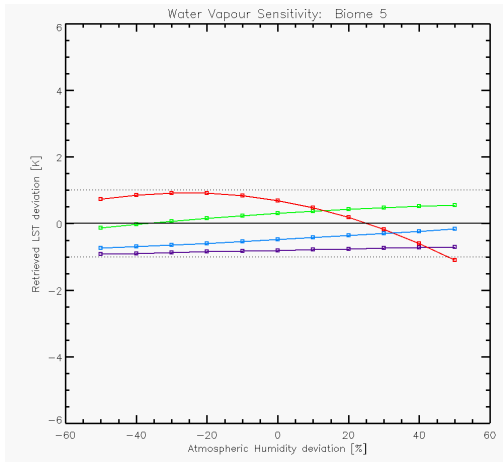
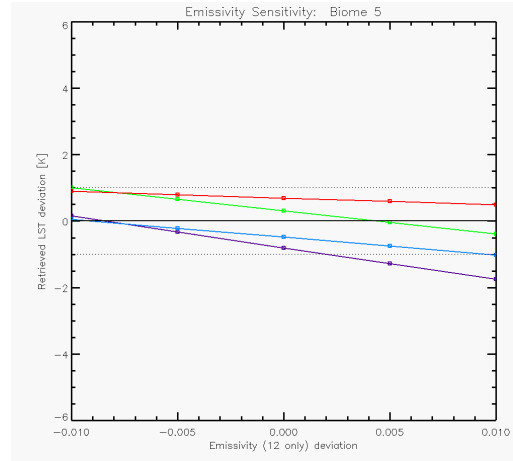
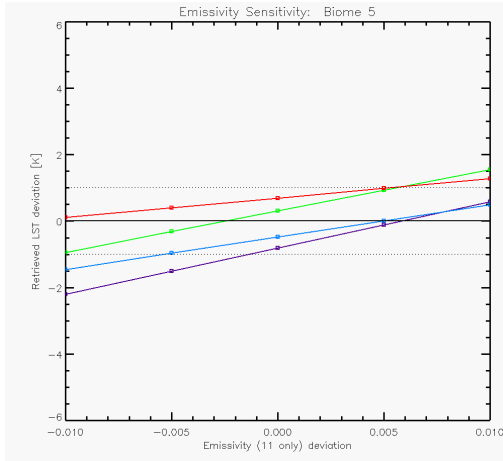


ALB2 Biome 3

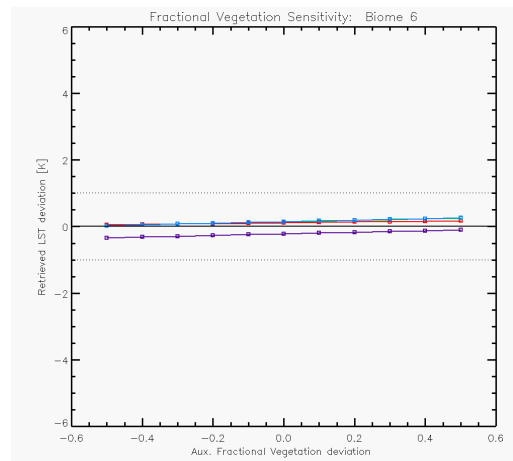
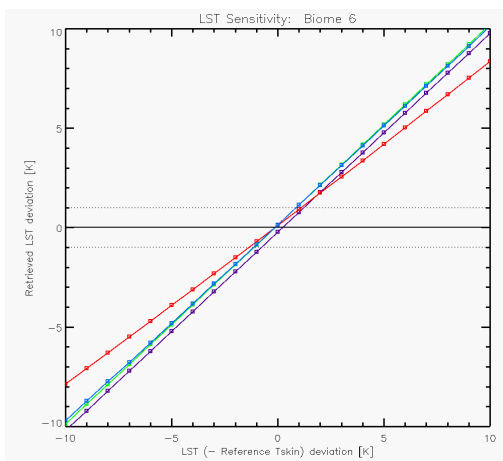
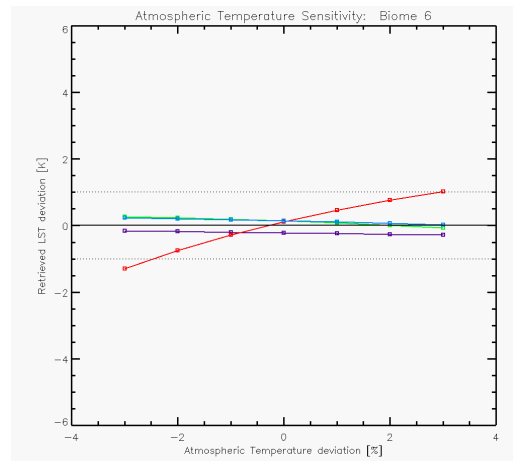
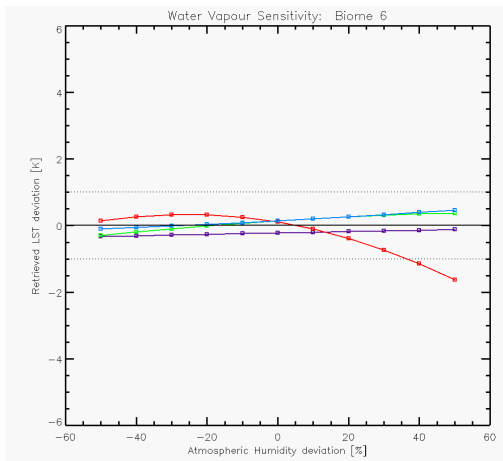
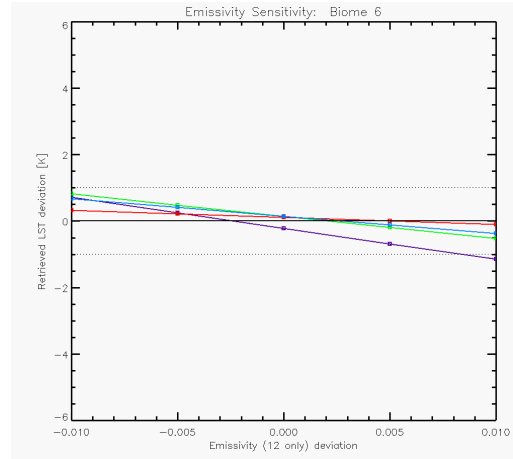
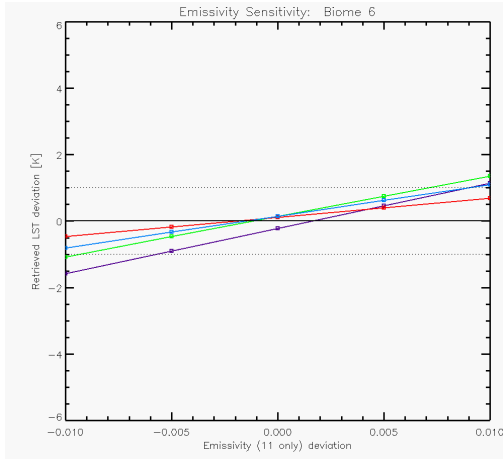
ALB2 Biome 4



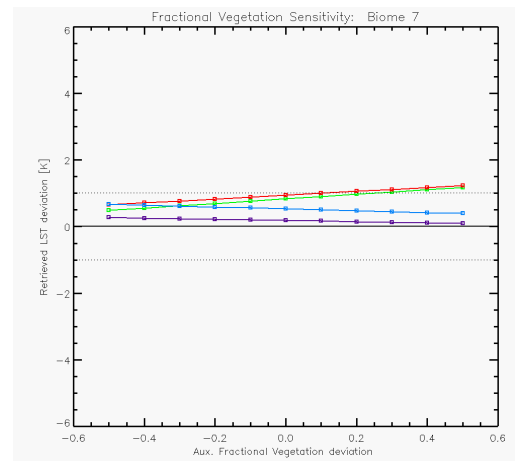
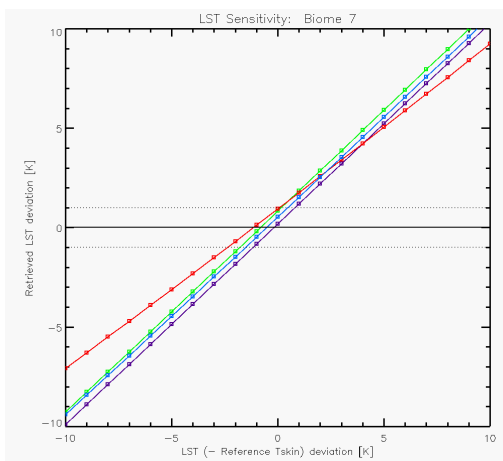
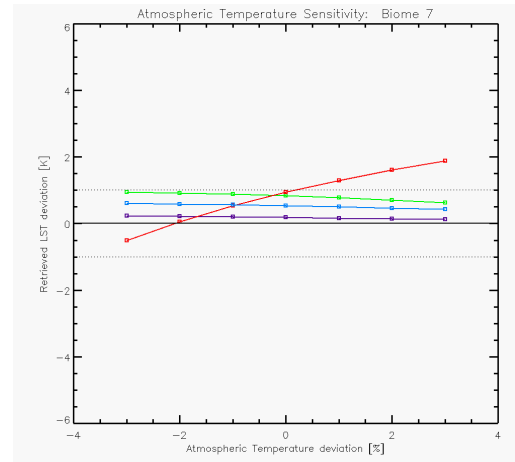
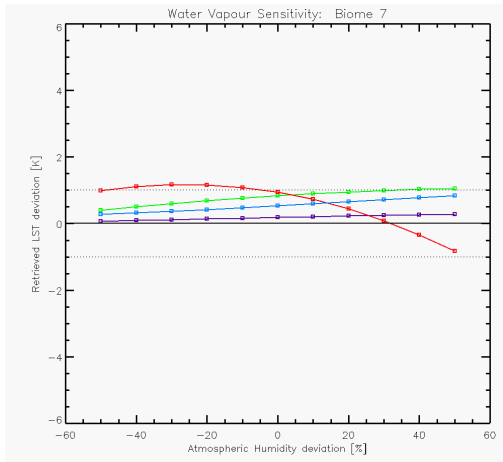
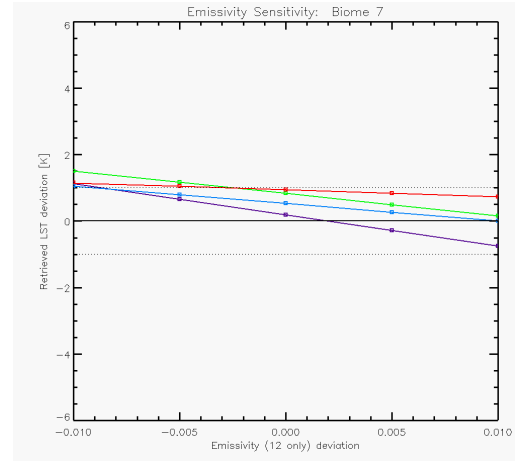
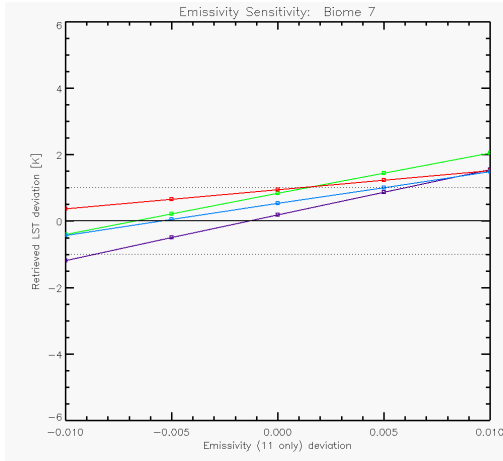
ALB2 Biome 5



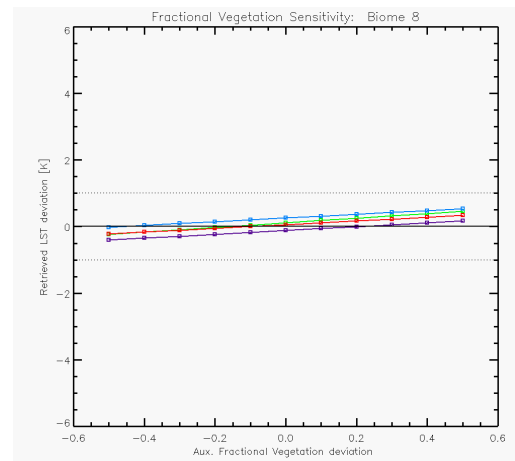
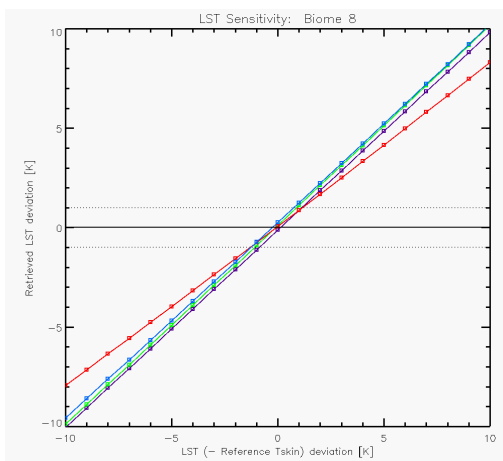
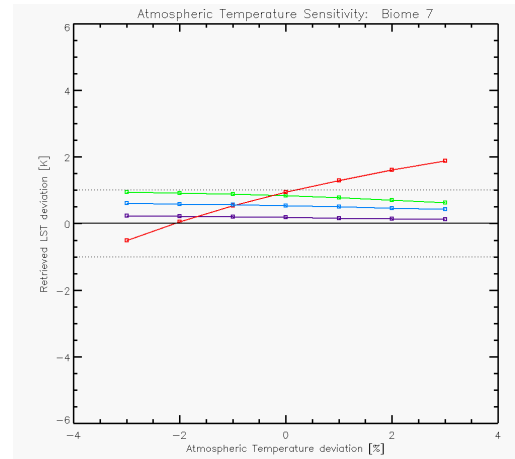
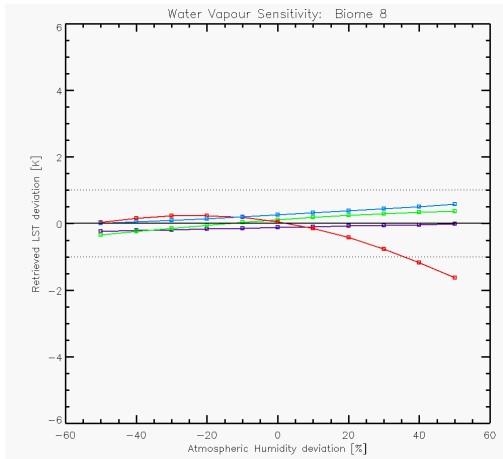
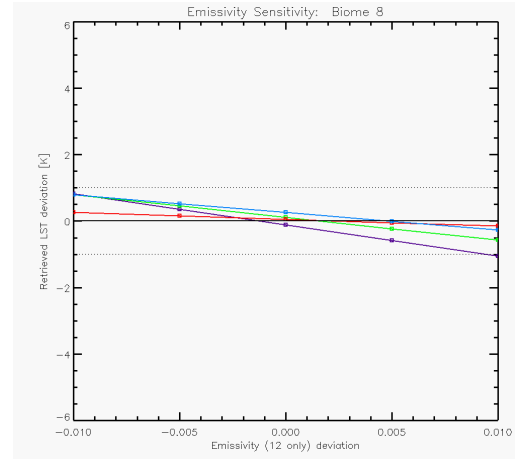
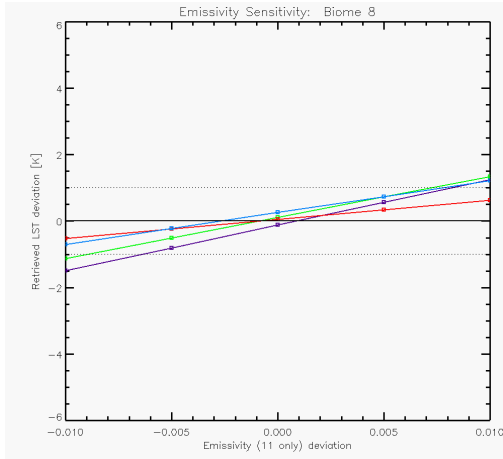
ALB2 Biome 6



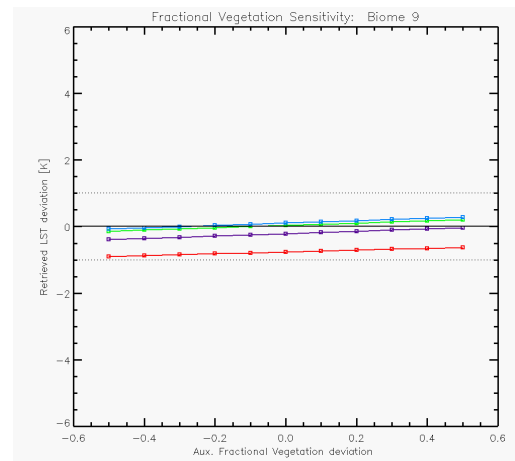
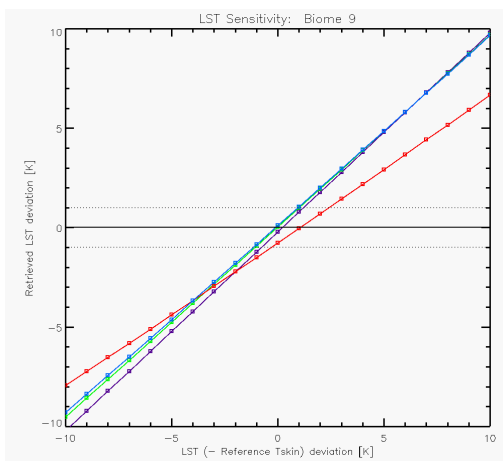
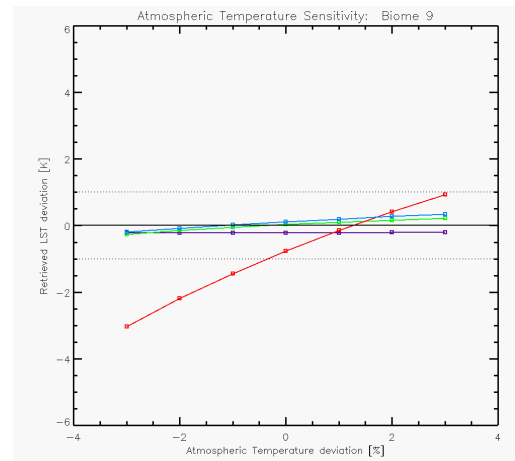
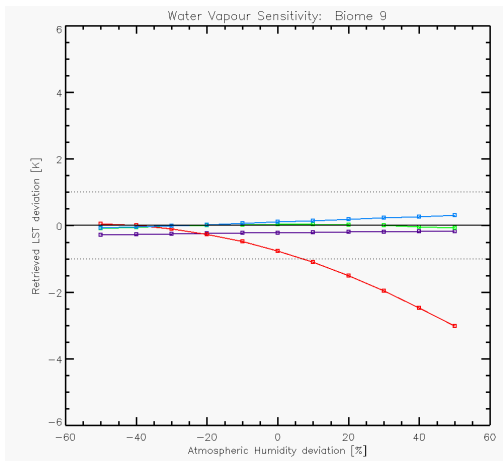
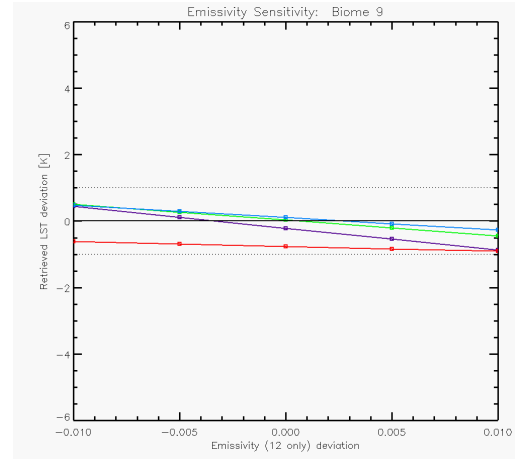
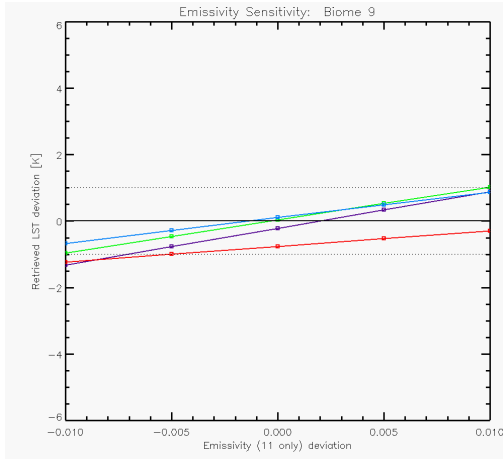
ALB2 Biome 7



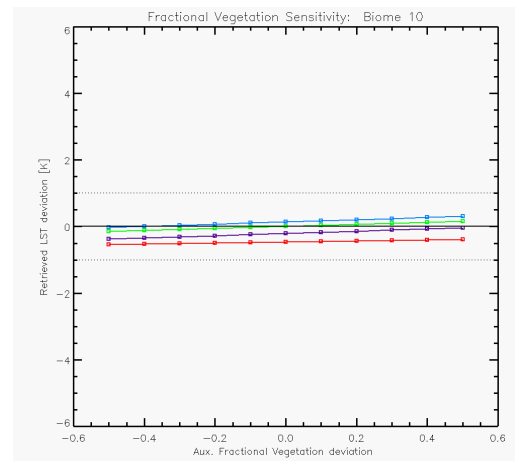
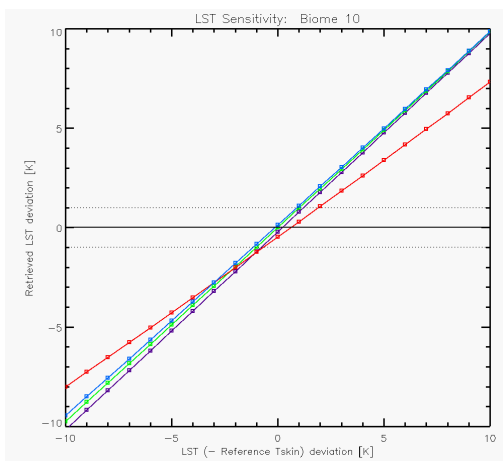
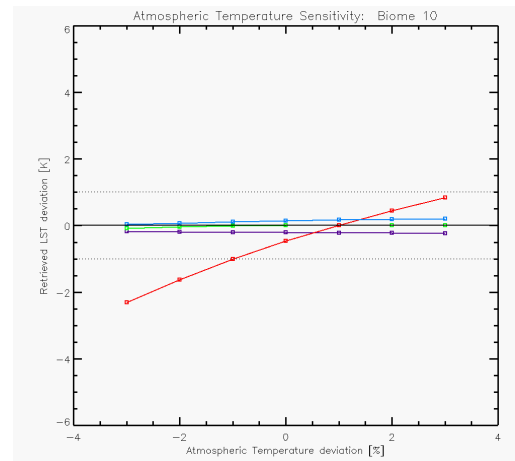
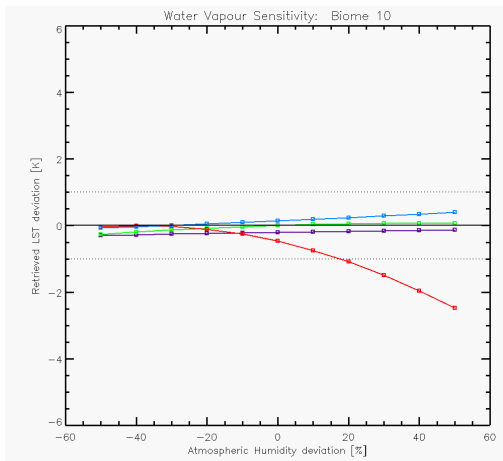
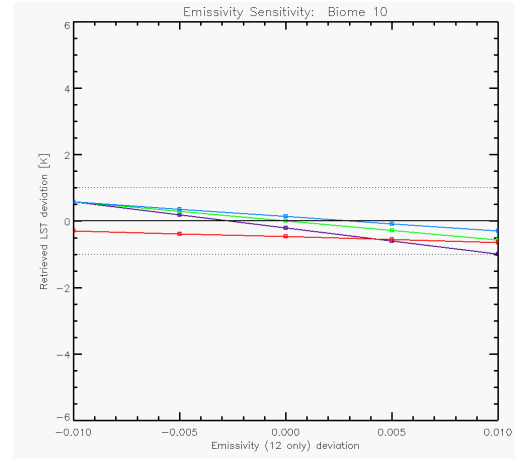
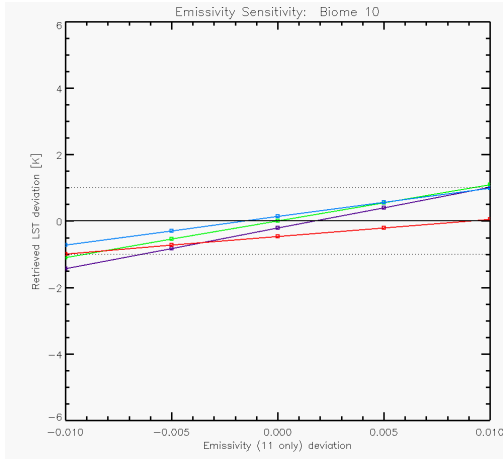
ALB2 Biome 8



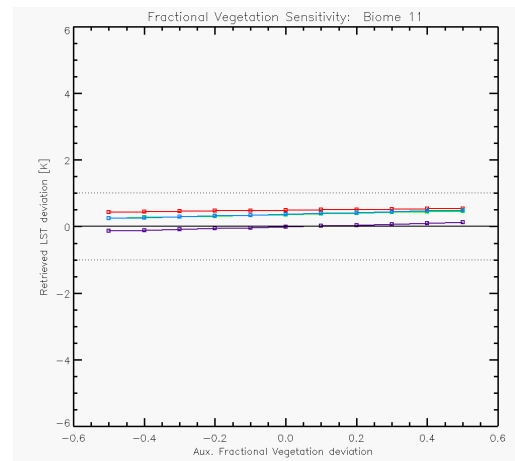
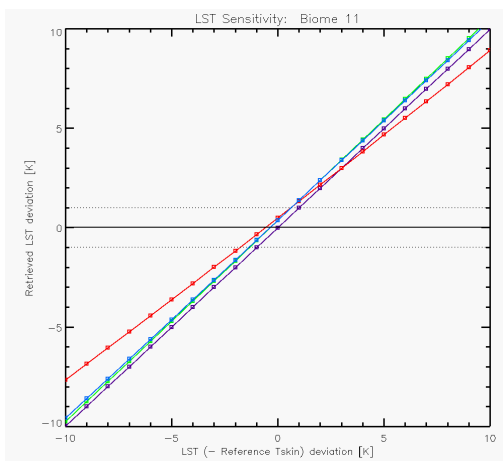
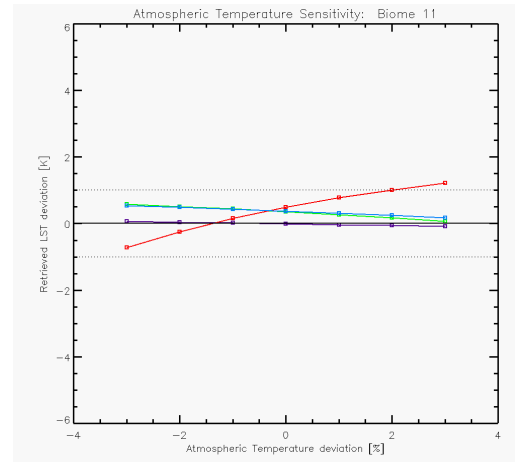
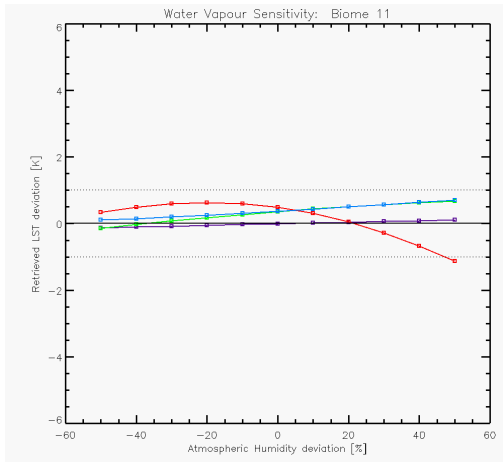
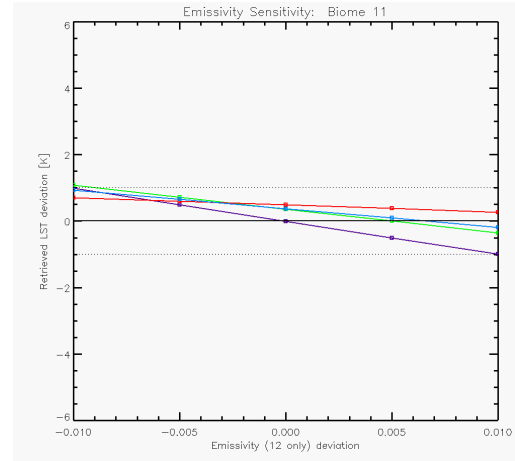
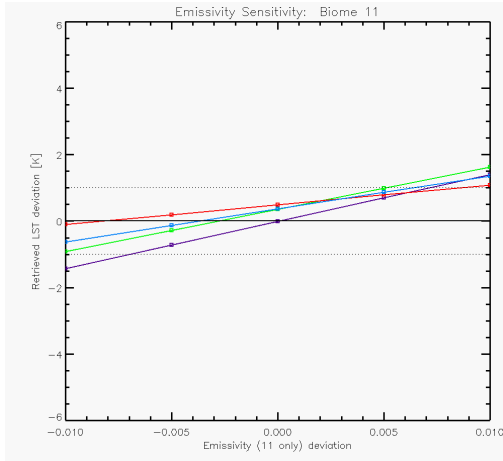
ALB2 Biome 9



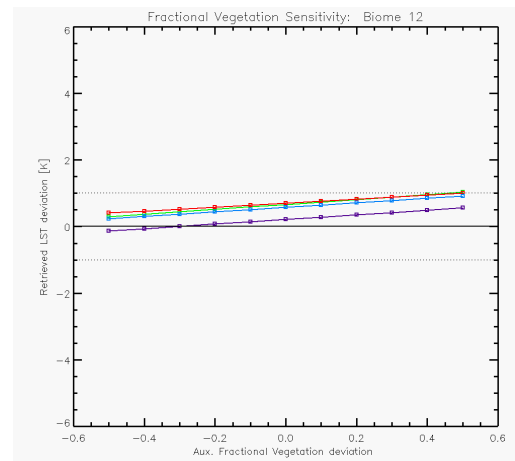
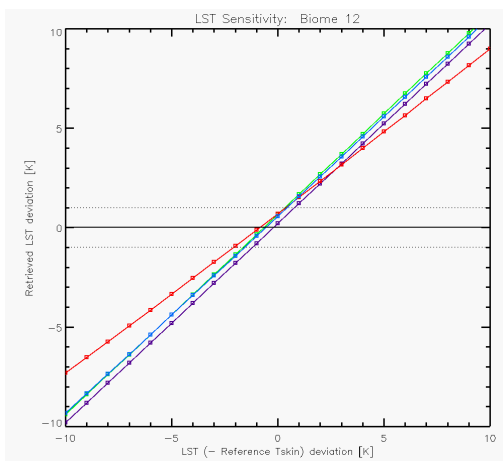
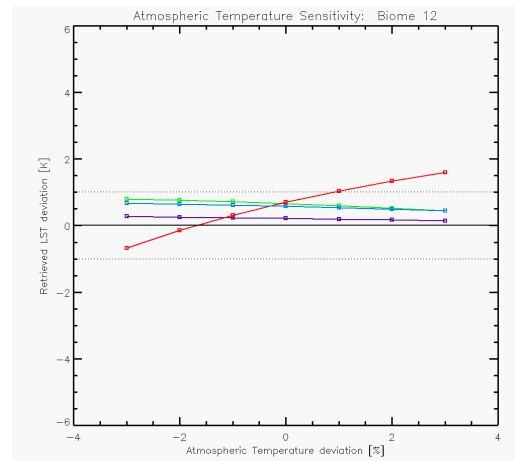
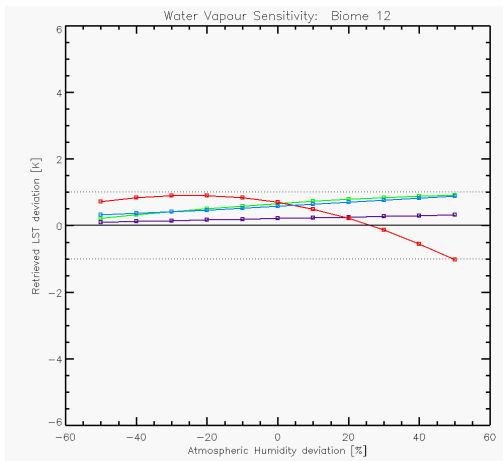
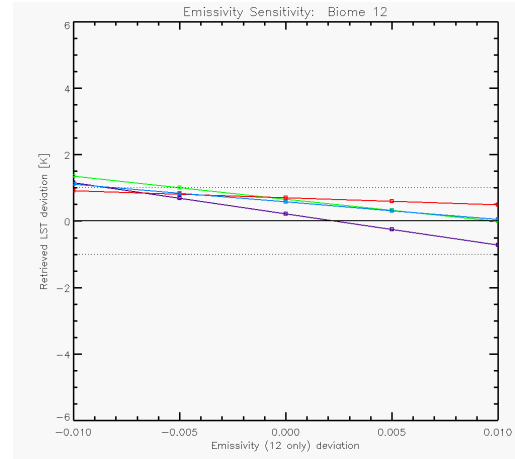
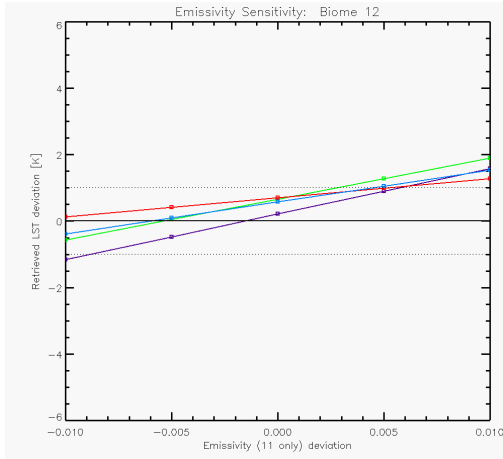
ALB2 Biome 10



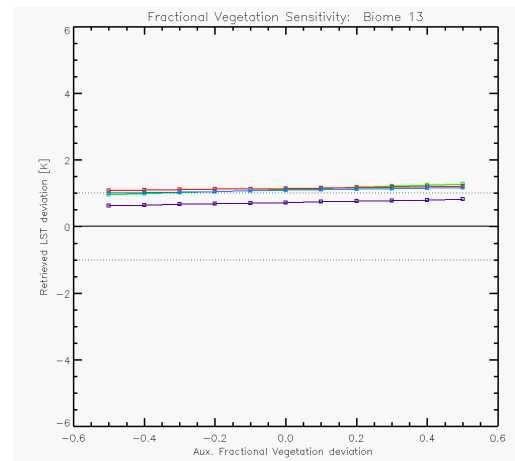
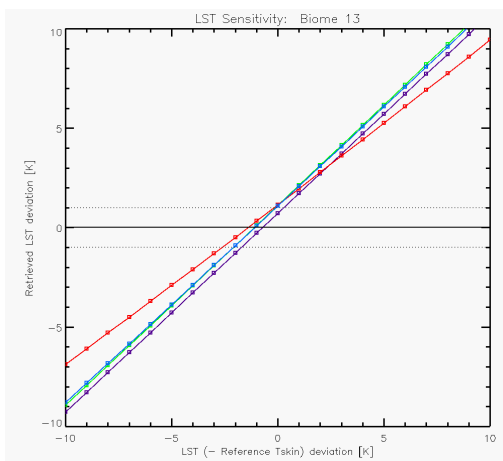
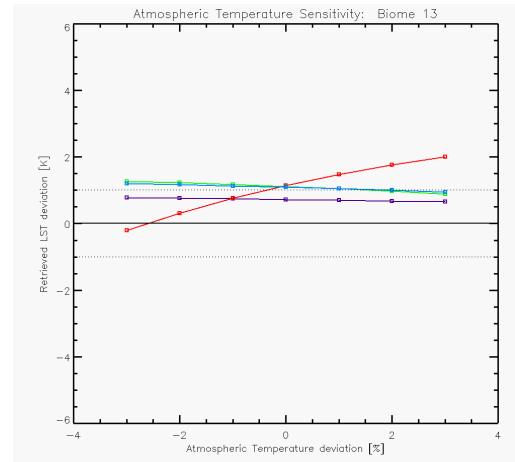
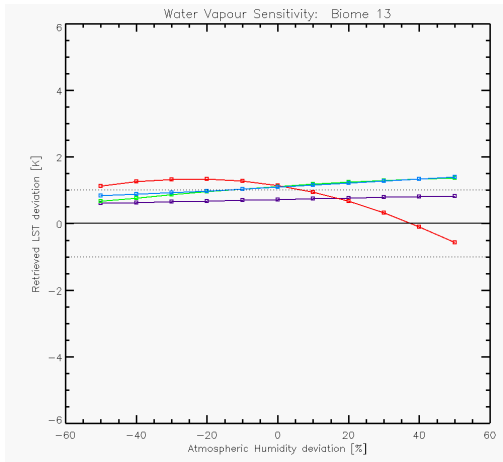
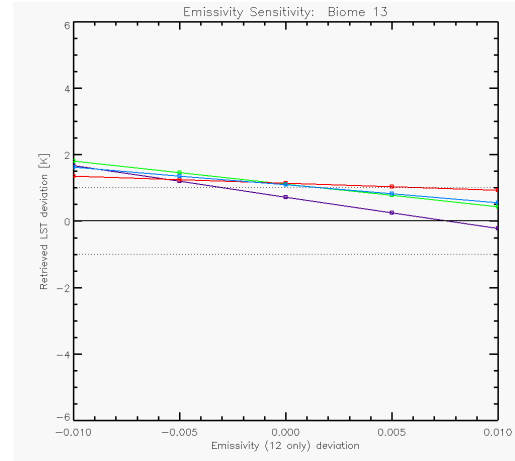
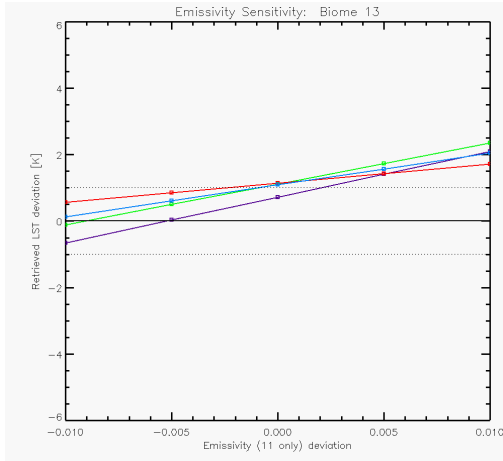
ALB2 Biome 11



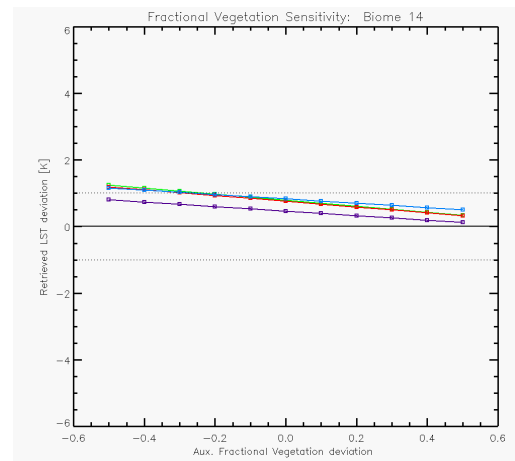
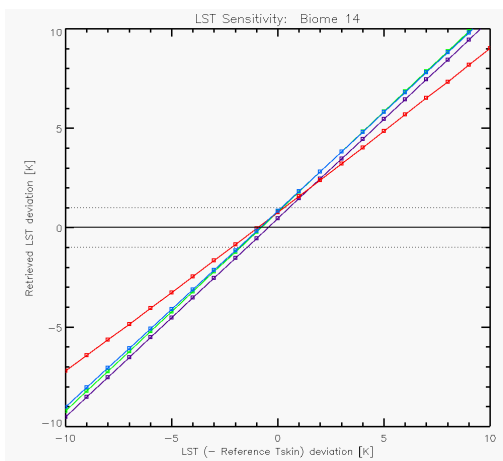
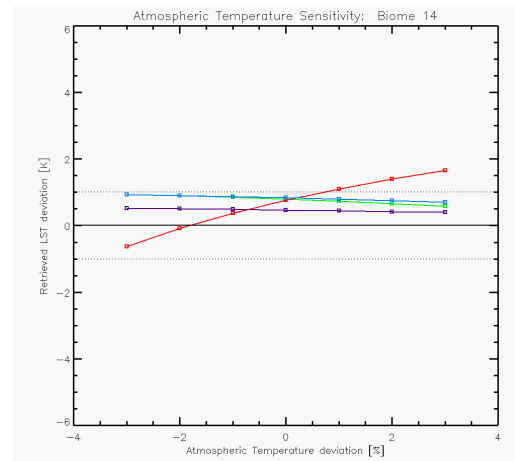
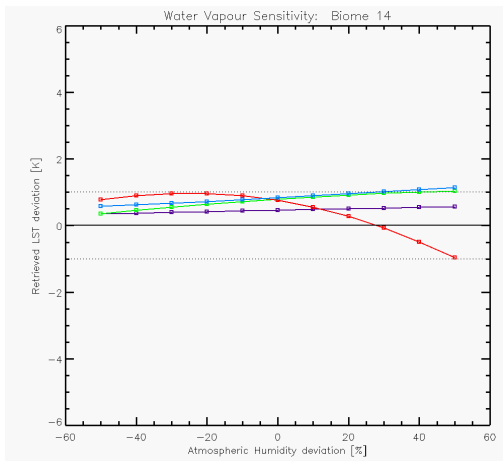
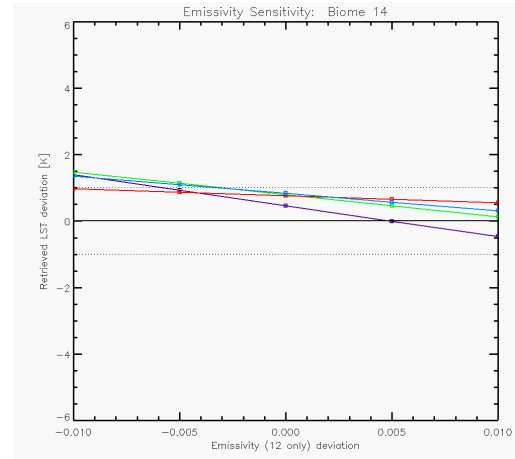
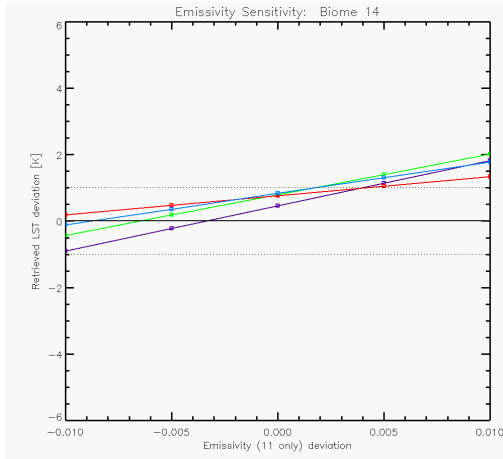
ALB2 Biome 12



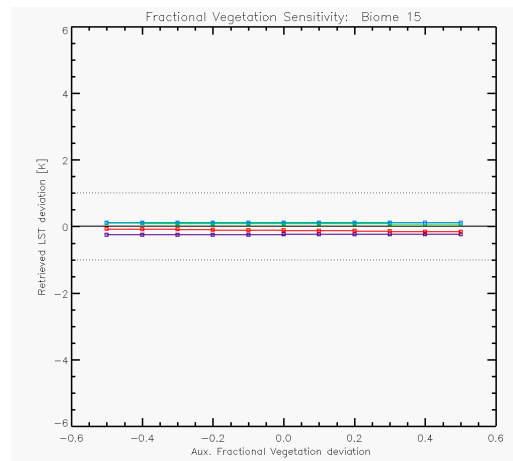
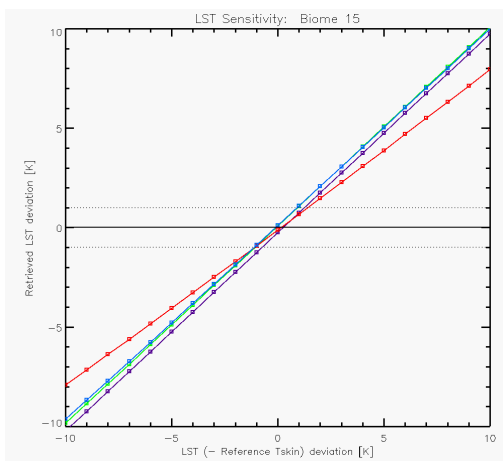
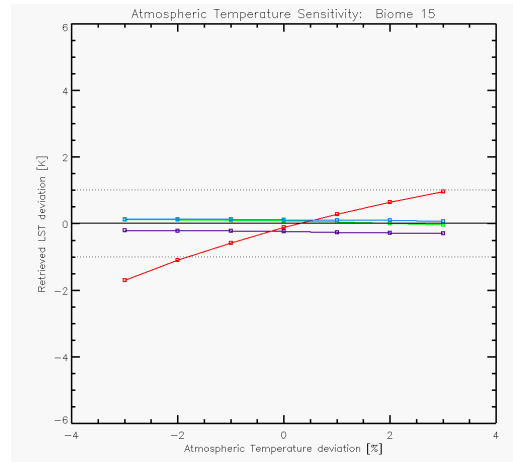
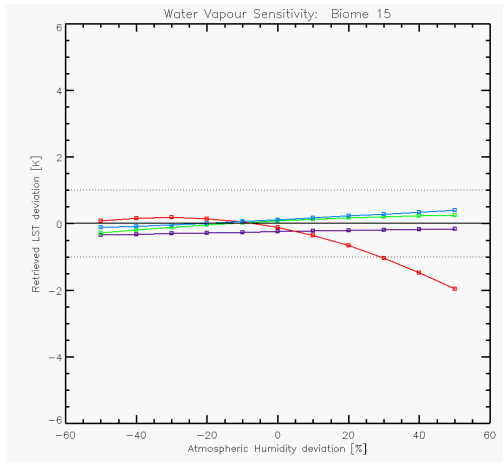
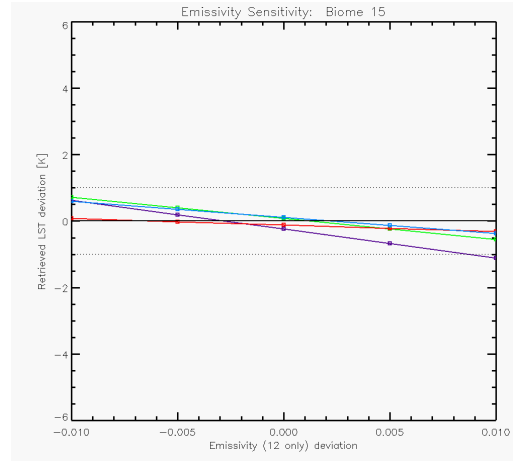
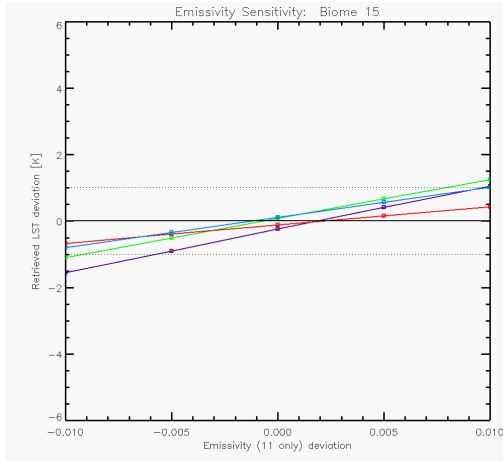
ALB2 Biome 13



ALB2 Biome 14

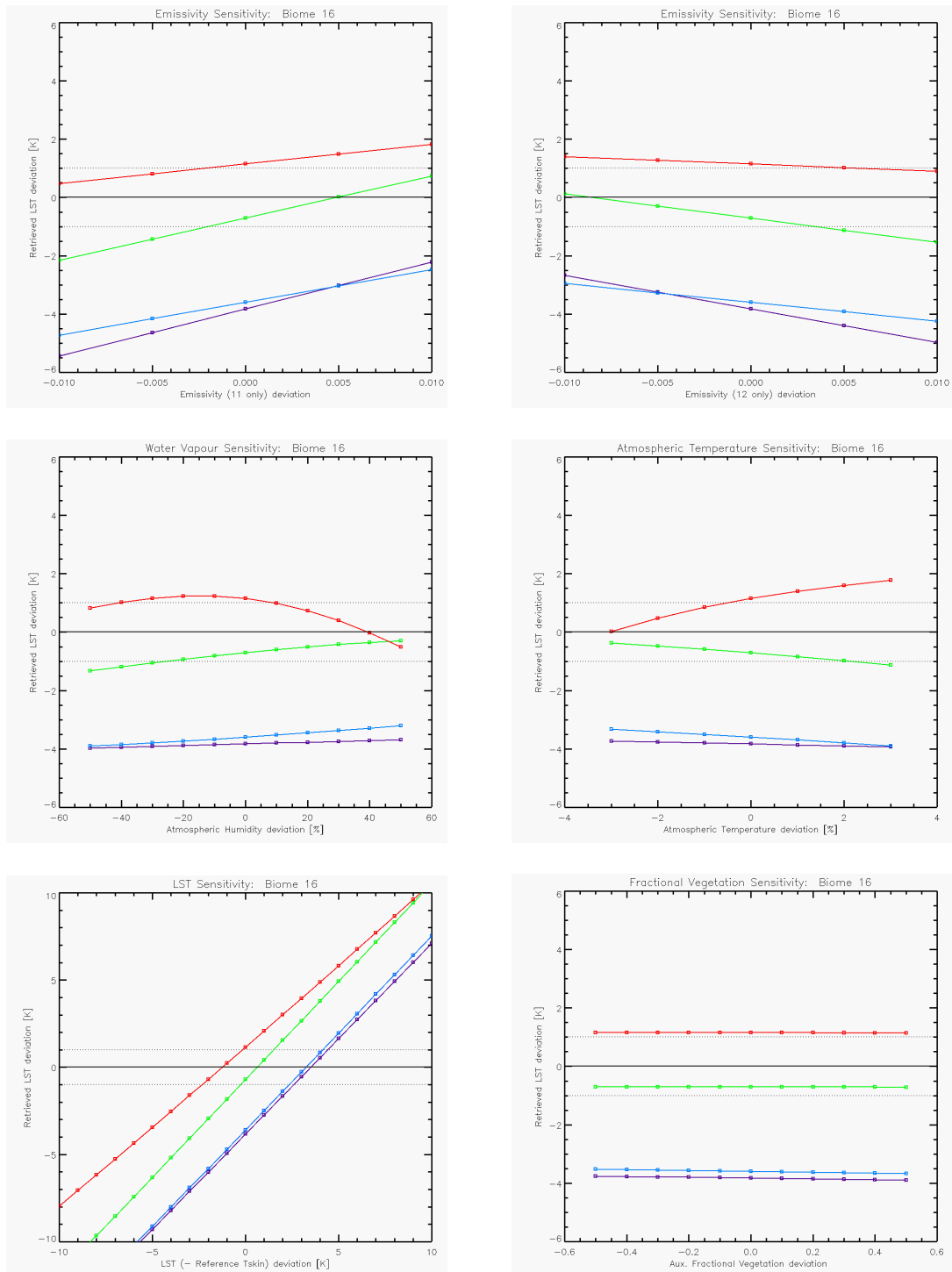


ALB2 Biome 15



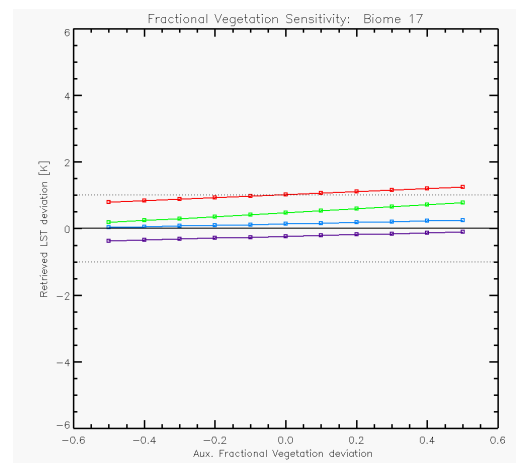
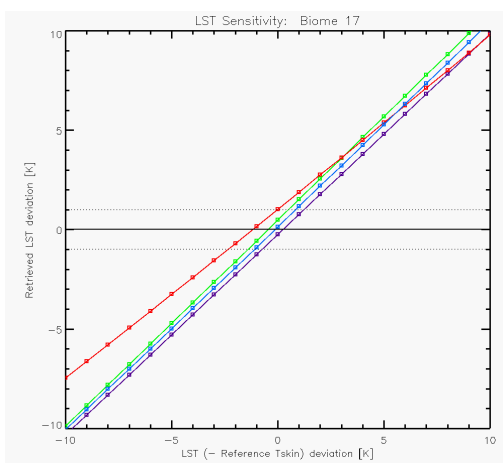
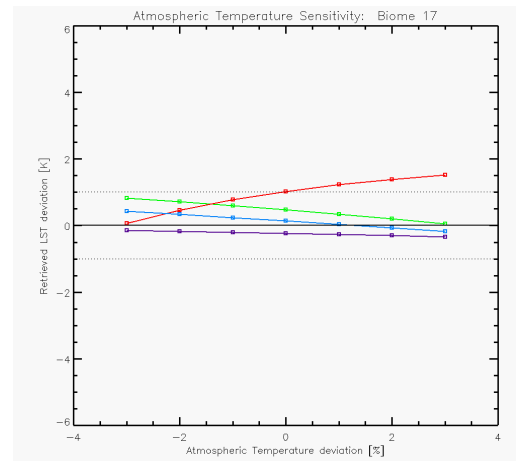
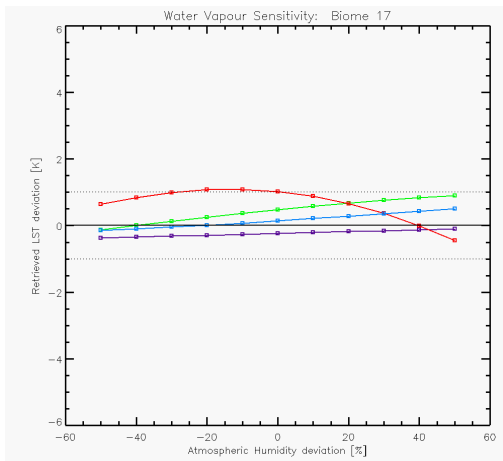
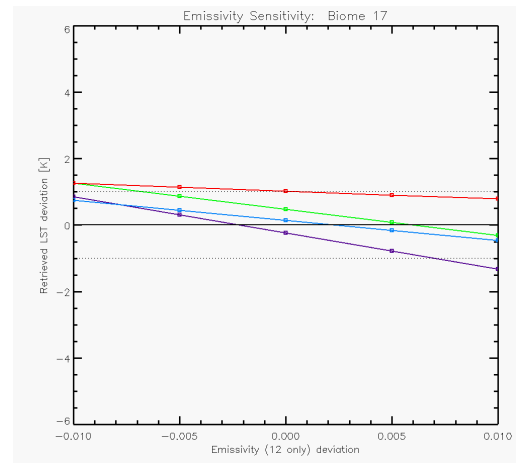
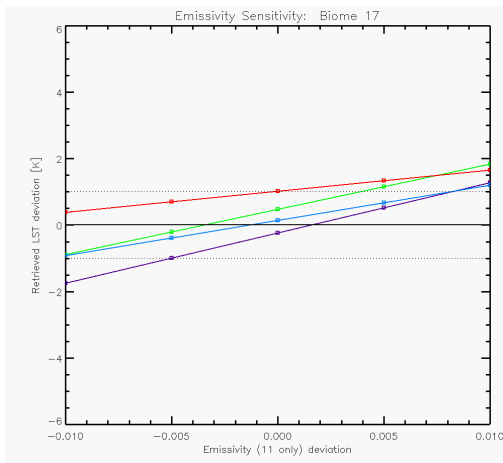


ALB2 Biome 16



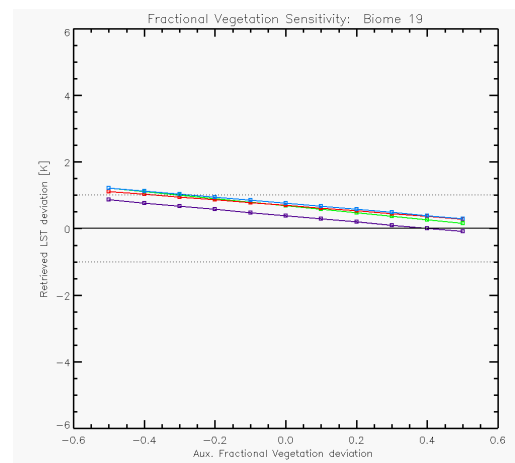
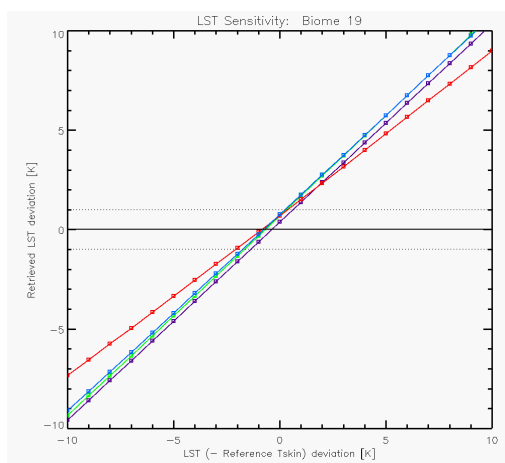
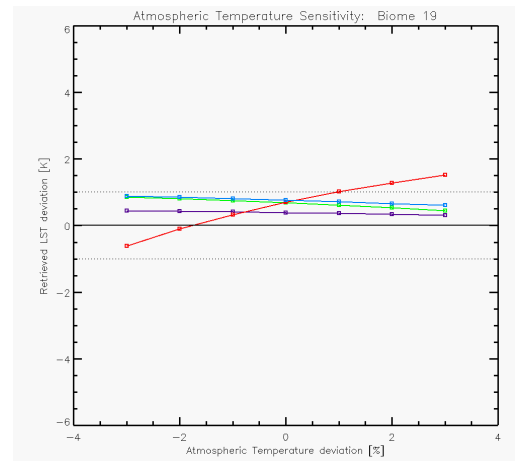
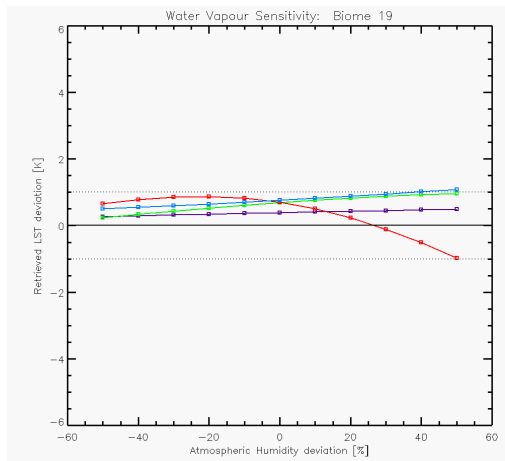
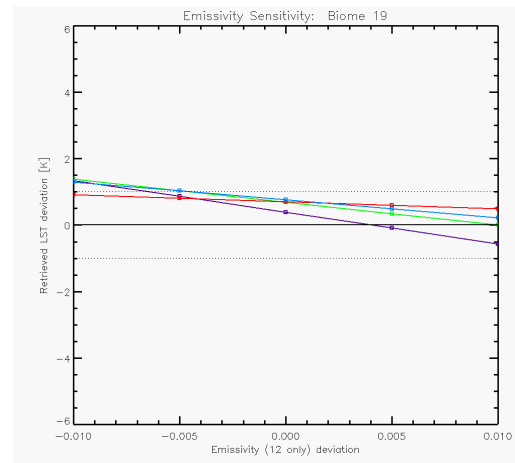
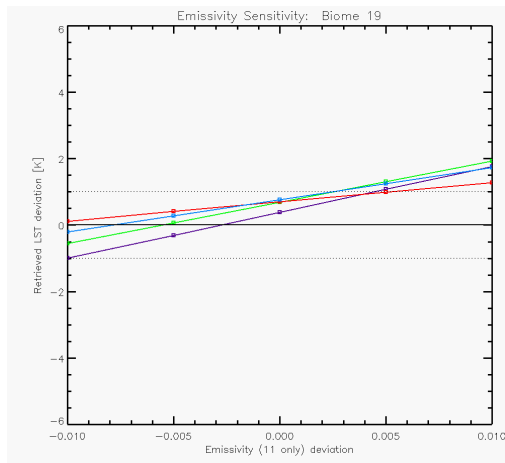


ALB2 Biome 17



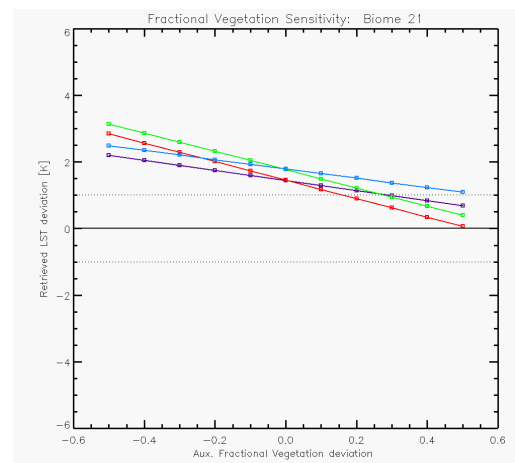
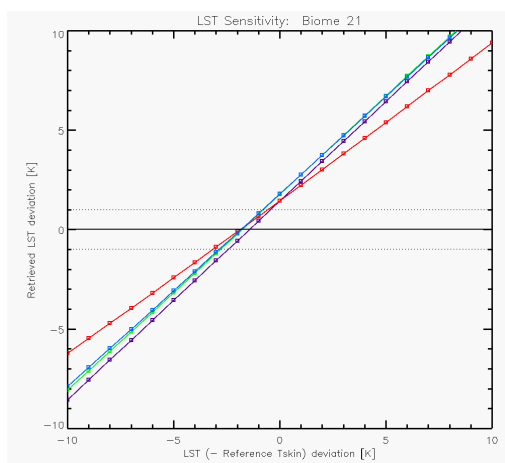
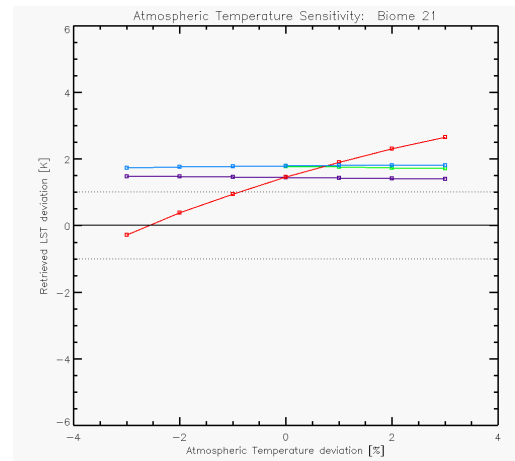
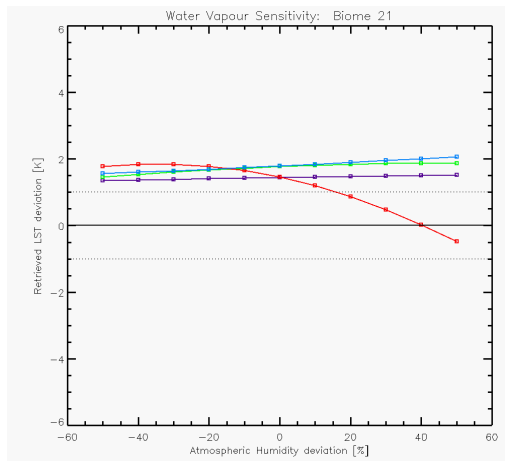
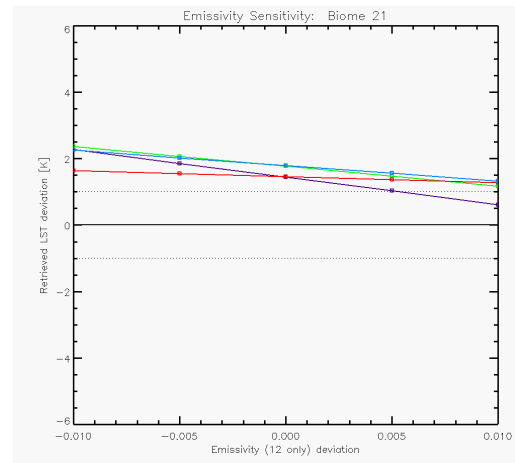
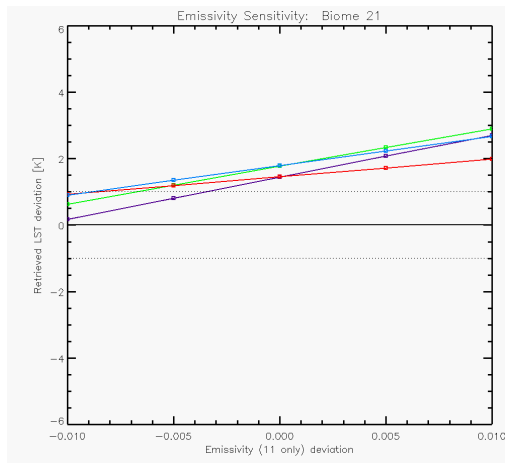


ALB2 Biome 19



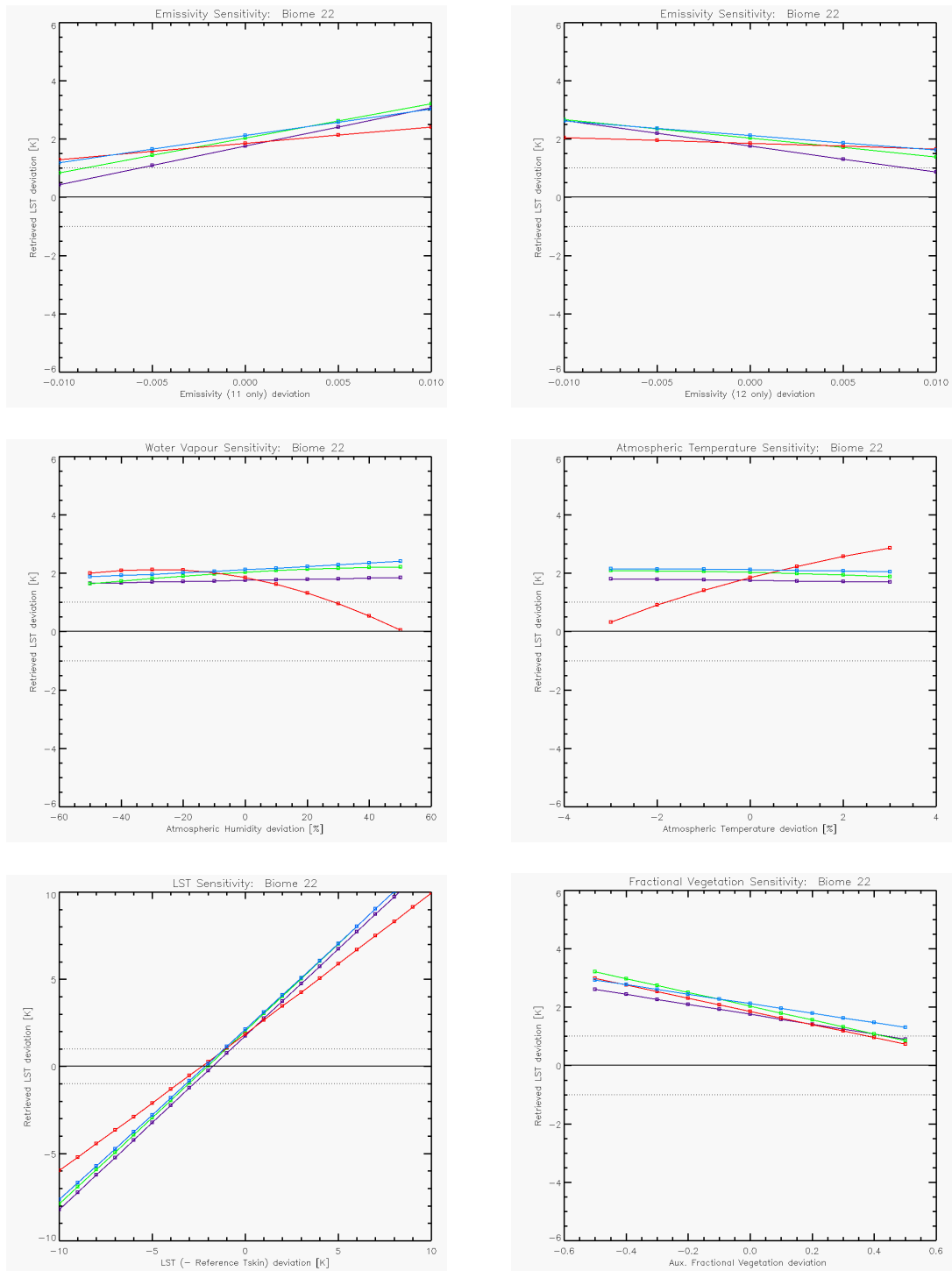


ALB2 Biome 21

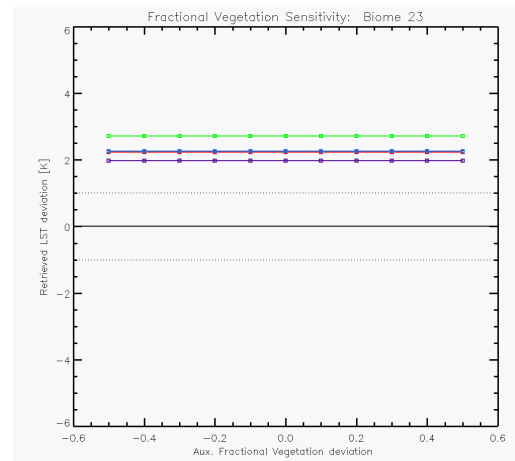
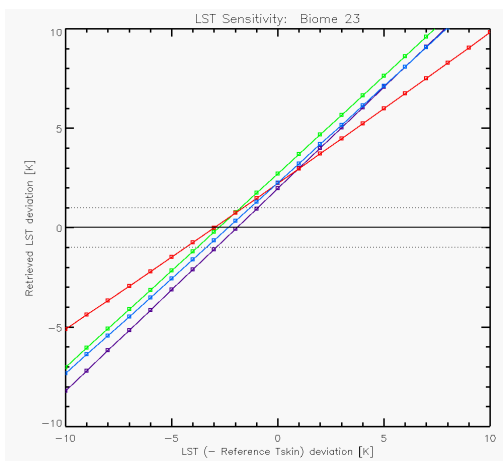
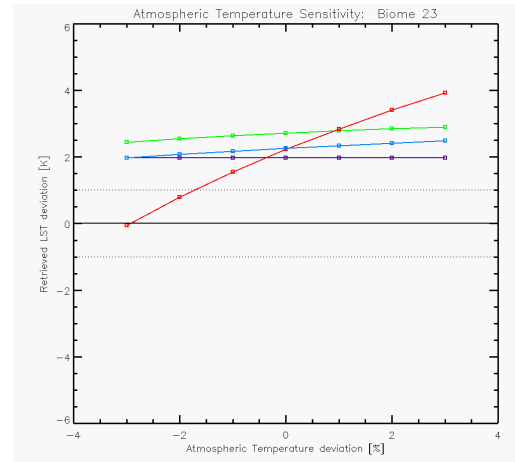
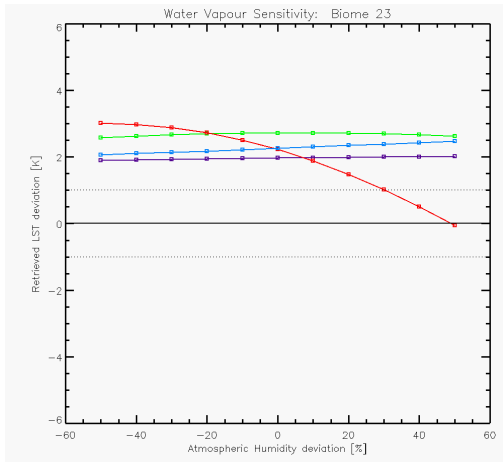
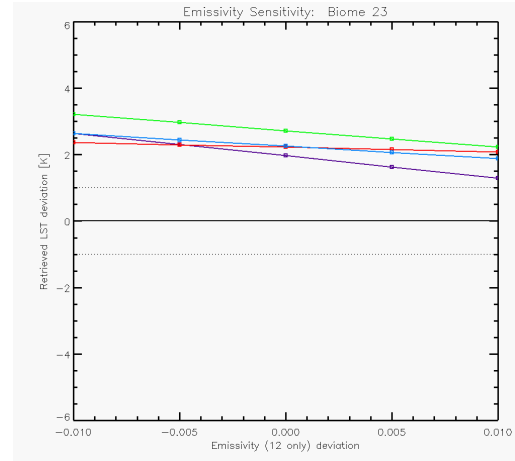
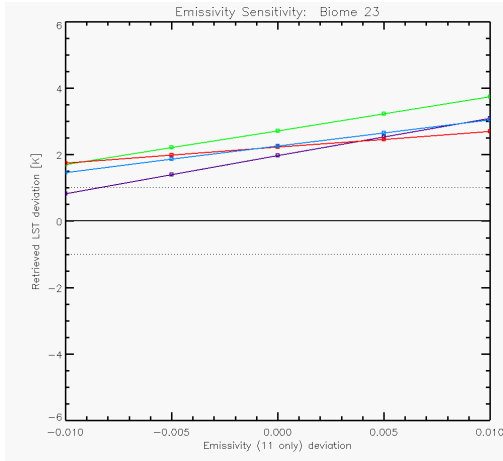




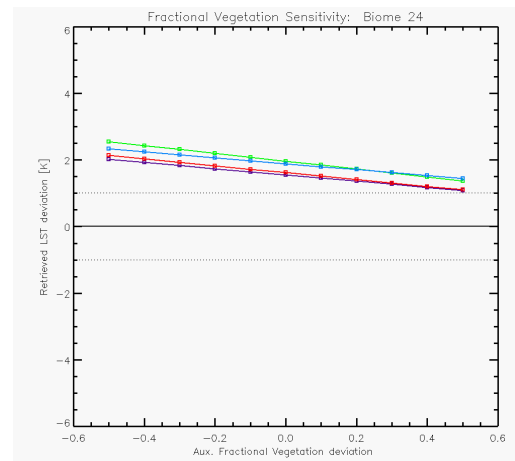
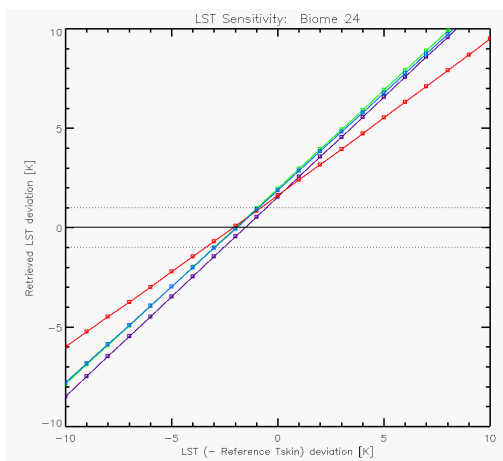
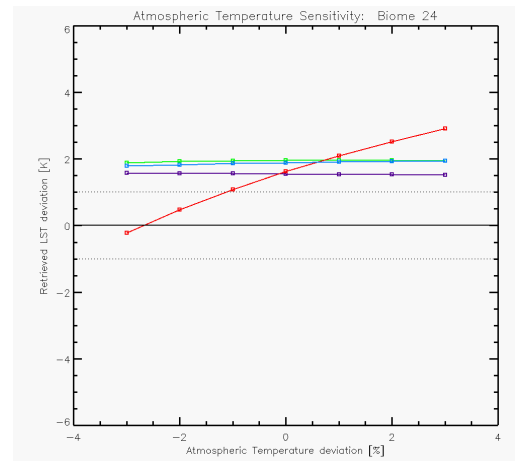
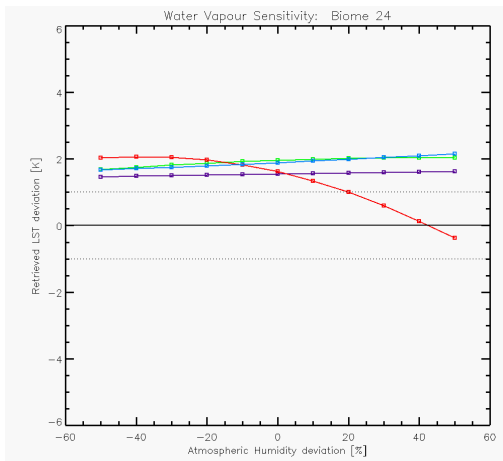
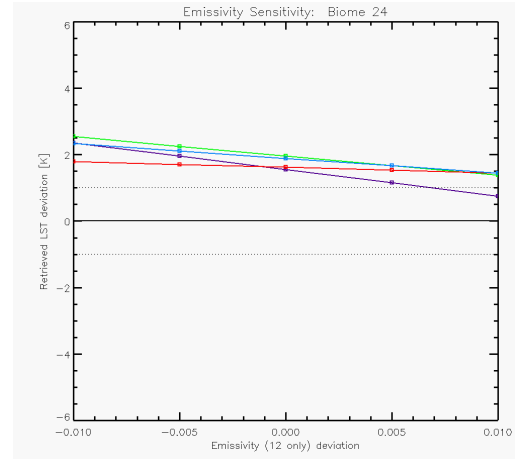
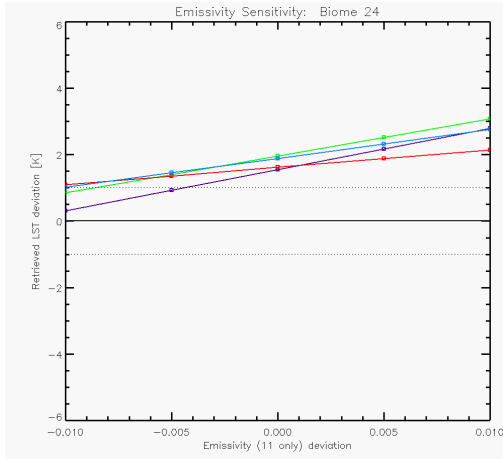
ALB2 Biome 22



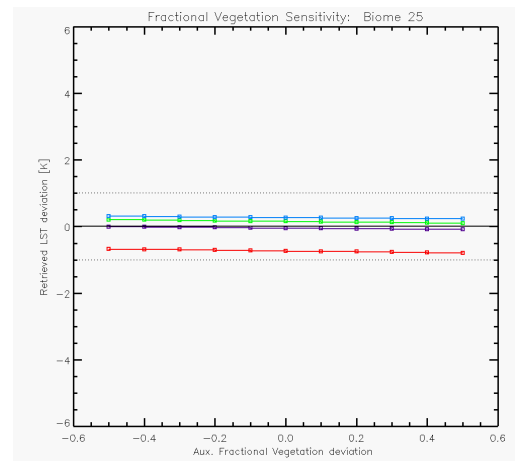
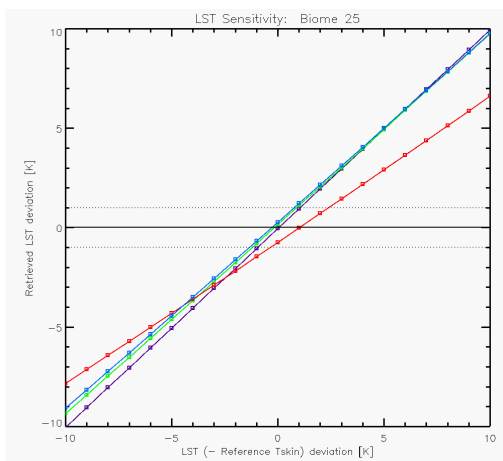
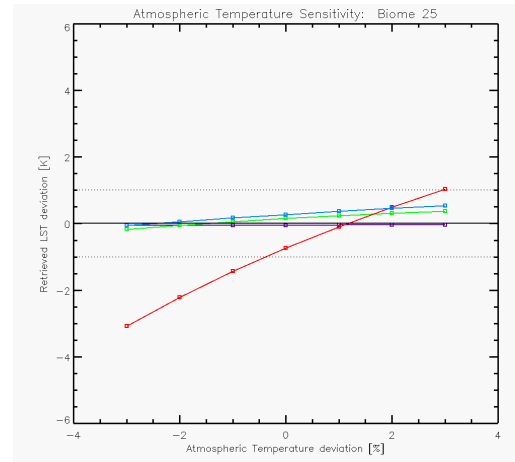
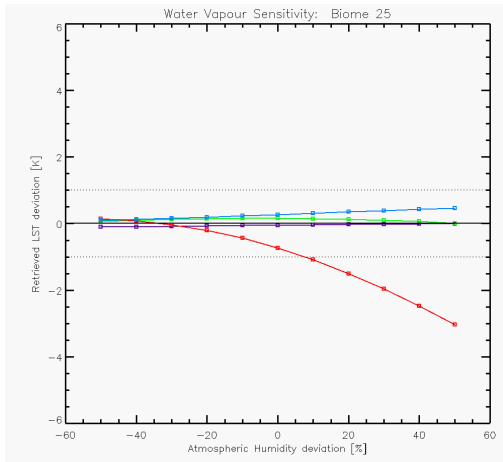
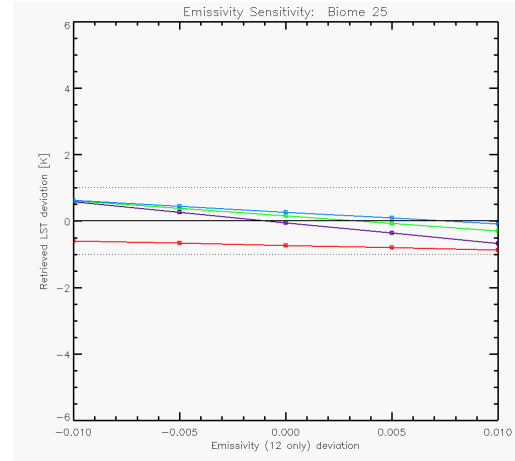
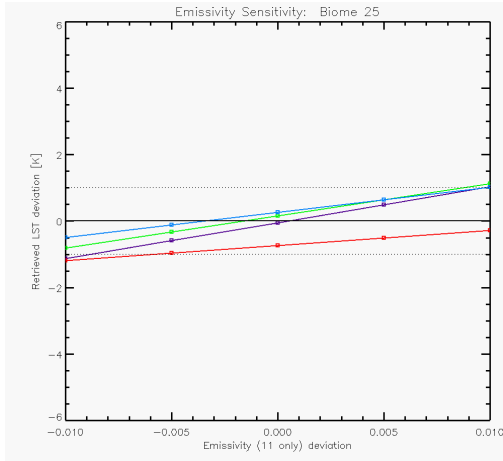
ALB2 Biome 23



ALB2 Biome 24

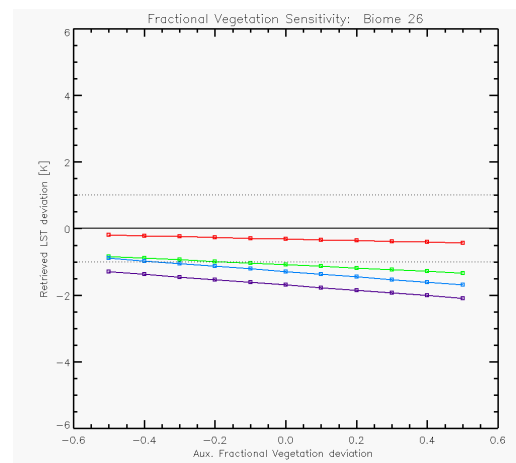
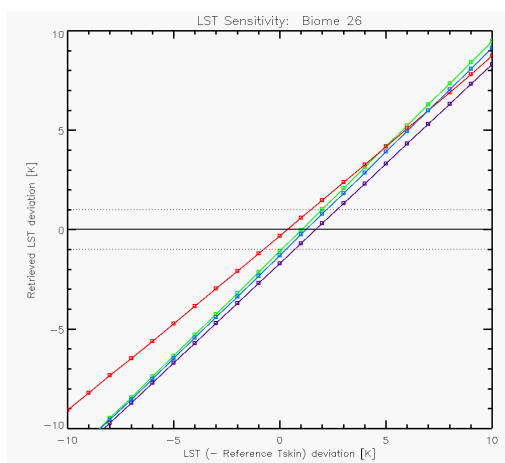
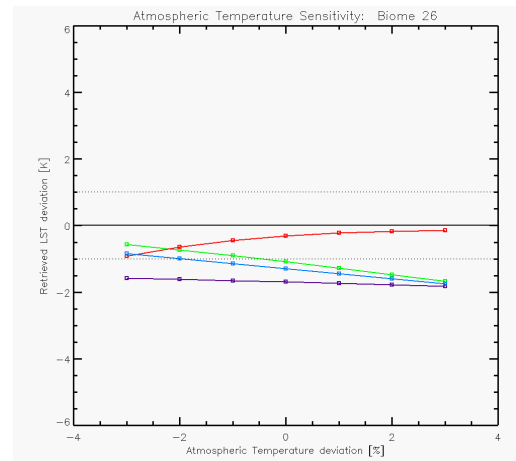
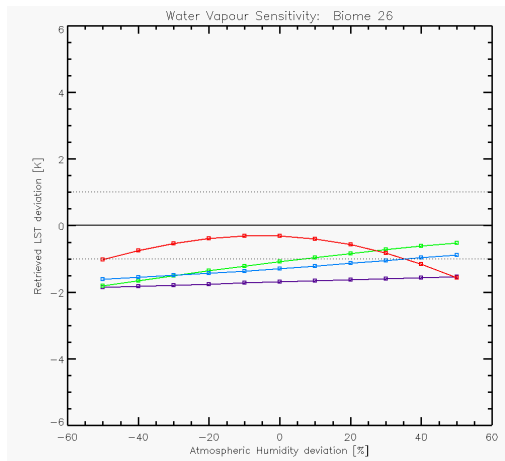
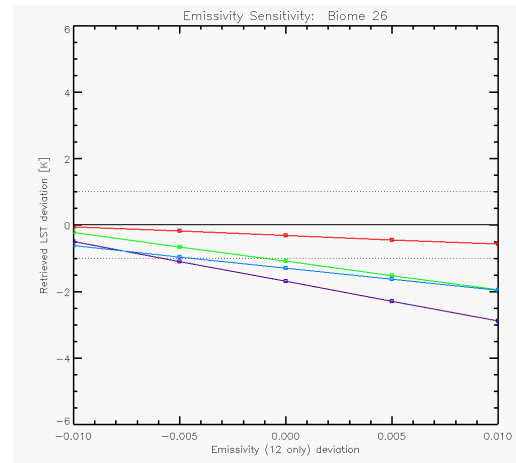
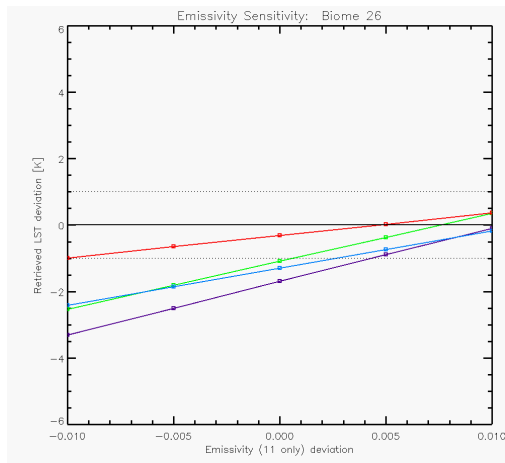


ALB2 Biome 25





ALB2 Biome 26





ALB2 Biome 27

